SINGLE EVENT KINETIC MODELING OF SOLID ACID ALKYLATION OF ISOBUTANE WITH BUTENES OVER PROTON-EXCHANGED Y-ZEOLITES

A Dissertation

by

JORGE MAXIMILIANO MARTINIS COLL

Submitted to the Office of Graduate Studies of
Texas A&M University
in partial fulfillment of the requirements for the degree of

DOCTOR OF PHILOSOPHY

December 2004

Major Subject: Chemical Engineering

SINGLE EVENT KINETIC MODELING OF SOLID ACID ALKYLATION OF ISOBUTANE WITH BUTENES OVER PROTON-EXCHANGED Y-ZEOLITES

A Dissertation

by

JORGE MAXIMILIANO MARTINIS COLL

Submitted to Texas A&M University
in partial fulfillment of the requirements
for the degree of

DOCTOR OF PHILOSOPHY

Approved as to style and content by:

Gilbert F. Froment (Chair of Committee)	Daniel F. Shantz (Member)
Dragomir B. Bukur (Member)	John P. Fackler (Member)
Kenneth R. Hall (Head of Department)	

December 2004

Major Subject: Chemical Engineering

ABSTRACT

Single Event Kinetic Modeling of Solid Acid Alkylation of Isobutane with Butenes over Proton-Exchanged Y-Zeolites. (December 2004)
Jorge Maximiliano Martinis Coll, B.S., Universidad Simon Bolivar
Chair of Advisory Committee: Dr. Gilbert F. Froment

Complex reaction kinetics of the solid acid alkylation of isobutane with butenes over a proton-exchanged Y-zeolite has been modeled at the elementary step level. Starting with a computer algorithm that generated the reaction network based on the fundamentals of the carbenium ion chemistry, the formation of over 100+ product species has been modeled in order to gain understanding of the underlying phenomena leading to rapid catalyst deactivation and product selectivity shifts observed in experimental runs. An experimental investigation of the solid acid alkylation process was carried out in a fixed bed catalytic reactor operating with an excess of isobutane under isothermal conditions at moderate temperatures (353-393 K) in liquid phase. Experimental data varying with run-time for a set of butene space-times and reaction temperatures were collected for parameter estimation purposes. A kinetic model was formulated in terms of rate expressions at the elementary step level including a rigorous modeling of deactivation through site coverage. The single event concept was applied to each rate coefficient at the elementary step level to achieve a significant reduction in the number of model parameters. Based on the identification of structural changes leading to the creation or destruction of symmetry axes and chiral centers in an elementary step, formulae have been developed for the calculation of the number of single events. The Evans-Polanyi relationship and the concept of stabilization energy were introduced to account for energy levels in surface-bonded carbenium ions. A novel functional dependency of the stabilization energy with the nature of the carbenium ion and the carbon number was proposed to account for energy effects from the acid sites on the catalyst. Further reductions in the number of parameters and simplification of the equations for the transient pseudohomogeneous one-dimensional plug-flow model of the reactor were achieved by means of thermodynamic constraints. Altogether, the single event concept, the Evans-Polanyi relationship, the stabilization energy approach and the thermodynamic constraints led to a set of 14 parameters necessary for a complete description of solid acid alkylation at the elementary step level.

TABLE OF CONTENTS

Page

ABSTRACT iii

TABLE OF CONTENTS iv

LIST OF FIGURES v

LIST OF TABLES vi

INTRODUCTION 1

CHEMISTRY OF ISOALKANE/ALKENES SOLID ACID ALKYLATION OVER PROTON-EXCHANGED Y-ZEOLITE AT MODERATE TEMPERATURES 5

- Chemistry of Hydrocarbon Transformations over Solid Acid Catalysts 5
- Elementary Steps in Solid Acid Alkylation 7
- Matrix Representation of Hydrocarbon Species 10
- Solid Acid Alkylation Reaction Network 12

EXPERIMENTAL INVESTIGATION 16

- Catalyst Characteristics: Proton-Exchanged Y-Zeolite 16
- Experimental Setup and Procedure 17
- Product Characterization by Gas Chromatography / Mass Spectrometry 19
- Experimental Results and Discussion 24

FUNDAMENTAL MODELING OF SOLID ACID ALKYLATION KINETICS 36

- Modeling Deactivation through Site Coverage 36
- Rate Controlling Steps and Liquid Sorption in Zeolites 38
- Rate Expressions at the Elementary Step Level 40
- The Single Event Concept 42
- Number of Single Events 44
- The Evans-Polanyi Relationship 48
- Stabilization Energies, Heats of Reaction and Protonation Equilibrium Constants 50
- Gas-Phase Enthalpies of Formation 54
- Carbenium Ion Energies 58
- Thermodynamic Constraints and Component Groups 61
- Rate Expressions at the Single Event Level 65

REACTOR MODEL FORMULATION & PARAMETER ESTIMATION 67

- The Transient Pseudohomogeneous One-Dimensional Model with Plug Flow 67
- The Objective Function 71
- Parameter Estimation 72
- Statistical Tests 75
- Results and Discussion 78

CONCLUSIONS AND RECOMMENDATIONS 86

LITERATURE CITED 88

APPENDIX 92

VITA 101

LIST OF FIGURES

Page

Figure 1. Proposed Elementary Steps for Solid Acid Alkylation at Moderate Temperatures 8
Figure 2. Hydrocarbon Representation by Boolean Matrices 11
Figure 3. Calculation of the t-butyl + 2-butene Oligomerization Step. 13
Figure 4. Reaction Network Scheme 15
Figure 5. Fixed Bed Isobutane Alkylation with Butenes Experimental Setup. 18
Figure 6. Reaction Product Total Ion Chromatogram for Fresh Catalyst 20
Figure 7. Reaction Product Total Ion Chromatogram after Deactivation 21
Figure 8. Major Product Yields vs. Processed Butene for Run 9 27
Figure 9. Minor Product Yields vs. Processed Butene for Run 9 28
Figure 10. Product Yields vs. Processed Butene for Run 1 29
Figure 11. Product Yields vs. Processed Butene for Run 2 29
Figure 12. Product Yields vs. Processed Butene for Run 3 30
Figure 13. Product Yields vs. Processed Butene for Run 4 30
Figure 14. Product Yields vs. Processed Butene for Run 5 31
Figure 15. Product Yields vs. Processed Butene for Run 6 31
Figure 16. Product Yields vs. Processed Butene for Run 7 32
Figure 17. Product Yields vs. Processed Butene for Run 8 32
Figure 18. Product Yields vs. Processed Butene for Run 9 33
Figure 19. Initial C_8-Alkanes and Final C_4/C_8-Alkenes Product Yields 34
Figure 20. Alkane Standard Enthalpy of Formation Parity Plot 56
Figure 21. Alkene Standard Enthalpy of Formation Parity Plot 57
Figure 22. Carbenium Ion Standard Enthalpy of Formation Parity Plot. 61
Figure 23. Performance of SQP and Marquardt Algorithms in Parameter Estimation 78
Figure 24. Parity Plot for O4 Product Yield 81
Figure 25. Parity Plot for [M+D+T] P8 Product Yield 81
Figure 26. Parity Plot for [M+D+T] O8 Product Yield 82
Figure 27. Parity Plot for P5, P6 & P7 Product Yields 82
Figure 28. Product Yield Evolution with Run-Time 83
Figure 29. Reach of the Deactivation Zone after 0.5 h of Run-Time: Product Yields 84
Figure 30. Reach of the Deactivation Zone after 0.5 h of Run-Time: Net Production Rates 85

LIST OF TABLES

Page

Table 1. Reaction Network Generation Elementary Steps and Rules 12
Table 2. Reaction Network Species Distribution by Type and Carbon Number 14
Table 3. Reaction Network Elementary Step Inventory. 15
Table 4. Identified Alkanes Distribution 22
Table 5. Identified Alkenes Distribution 23
Table 6. Experimental Program 24
Table 7. Product Yields from Run 5 26
Table 8. Product Yields from Run 9 27
Table 9. Examples of Symmetry Transformations on Elementary Steps 46
Table 10. Formulae for the Estimation of the Number of Single Events 48
Table 11. Alkane Standard Enthalpy of Formation 55
Table 12. Alkene Standard Enthalpy of Formation 57
Table 13. Isodesmic Reactions 59
Table 14. Gas Phase Carbenium Ion Standard Enthalpy of Formation 60
Table 15. Non-Branching Isomerization Equilibrium Test 62
Table 16. Group Contribution Method for Liquid Heat Capacity 64
Table 17. Group Contribution Method for Enthalpy Change of Vaporization 65
Table 18. Parameter Constraints Summary 74
Table 19. Parameter Estimates 79

INTRODUCTION

Under the legal framework established by the Clean Air Act[1], oil refiners have been under increasing pressure to produce more environmentally friendly fuels in order to satisfy the increasing energy demand of a growing transport sector. Thus, in response to more stringent regulations, innovative fuel formulations such as reformulated gasolines RFG and boutique fuels have been introduced into U.S. markets in order to satisfy escalating mandatory reductions on regulated emissions such as Volatile Organic Compounds (VOC), Nitrogen Oxides (NO_x), Particulates (PM) and Carbon Monoxide (CO). However, in spite of their success on reducing air pollution, RFG must still overcome technical challenges in terms of minimizing the environmental impact of the processes and the additives involved in their production.

The production of RFG involves the addition of increasing volumes of clean octane number boosters such as oxygenates, reformate and alkylate to the gasoline pool. This pool is mainly conformed by a mixture of the most readily available volumes of gasoline cuts in the refinery such as the straight-run naphtha from crude oil distillation unit and the conversion naphtha from either the fluid catalytic cracking or the thermal cracking units. However, naphtha from conversion processes often requires extensive hydrodesulphurization before entering the pool because of their elevated sulphur content, resulting in a significant octane number reduction due to extensive alkene hydrogenation. As a result, the production of large volumes of low-sulphur gasoline usually implies also low octane numbers, making necessary the inclusion of octane boosters in their formulation.

The sustained use of oxygenates such as MTBE (Methyl Tert-Butyl Ether) in RFG is currently under scrutiny because of their high solubility in water. This property makes oxygenates strong candidates for aquifer pollution and limits their future as a major component on any new gasoline formulation. In addition, tightening regulations on benzene content, which is a strong carcinogen, are also putting caps on the amount of reformate that can go into the gasoline pool. This scenario makes alkylate, which has a very high octane number and almost no sulphur, olefin or aromatic content, the most promising fuel component for the future of any new RFG formulation.

This dissertation follows the style and format of *Industrial & Engineering Chemistry Research.*

Alkylate was first produced in 1932 when Ipattieff and Pines[2] at UOP discovered that, at low temperatures (<300 K), light alkenes react with isoalkanes in solutions of strong acids such as $AlCl_3$/HCl or BF_3/HF to produce highly branched heavier alkanes. By the 1940s, alkylate was commercially produced worldwide by contacting at sub-ambient temperatures concentrated liquid sulfuric acid or anhydrous hydrogen fluoride with a mixture of butenes highly diluted in isobutane.

The use of liquid acids in alkylation involves the production of hazardous by-products such as acid soluble oils (ASO) and heavy polymers that must be continuously purged out of the reactor in order to avoid alkylate yield degradation. Consequently, during the last two decades, increasing safety and environmental concerns associated with the use of either these two toxic acids and the disposal of their related ASO have aroused together with significant efforts to come up with alternative technologies based on solid acid materials.[3]

To date, numerous solid acids including zeolites, silica supported Lewis acids and sulfated metal oxides have been widely tested as promising catalytic for solid acid isobutane/butene Alkylation.[4,5,6] In order to carry out solid acid alkylation over these materials, higher temperatures (320-390 K) compared to the use of liquid acids (280-300 K) are required to compensate for lower acidity levels. In spite of all the advantages associated with the use of solid acid materials, their evolution into a commercial process has been hindered by the observation of a very rapid catalyst deactivation after only few hours of operation when starting at high butene conversion levels. Moreover, this deactivation process is always accompanied by a selectivity shift towards highly unsaturated products.

In the solid acid alkylation of isobutane with butenes with fresh catalyst, an alkylate-like product mostly made out of isoalkanes in the C_8 carbon fraction is initially obtained. As the catalyst deactivation proceeds, increasing amounts of isoalkenes within the C_5-C_{10} carbon fraction are observed to replace C_8-isoalkanes until they become the majority of the reaction product.[7] This observed decrease in alkylate yield with time makes the fixed bed operation for this process unsuitable for commercial application. Still, important efforts to overcome the catalyst deactivation have been made not only to improve both activity and stability on catalysts themselves, but also to deal with their rapid deactivation by looking for alternative contacting schemes and regeneration methods. These efforts include testing fluidized beds (slurry) or transport (riser) reactors as well as regenerating spent catalysts by means of combustion of carbonaceous deposits, ozone treatment, hydrogenation and supercritical media operation.[8]

Currently, it is widely accepted that deactivation in solid acid alkylation is produced by the irreversible adsorption of oligomers on the catalyst acid sites. From experiments where Temperature Programmed Oxidation (TPO) is applied to characterize carbonaceous deposits on spent Y-zeolites, Querini demonstrated that only partial removal of these strongly adsorbed species can be achieved by combustion in air at temperatures within the 285-500°C range. In this work, Querini claims that the high temperature transformation of these adsorbed species from aliphatic structures to aromatics ones is responsible for limiting regeneration by creating stronger interactions between the adsorbed species and the acid sites. Further experiments show that the inclusion of small amounts of noble metals such as platinum to the catalyst formulation results in no significant reduction of the regeneration temperature in the extent needed to avoid oligomer condensation. Finally, extraction with organic solvents and supercritical fluids has also proven unsuccessful for spent catalyst regeneration. Here, solid microporosity resulted responsible of preventing the removal of large oligomers out of the catalyst framework.[9]

In general, alkylate chemical composition comprises a large number of isoalkanes and isoalkenes within the C_5-C_{10} carbon fraction. In the particular case of isobutane alkylation with butenes, isoalkanes with carbon number of eight constitute most of the reaction product. This fraction is largely made up of trimethylpentanes (TMP) and dimethylhexanes (DMH) followed by important amounts of methylheptanes (MH). For every carbon number, isomers with a tertiary carbon atom in the 2-position predominate over all other species. Moreover, the distribution of these species within the same carbon fraction is far from their equilibrium composition.[10] An overall product distribution with such a large variety of species clearly illustrates the complexity of its corresponding reaction network.

The underlying chemistry behind the acid-catalyzed transformation of hydrocarbons is the carbenium ion chemistry. In the particular case of solid acid alkylation of isoalkanes with alkenes, eight types of elementary steps have been identified to be responsible for the transformation of the original two molecules into more than a hundred different species present in the product. These elementary steps include alkene (de)protonation, intramolecular hydride shift, methyl shift, protonated cyclopropane (PCP) branching, oligomerization, β-scission and intramolecular hydride transfer. Consequently, thousands of these elementary steps governed by the rules of the carbenium ion chemistry constitute the reaction network for this process.[11,12]

Clearly, the complexity of the corresponding reaction network for alkylation makes difficult the formulation of kinetic models at the elementary step level for this process. Such a predictive

model requires hundreds of rate coefficients and consequently an unrealizable amount of experimental data. Nevertheless, the current computational capabilities and numerical methods in parameter estimation can only properly handle some tens of parameters and even in the case they could be estimated, their validity would be severely limited by uncertainty.

The concept of single-event kinetics, introduced by Froment[13] in the late 1980s, allows dealing with the difficulties of accounting for a large number of species and reactions by significantly reducing the number of model parameters required at the elementary step level description. This reduction is achieved by means of identifying a set of invariants in the transition state theory formulation for the rate of each elementary step. Furthermore, the introduction of reasonable assumptions and thermodynamic constraints in the mathematical model formulation leads to an even more substantial reduction in the number of model parameters making possible to describe very complex kinetics in terms of a small set of parameters.

If the reaction kinetics of the solid acid alkylation of isobutane with butenes were properly described by means of the carbenium ion chemistry, a single event kinetics formulation for this complex reaction set could be formulated in order to model those relevant phenomena that characterize the reacting flow for this process: selectivity shifts and rapid catalyst deactivation.

The scope of the present research work is to model the kinetics of solid acid alkylation of isobutane with butenes over a proton-exchanged Y-zeolite, carried out in a fixed bed continuous reactor, under isothermal conditions, at moderate temperatures (80-120°C), and with a large excess of isobutane. More specifically, the objective is to achieve a description of the fixed bed solid acid alkylation process at the elementary step level.

CHEMISTRY OF ISOALKANE/ALKENES SOLID ACID ALKYLATION OVER PROTON-EXCHANGED Y-ZEOLITE AT MODERATE TEMPERATURES

Chemistry of Hydrocarbon Transformations over Solid Acid Catalysts

In order to construct a kinetic model of any reacting set at the elementary step level, an appropriate description of the chemistry that governs the transformations within the species is required. In the particular case of the transformations of hydrocarbons over solid acids, the most widely accepted description of the governing chemistry for a very wide range of temperatures and acidities is based on the relative stability of carbenium ions in solution. This approach states that carbenium ions, which are formed as the result of protonation of alkenes/aromatics by Brönsted acids and further stabilized by solvation, work as reaction intermediates with increasing reactivity according to their relative stabilities (allylic > tertiary > secondary > primary < methyl)[14].

Recent studies have revealed a different nature of the intermediates for solid acid-catalyzed reactions. Based on *ab initio* calculations for several different acid-catalyzed elementary steps on zeolite clusters, Kazansky[15] has proposed that surface alkoxides are in fact the most energy favored species to serve as stable reaction intermediates. In his view, a covalent carbonyl bond is responsible for binding the alkoxide to the catalytic surface. Thus, as the reaction proceeds, the carbonyl bond stretches until a highly polarized carbenium ion-like structure becomes a transition state towards the reaction products. As a result, the nature of the resulting carbenium ion-like structure serving as transition state determines the effective energy barrier for the reaction, and therefore, its relative reactivity[16].

Consequently, the rules of the carbenium ion chemistry currently known to govern the transformation of hydrocarbons in solution also determine the hydrocarbon reactivity over solid acids. This similarity, supported by an overwhelming amount of experimental evidence in the field of heterogeneous acid catalysis, constitutes the basis for this research work's approach of describing the barely known chemistry of surface alkoxides by means of surface-bonded carbenium ions acting as reaction intermediates. The two approaches become equivalent only after the introduction of the concept of stabilization energy, a concept that accounts for the energy differences between gas phase carbenium ions and their corresponding surface-bonded intermediates (surface alkoxides).

The two most relevant variables that control the hydrocarbon reactivity in acid catalysis are temperature and acidity strength. In the absence of superacidity (Hammet Acidity Number Ho > -11.2), alkene or aromatic protonations carried out over Brönsted acid sites serve as initiation steps in the formation of intermediates at low and moderate temperatures (<200°C).[17] Under these conditions, both methyl and primary carbenium ions are barely formed and therefore only reaction products involving tertiary and secondary ion intermediates are often observed.

In processes where the reaction temperature is well above 200°C, the available energy becomes high enough to allow alkanes and cycloalkanes to interact directly with acid sites. In those cases, pentavalent carbonium ion complexes are formed through hydride abstraction elementary steps. Carbocations with a coordination numbers of five are defined as carbonium ions. Once formed, these species degenerate rapidly into either a secondary carbenium ion plus hydrogen or a tertiary carbenium ion plus methane. Other routes to activate barely reactive hydrocarbons at moderate temperatures such as alkanes and cycloalkanes are possible by adding a metal function to the catalyst in order to catalyze (de)hydrogenation reactions or by using superacids capable to carry on these high temperature elementary steps at much lower temperatures.

A large variety of industrial processes is based on solid acid catalysis. In fact, most of these processes share a common ground in the carbenium ion chemistry even though they might express completely different types of transformations depending on not only their corresponding temperature and acidity levels but also on the nature of their feedstock and contacting schemes. For instance, Alkylation and Fluid Catalytic Cracking both have oligomerization, and its reverse step, β-scission, among their principal elementary steps. Thus, breaking large molecules in Fluid Catalytic Cracking requires high temperature and significant acidity in order to favor endothermic β-scission steps over oligomerization, whereas low temperatures and even stronger acidity is necessary in Alkylation for exothermic oligomerization steps to overcome β-scission aiming to form large molecules out of smaller ones. In such a way, several acid and metal/acid catalyzed processes can be better understood by revealing how their underlying carbenium ion chemistry expresses as a function of acidity and temperature.

Moreover, when combined with other important phenomena such as (de)hydrogenation, hydrogenolysis (protolytic α-scission) and carbonium ion chemistry, the approach of using a constrained expression of the carbenium ion chemistry based on the temperature and acidity conditions of each process plus its further integration with the single event kinetics modeling has the potential to improve predictive capabilities and applicability of most current process models.

Thus, common ground chemistry would result in better kinetic models for several important processes ranging from Alkylation (high acidity strength & low temperature) and Fluid Catalytic Cracking (moderate acidity strength & high temperature) to Isomerization (low acidity & moderate temperature), Naphtha Reforming (low acidity & high temperature), Hydrodesulphurization (low acidity & moderate temperature) and Hydrocracking (moderate acidity & high temperature).

Summarizing eight types of elementary steps are proposed to represent the chemistry of the isobutane/butenes alkylation on a proton-exchanged zeolite at moderate temperatures (80-120°C). These elementary steps are alkene (de)protonation, intramolecular hydride shift, methyl shift, protonated cyclopropane (PCP) branching, oligomerization, β-scission and intramolecular hydride transfer. Under the solid acid alkylation conditions, no alkane adsorption on the zeolite and no pathways involving methyl or primary carbenium ions need to be considered.

Elementary Steps in Solid Acid Alkylation

Figure 1 presents examples for each type of elementary step proposed to model the chemistry of solid acid alkylation over zeolites at moderate temperatures. Here, every type of elementary step involves one or two surface-bonded ion(s) as stable intermediate(s). Moreover, it assumes that these steps are elementary in the sense that no other species along the reaction coordinate (minimum energy trajectory from reactants to products on the potential energy surface) but reactants and products occupy energy minima. Even though this condition is not necessarily satisfied in all the proposed elementary steps, it implicitly assumes that any additional intermediate will be very short-lived and will have with almost no contribution to the energy barrier. For instance, there is evidence of the existence of short-lived species either in the PCP-branching mechanism (protonated cyclopropane intermediate) or in the alkene (de)protonation mechanism (Π-complex intermediate) that are of course neglected.[18]

Alkene protonation constitutes the initiation step. This reaction is the result of the interaction between an alkene's double bond and an acid site's proton to produce a surface-bonded carbenium ion. Here, the most likely outcome can be predicted from the Markovnikov's rule, which states that the most substituted carbon on the double bond will bear the positive charge. In general, this elementary step is known to be fast and exothermic. Therefore, it is favored over desorption by decreasing temperature and by increasing acid strength.

On the other hand, the reverse elementary step or the **deprotonation** of a surface-bonded carbenium ion works as a termination step. This step allows the alkene to be desorbed from the surface and restores a proton back on the acid site. As an endothermic reaction, it proceeds with a higher energy barrier than protonation so that the reaction is favored with increasing temperature. In general, a double bond will be formed between any of the carbons on α-position (unless it has 4 carbon substituents) and the carbon bearing the positive charge.

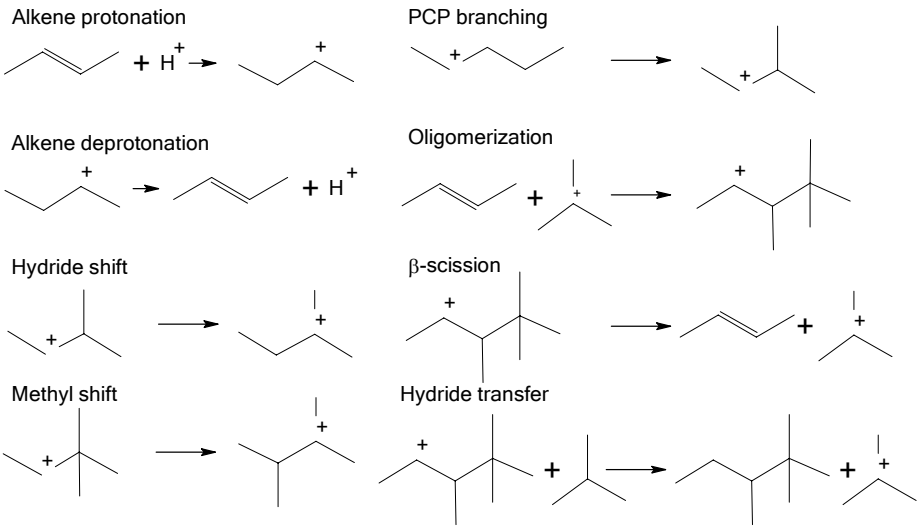

Figure 1. Proposed Elementary Steps for Solid Acid Alkylation at Moderate Temperatures.

Based on this description, it is inferred that at moderate temperatures the Y-zeolite will show a strong affinity for alkenes. The experimental observation that no significant amount of C_9+ species are present in the reaction products, corroborates this inference and supports the introduction of irreversibly adsorbed carbenium ions as catalyst deactivating agents.

Hydride shifts and **methyl shifts** are non-branching isomerization steps. These two slightly exothermic elementary steps proceed through the exchange of a hydride/methyl substituent and a positive charge between two adjacent carbon atoms. In general, stability differences between the charged bearing carbon and its neighbor in α-position happen to be the driving force for this elementary step. Therefore, non-branching isomerization reactivity follows a trend in energy difference towards more stable configurations: tertiary-to-secondary > tertiary-to-tertiary > secondary-to-secondary > secondary-to-tertiary.

Although a methyl or a hydride shift can both change the position of substituents within a molecule, they are not able to modify its overall degree of branching. The skeletal rearrangement involving changes in the final degree of branching of an ion goes through a **PCP-branching** elementary step. First proposed by Brouwer *et al.*[19] in 1972, the protonated cyclopropane (PCP) mechanism is successful in explaining the experimental observation that n-butane does not isomerize to isobutane in the presence of strong liquid acids such as HF/SbF_5 under conditions where n-pentane and n-hexane quickly isomerize to 2-methyl-butane and 2-methyl-pentane respectively (the mechanism goes through a primary carbon intermediate only for n-butane).

According to Brouwer's mechanism, two different routes are possible in PCP-branching depending upon which bond within the protonated cyclopropane structure breaks: α-cleavage or β-cleavage. Depending on the reactant molecular structure and the position of the charge both routes can yield products with a higher degree of branching or not, and even in some cases, a given route might yield the same reactant structure but with two of their carbon exchanged in what constitutes a so-called scrambling reaction.

Oligomerization proceeds according to the rules of electrophilic addition of alkenes to carbenium ions. These rules establish that because of the attack of an alkene's double bond to a charge-bearing carbon atom in a surface-bonded ion, a new sigma bond is created between the charge-bearing carbon atom and the less substituted carbon on the double bond, leaving its companion at the double-bond electron-deficient so that a new carbenium ion is formed. This elementary step is highly favored at low temperatures due to its exothermicity. It also has a fundamental role in the Alkylation process being responsible not only for the formation of many isomers at the C_8 carbon fraction but also in the further formation of irreversibly adsorbed ions (C_9+) to which the present study assigns the role of deactivation agents.

Whereas oligomerization increases the average carbon number of the reaction product, its reverse step, **β-scission**, spreads the reaction product distribution with respect to the carbon number towards shorter chain lengths. This step breaks bonds between carbons on α- and β-position with respect to the charge-bearing carbon atom. As a consequence of its endothermic nature, β-scission elementary steps are strongly favored by increasing temperatures. On β-scission, long and highly branched carbon chains are more reactive because of an increased availability of carbon atom in β-position that would yield either tertiary or secondary carbenium ions. In addition, reactivity increases with carbon number due to increasing surface concentrations and larger enthalpy contributions to the rate coefficient.[20] In general, no product fragments smaller than propene or sec-propyl ion can be formed through this step.

Figure 1 shows **hydride transfer** as the only proposed elementary step in which alkane molecules participate. This elementary step proceeds when a hydrogen atom attached to a highly substituted carbon atom is attacked by a surface-bonded carbenium ion so that a hydride ion transfer between them happens.

Since the relative stability of the carbenium ions increases with carbon number, it is expected that tertiary-to-tertiary and secondary-to-secondary hydride transfers would be favored. Here, a low molecular weight surface-bonded ion attacked by a larger isoalkane results in a net chain growth effect for the product. However, the role of hydride transfer in isoalkane alkylation with alkenes turns out to be exactly the opposite. A net chain control effect is obtained by promoting the desorption of large surface-bonded ions as alkanes through hydride transfer when the process runs under a large excess of some low-molecular-weight isoalkane such as isobutane.

Matrix Representation of Hydrocarbon Species

On the construction of the reaction network, molecules are numerically represented by Boolean matrices so that every elementary step transformation can be properly described by a set of linear algebraic operations. Starting by labeling carbon atoms in no particular order, the Boolean matrix description exhibits a value of one (1) for every C-C sigma bond (node) present in the molecule. In addition, this description takes advantage of the unused space at the diagonal in storing the hybridization state of each carbon atom as either one (sp^2 planar triangular) or zero (sp^3 tetrahedral). Thereby, the hybridization state vector allows a full description of alkanes (only sp^3 carbons), alkenes (two sp^2 carbons) and carbenium ions (one sp^2 carbon) as Boolean matrices without requiring additional information. Figure 2 illustrates this method by means of some examples.

In the Boolean matrix representation of a hydrocarbon species, no specific sequence is imposed when numerating the carbon atoms within the chain. Consequently, a characteristic vector containing a full set of the Boolean matrix eigenvalues, sorted by value, is created in order to identify different representations of the same species. The calculation of a real set of eigenvalues for the Boolean matrix is always possible because all these matrices are symmetric by definition. In contrast, there is no guarantee of uniqueness from the characteristic vector approach. In fact, it was found that within a large set of species (>10,000) there is at least one chance in ten

thousand to find out two different species with the same characteristic vector. Therefore, in addition to the characteristic vector, a second auxiliary vector is calculated based on Golender's graph potentials. This topological method provides with an effective recipe to find out graph invariants within the Boolean matrix representation based on analogies with electrical networks.[21]

From the Boolean matrix representation of a hydrocarbon species, relevant information such as the degree of substitution for each carbon atom (primary, secondary, tertiary, quaternary) and their relative positions (α, β, γ) with respect to the carbon atom carrying the charge can be easily obtained. Yet, this representation does not intent to provide complete information about a molecule or ion configuration. For instance, it cannot distinguish between the two possible 2-butene stereoisomers: cis-2-butene and trans-2-butene.

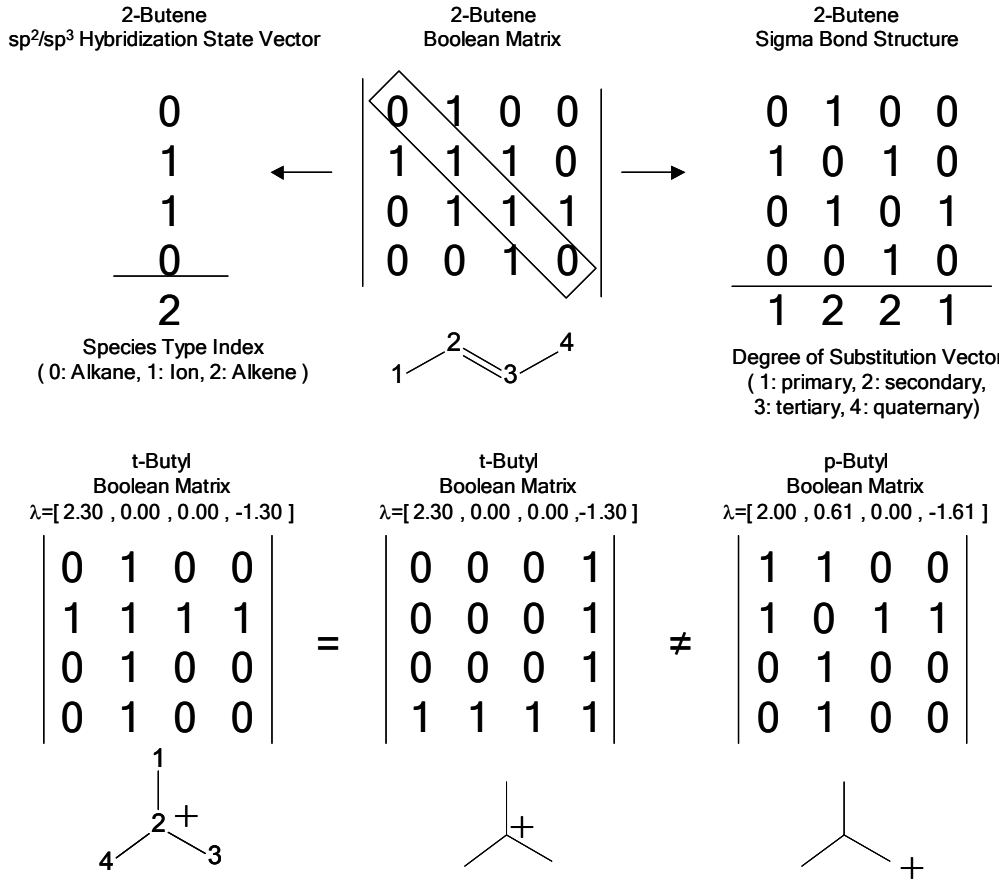

Figure 2. Hydrocarbon Representation by Boolean Matrices. First row: 2-butene Boolean matrix representation decomposed into the sigma bond structure and the hybridization vector. Second row: two equivalent t-butyl Boolean matrix representation (same characteristic vector **λ**) compared to p-butyl (different **λ** vector).

Solid Acid Alkylation Reaction Network

The computer code generates the reaction network in terms of elementary steps. Starting with the protonation of 1-butene, every molecule is consecutively tested for reactivity based on the rules presented in Table 1. These rules are based either on the fundamentals of the carbenium ion chemistry or experimental observations. The generation process stops when no new molecules or reactions show up after testing for all the elementary steps.

Table 1. Reaction Network Generation Elementary Steps and Rules. C+: charge-bearing carbon atom. Cdb: double-bonded carbon atom. Cα: α-position carbon atom. Cβ: β-position carbon atom. Ca: alkane's carbon atom. n: ion carbon number. p: primary carbon atom. s: secondary carbon atom. t: tertiary carbon atom.

Elem. Step	Assumptions	(C+,Cα) Transformations	(C+,Cα) Distribution	Rules
Alkene protonation	Markonikov: only most substituted carbon on double bond reacts: No	(Cdb→C'+,Cdb→C'α)	(s,p):29,(s,s):36 (s,t):23,(t,p):26 (t,s):23,(t,t):10	C'+ = or{Cdb,Cdb} C'+ >= Secondary C'α >= Primary Cn, n < 9
Alkene deprotonation	Markonikov: only most substituted α-carbon reacts: No	(C+→C'db,Cα→C'db)	(s,p):29,(s,s):36 (s,t):23,(t,p):26 (t,s):23,(t,t):10	C'db = C+, C'db=Cα C+ >= Primary Cα >= Primary Cn, n < 9
Hydride shift	Only shift transfers occur: No Only most substituted α-carbon reacts: No	(C+→C'α,Cα→C'+)	(s,s):34,(s,t):23 (t,t):8	C'+ = Cα Cα < Quaternary Cα >= C+ Cn, n < 9
Methyl shift	Only shift transfers occur: No All β-methyls can react: Yes	(C+→C'α,Cα→C'+)	(s,t):18,(s,q):9 (t,q):2	C'+ = Cα - 1 Cα >= Tertiary Cβ = Primary Cα -1 >= C+ Cn, n < 9
PCP branching	Only transfers towards more stable carbons may occur: Yes	α-cleavage: (C+→or{C'+,C'β},Cα→or{C'β,C'+}) β-cleavage: (C+→C'α,Cα→or{C'β,C'+})	(s,s):48,(s,t):38 (t,t):28	α: C'+ = or{C+,Cα-1} β: C'+ = or{Cα-1,Cβ+1} Cβ <= Tertiary Cn, n < 9
Oligomerization	Only most substituted carbon on double bond reacts: No	(C+→C'β,Cdb→C'+)	(s,s):240,(s,t):109 (t,s):139,(t,t):66	Cdb<=C+ C'+ = max{Cdb,Cdb} Cn, n < 9
β-scission	Only most substituted β-carbon reacts: No Irreversibly adsorbed ion carbon number limit < 9	(C+→C'db,Cβ→C'+)	(s,t):240,(s,q):139 (t,t):109,(t,q):66	C'+>=C'db C'+ = max{Cβ} - 1 C'db=C+ C'db=Cα - 1 Cβ > Secondary Cn, n < 13
Hydride transfer	Only most substituted aliphatic carbon reacts: Yes	(C+→C'a,Ca→C'+)	(s,t):988,(t,t):532	C+ >= Secondary Ca > Secondary Cn, n < 9

Details about every matrix operation involved in the generation of each elementary step in the reaction network can be found in Clymans and Froment (1984)[22] as well as in Baltanas and Froment (1985).[23] For instance, by following the rules stated for the oligomerization elementary step on Table 1, Figure 3 illustrates the matrix operations involved in the formation of 2,2,3-trimethyl-pentyl(4) from the addition of a 2-butene molecule to a surface-bonded t-butyl ion. The mathematical execution of this elementary step starts with the identification of the carbon atom carrying the charge at the t-butyl by means of the hybridization state vector. Then, the degree of substitution at the two double-bonded sp^2-hybridized carbon atoms on the alkene are determined in order to select the carbon atom(s) that would comply with their corresponding rules. Next, after checking that the ion carbon number is less than the reactivity limit, the reaction product matrix is obtained by concatenating the two sigma bond structure matrices from the original reactant species followed by the addition of a similar-size matrix containing the new created sigma bond as well as the new hybridization state vector.

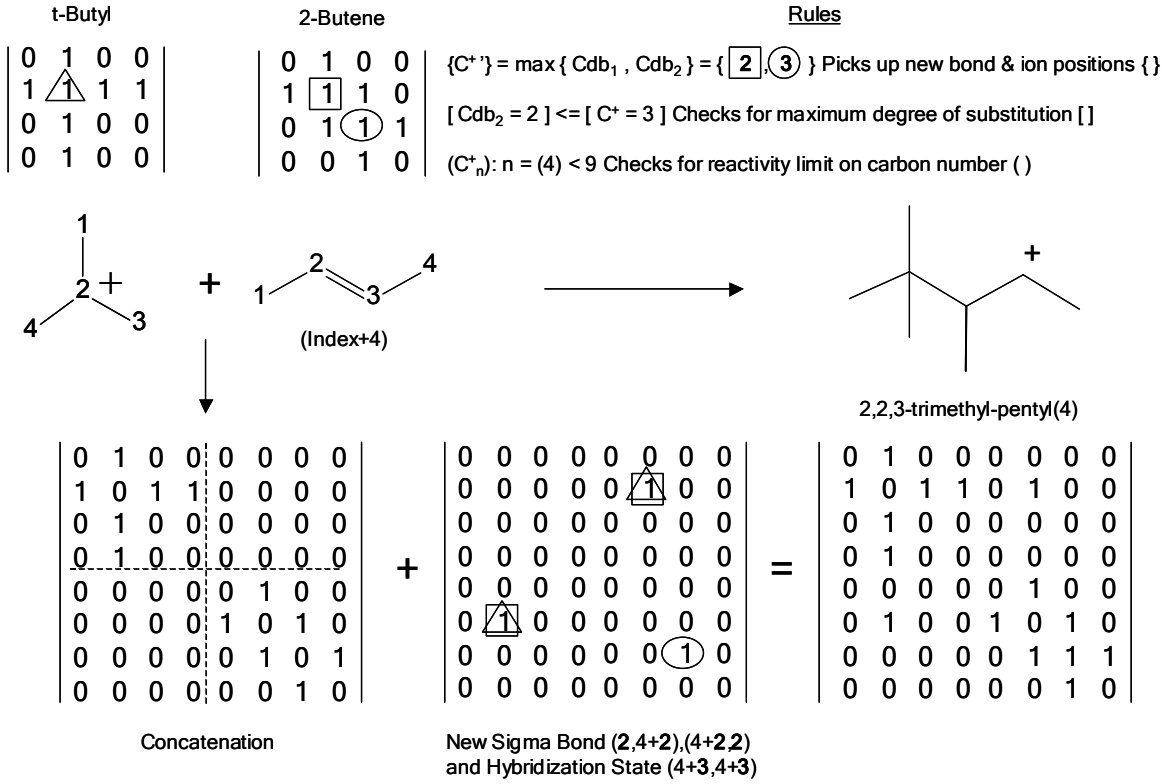

Figure 3. Calculation of the t-butyl + 2-butene Oligomerization Step.

Tables 2 and 3 present a summary of the results in terms of the distribution of species and elementary steps for the reaction network. Here, adsorption of C_9+ carbenium ions is assumed to be irreversible based on the well-established fact that the relative stability of carbenium ions increases with the ion carbon number together with the values of the alkene protonation equilibrium constant. In consequence, a minimum cut point temperature is set for deprotonation to proceed.

In the particular case of the reaction set under study the cut point in terms of carbon number is effectively set at C_9. Nevertheless, it is relevant to recognize that in terms of reactivity, the irreversibly adsorbed condition does not preclude these species to react through all the other elementary steps. Besides, the appropriate approach to the reactivity of the irreversibly adsorbed ions with respect to other species is one that accounts for the incremental concentration of these ions on the surface so that faster rates of reaction should in fact prevail for these species.

Consequently, the approach adopted on the reaction network generation is one where the only transformations allowed to operate on the irreversibly adsorbed ions are the oligomerization and the β-scission elementary steps. Any other elementary step involving these species is prevented to proceed since either they reach equilibrium (isomerization steps) or they are highly unlikely to happen under the current reaction conditions (hydride transfer).

Table 2. Reaction Network Species Distribution by Type and Carbon Number. Conditions imposed to the reaction generation algorithm includes preventing the formation of species with carbon number larger than C12 and the formation of any primary carbenium ion as intermediate.

	C_3	C_4	C_5	C_6	C_7	C_8	C_9	C_{10}	C_{11}	C_{12}	Total
Alkanes	0	2	2	4	7	16	0	0	0	0	31
Alkenes	1	3	5	10	22	62	0	0	0	0	103
Carbenium Ions											
Primary	0	0	0	0	0	0	0	0	0	0	0
Secondary	1	1	3	4	11	30	15	47	109	197	418
Tertiary	0	1	1	3	6	17	4	15	31	123	201
	1	2	4	7	17	47	19	62	140	320	619
Total	2	7	11	21	46	125	19	62	140	320	753

As shown in Table 2, the reaction network generation predicts the existence of 78 reversibly adsorbed carbenium ions serving as reaction intermediates whereas 541 irreversibly adsorbed ions occupying catalytic acid sites will cause the catalyst to deactivate. On the other hand, 134 species are expected to show up in the reaction product. Table 3 presents a summary of the elementary step inventory of the reaction network. Application of the rules stated on Table 1 guarantees a correct match between the number of elementary steps of a given type and its

corresponding reverse step.

Table 3. Reaction Network Elementary Step Inventory.

Overall Reaction Type	Elementary Step Type	Occurrence
Alkene Adsorption/Desorption (Initiation/Termination)	Alkene Protonation	147
	Alkene Deprotonation	147
Non-branching Isomerization	Hydride Shift	65
	Methyl Shift	29
Branching Isomerization	PCP Branching	114
Chain Growth/Cracking	Oligomerization	554
	β-Scission C_6-C_8 + C_9-C_{12}	13+541
Chain Transfer (Termination)	Hydride Transfer	1520
	Total	3130

Accounting for the elementary steps leads to complex reaction networks. Figure 4 presents the resulting overall reaction scheme for this process after grouping 753 species and 3130 transformations according to nature, carbon number and degree of branching for all the species.

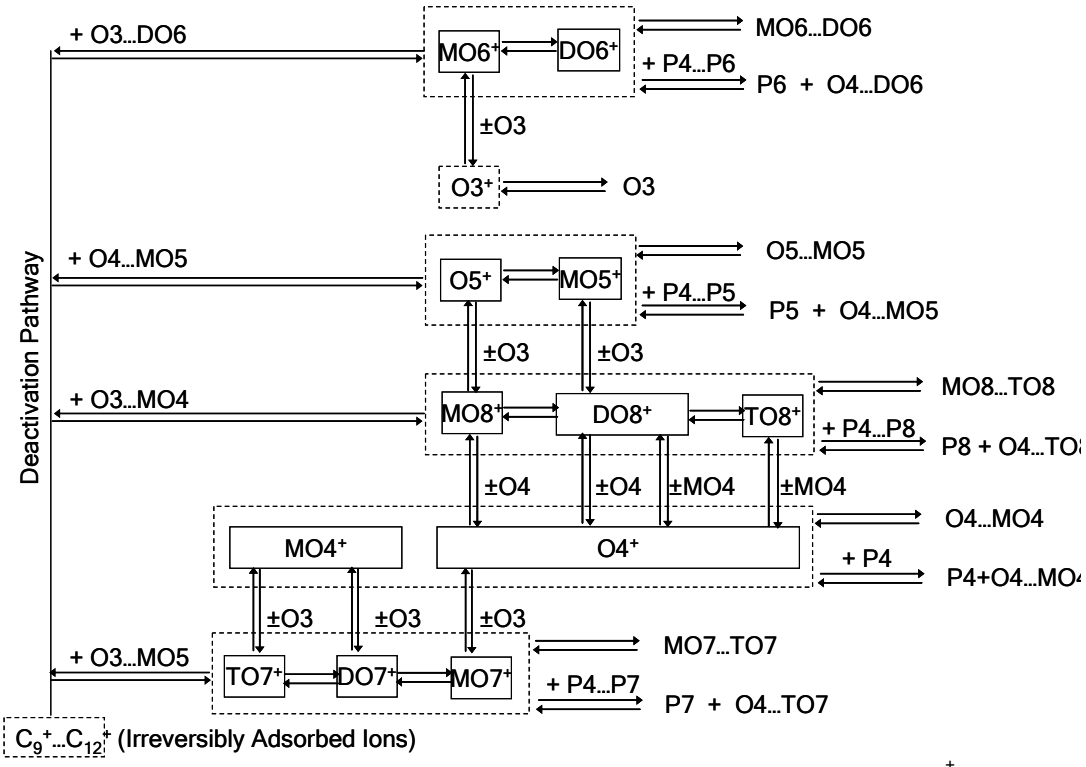

Figure 4. Reaction Network Scheme. Species are grouped based on type (O:alkene, P:alkane, O^+:carbenium ion), degree of branching (M: mono-, D: di-, T: tri-substituted) and carbon number. Species within dotted boxes correspond to surface-bonded ions. Species within solid boxes correspond to reversibly adsorbed ions. Feedstock: O4 & P4.

EXPERIMENTAL INVESTIGATION

Catalyst Characteristics: Proton-Exchanged Y-Zeolite

Zeolyst International CVB600, a proton-exchanged Y-zeolite (crystalline aluminosilicate) with SiO_2/Al_2O_3 molar ratio of 5.2 and approximate surface area of 660 m^2/g, will serve as solid acid catalyst for the experimental investigation. The selection of a protonic faujasite (hexagonal faced supercage) with a low Si/Al ratio pursues to maximize the density of Brönsted (proton donor) acid sites with respect to the Lewis (electron receptor) ones. Higher acid density reduces the distance between Brönsted acid sites enhancing their ability to catalyze bimolecular reactions such as hydride transfer.

On the other hand, for most zeolitic materials as the density of acid sites increases, their acid strength decreases. Therefore, a balance between acid density and strength exists depending on the Si/Al ratio of the material. For instance, pure silica has no acidic character but as soon as a few aluminum atoms are included in the framework (high Si/Al ratio), a strong acid character arises from the appearance of unbalanced charges around the location of the aluminum atoms. Based on this, the zeolite selection for the experimental investigation is not only based on maximizing the acid density but also on keeping the acid strength high enough so that no high temperatures are required for all the elementary steps to readily proceed.

Moreover, this investigation assumes that the amount of Brönsted acid sites available in the protonated Y-zeolite corresponds to its total cation exchange capacity (CEC). Thus, the CEC for a typical faujasite with Si/Al of about 5.2 should properly represent a good estimate for the Brönsted acidity of the fresh catalyst.

Previous to catalyst loading in the reactor, the original Y-zeolite powder with an average particle size of 80 μm was pelletized, crushed and sieved to a pellet size range of 210-425 μm. This procedure pursues to minimize any internal diffusion resistance in the contactor and to better approximate plug-flow conditions by increasing the reactor diameter to particle diameter ratio. Along with the pretreating procedure, the catalyst was dried in air at 120°C and subsequently calcinated at 450°C. Once loaded in the reactor, the catalyst was dried again for 4 hours at 120°C under 2.4 bar with a continuous stream of nitrogen at 100 ml/min Std. Immediately after drying, the solid was activated by increasing the temperature to 400°C for over 12 hours.

Experimental Setup and Procedure

Figure 5 shows a flow diagram of the experimental setup. The alkylation reaction of isobutane with 1-butene is carried out in liquid phase along a 16.4 ml fixed bed reactor loaded with a predetermined amount of proton-exchanged Y-zeolite diluted 1:1 in 425-600 μm glass beads. A thermocouple within a thermo-well monitors the catalyst bed temperature (353-393 K) while the reactor wall temperature is controlled by means of a heating tape rolled over an insulated aluminum rod. The experiment starts with the syringe pumps feeding isobutane and 1-butene (99.5% purity) at the desired pressure and flowrate down flow into the reactor vessel. Immediately after the pumps, the reaction mixture is passed thorough a trap loaded with USY zeolite at room temperature in order to remove peroxides and water that otherwise would poison the catalyst. Out of the reactor, alkylation products depressurize through a backpressure regulator (BPR) and heat up to 390 K with a heating tape. Finally, eighth 10.3 μl loops are available for storage of the samples pending injection into a Gas-Chromatography/Mass-Spectrometry (GC/MS) as the purge gas stream follows towards a 1 ft^3 wet meter accumulator in order to measure its flowrate.

The objective of every experimental run is to determine the resulting reaction product yields as a function of run-time, butene space-time and isothermal reaction temperature. Thus, once the operating pressure and the isobutane/1-butene flowrates at the feeding pumps were properly calibrated against flow measurements at the purge gas wet meter, their corresponding values were fixed for every experimental run so that all the different butene space-time values to be tested could be achieved just by varying the amount of catalyst loaded in to the reactor.

In general, an experimental run comprises three main procedures: the startup procedure, the data collection procedure and the shutdown procedure.

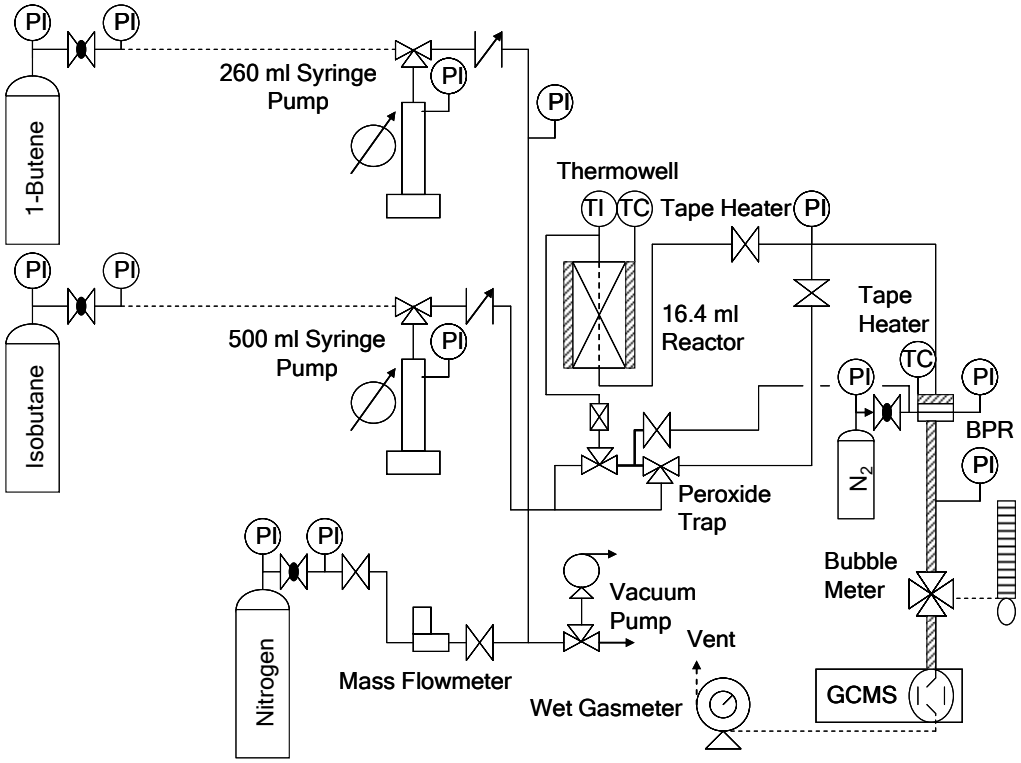

Figure 5. Fixed Bed Isobutane Alkylation with Butenes Experimental Setup.

The **startup procedure** begins a leak test performed by increasing the pressure up to 1.5 times the operating pressure with nitrogen and observing if a pressure drop of less than 1% of the original pressure occurs after two or more hours under this condition. After the leak test has been certified, the plant startup goes as follows:

1. Reach the operating pressure of 35 bar with nitrogen.
2. Load both syringe pumps with isobutane and 1-butene by cooling their walls with ice.
3. Reach operating pressure in the syringe pumps by moving the piston.
4. Wait for the syringe pumps cylinders to reach thermal equilibrium.
5. Set the back pressure regulator heating tape temperature at 390 K.
6. Align the purge gas line and set a nitrogen flow rate of 100 ml/min Std.
7. Shutdown nitrogen and introduce isobutane at the required flow rate of 140 ml/min Std.
8. By-pass the reactor.
9. Introduce 1-butene at the required flow rate of 18 ml/min Std.
10. Monitor the reaction mixture flowrate (wet meter) and composition (GC/MS).
11. Increase the reactor temperature up to operating conditions (353, 373 or 393 K).
12. Set the reactor on stream and zero the run-time.

The plant startup is followed by the **data gathering procedure** during which the necessary experimental data for the calculation of the reaction product yields is collected. This procedure is as follows:

1. Wait 30 min to achieve steady conditions.
2. Start taking product samples at the 10.3 μl sampling loop every 15 min (8 loops available).
3. Begin the analysis of the first sample loop at the GC/MS (45 min analysis).
4. Start recording wet meter readings every 5 min in digital format.
5. Once all loops are filled with product sample, switch to a 45 min sampling frequency.
6. Monitor operating pressure and temperatures with run-time.
7. After 8 hours of run-time and 15 product samples analyzed start the shutdown procedure.

Finally, the **shutdown procedure** goes as follows:

1. Cut off the 1-butene feed by turning off the syringe pump and closing the pump valve.
2. Turn off the reactor heating tape.
3. Cut off the isobutane feed by turning off the isobutane syringe pump and closing its valve.
4. Introduce nitrogen at high flow rate.
5. Decrease the pressure until it reaches 0 psig.
6. Close inlet/outlet valves, shutdown nitrogen and turn off energy supply.

Product Characterization by Gas Chromatography / Mass Spectrometry

The solid acid alkylation of isobutane with 1-butene in liquid phase can produce over a hundred different species in the carbon number range of C_3-C_9. In general, a large number of isoalkanes and isoalkenes within the C_8 carbon fraction constitute most of the reaction product. This fraction largely comprises mono- di- and tri- substituted isomers with a tertiary carbon atom in the 2-position. Therefore, a powerful analytical technique, capable of identifying and quantifying such a diversity in the product composition is required. Thus, a combination of gas chromatography (GC) with electro-ionization detection (EID) and mass spectra generation (MS) was selected as the appropriate tool for determining the reaction product composition. An HP GCD1800C Gas Chromatograph with EID was calibrated and configured for this purpose.

The chromatographic separation of over one hundred different alkanes and alkenes in the carbon number range of C_3-C_9 requires the use of a polar column stationary phase. A 30 m x 0.25 mm I.D. PLOT-Al_2O_3-S column, capable of resolving all C1-C8 isomers including propylene from isobutane was installed into the GC/MS. A calibrated separation method with 1.2 ml/min of helium as the carrier gas and a temperature program of 55°C (3 min)+7.5°C/min x 6 min=100°C (2 min)+8.5°C/min x 10 min=185 °C (8 min)+10°C/min x 2 min=215°C (6 min) for a total of 38 min was set for a 10.3 µl gas sample loop 40:1 split injection at 200°C in order to obtain the desired separation.

Figure 6 and 7 show the typical resolution achieved at the total ion chromatogram for two reaction products before and after deactivation. From the figures it can be easily observed how the selectivity shift due to deactivation changes the product composition from an C_5-C_8 isoalkane rich product to a C_8-isoalkene.

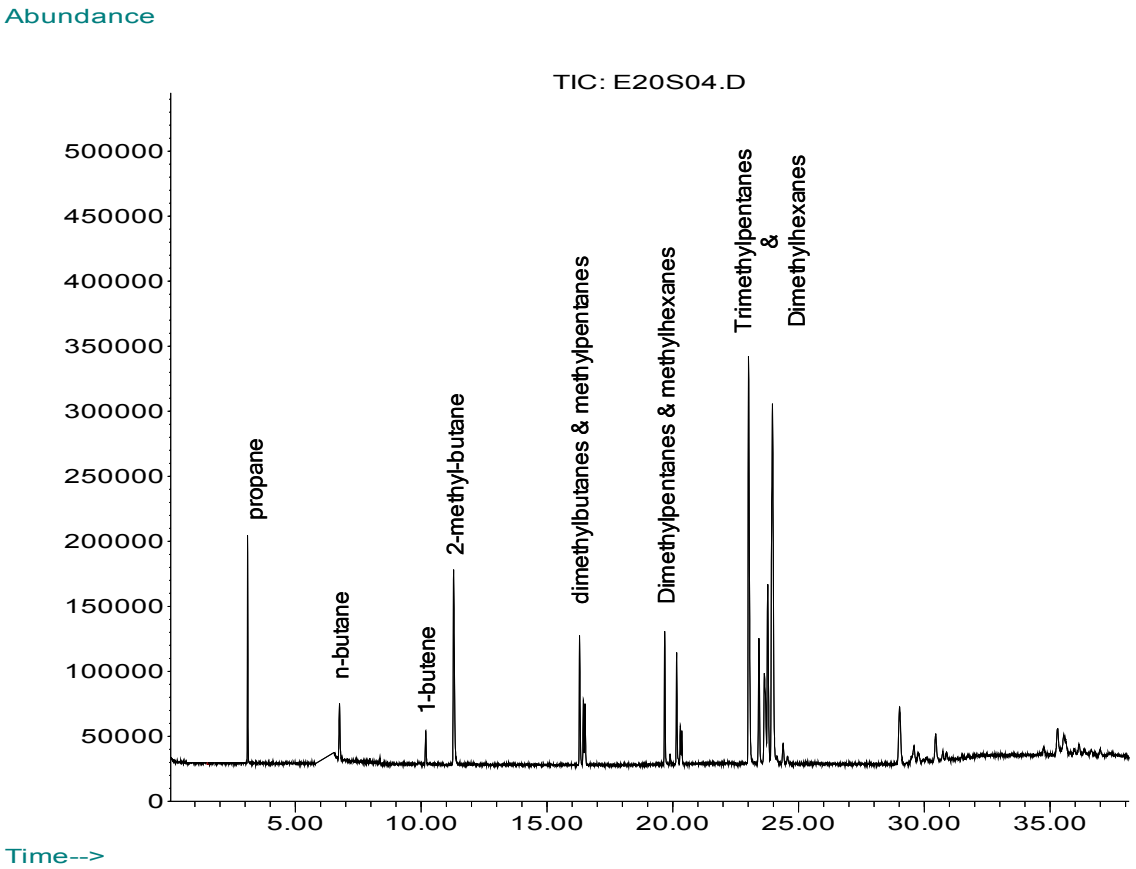

Figure 6. Reaction Product Total Ion Chromatogram for Fresh Catalyst. Experimental run with temperature = 80°C, butene space-time = 1.8 h^{-1} at run-time=0.5 h.

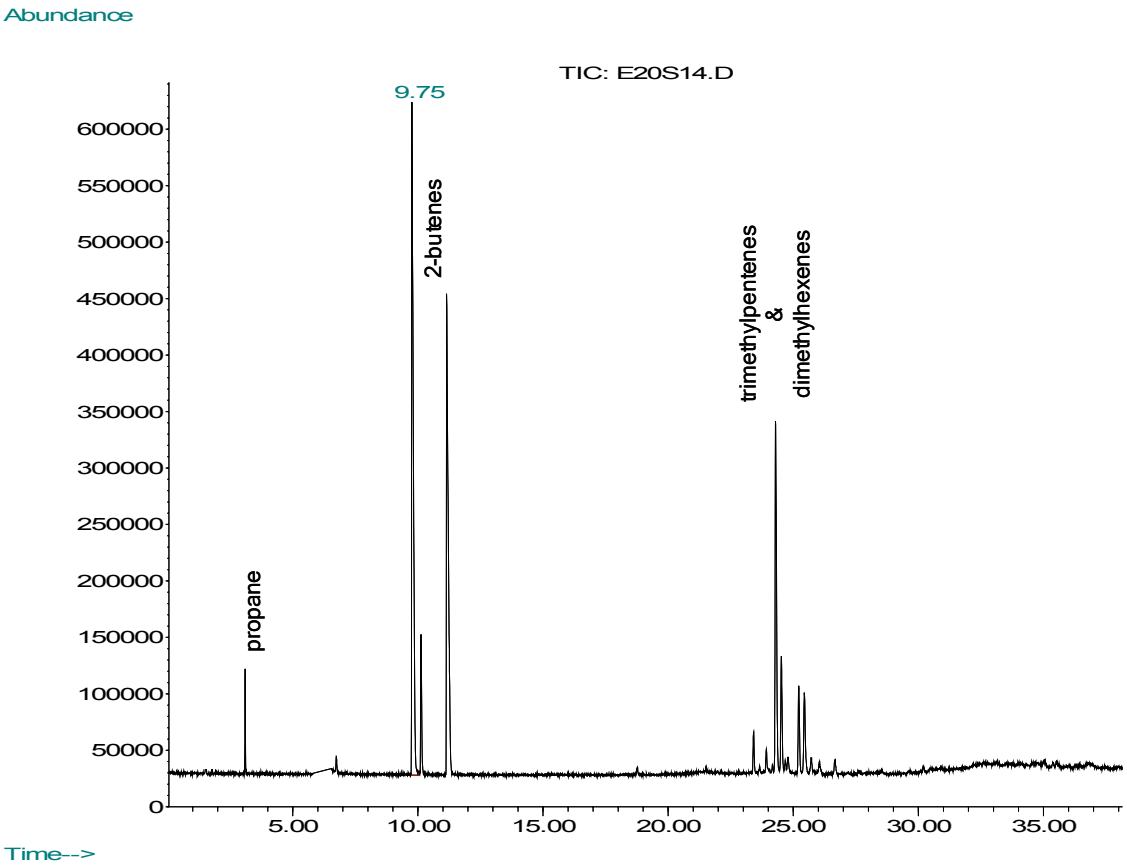

Figure 7. Reaction Product Total Ion Chromatogram after Deactivation. Experimental run with temperature = 80°C, butene space-time = 1.8 h^{-1} at run-time=6.5 h.

The quantitative analysis of the product sample is based on the experimental observation that no propane is produced by this reaction set. Therefore, since the only source of propane is the constant supply of isobutane containing 0.30±0.05 mol % of propane as impurity, it turns out to be very convenient to define propane as an internal standard for the quantitative determination of the reaction product composition. In addition to propane conservation, response factors for every single identified species are still needed to account for response differences at the detector. Consequently, relative response factors with respect to 3-methyl-pentane were determined for as many species as possible (propane, 1-propene, n-butane, isobutane, 1-butene, n-pentane, 1-pentene, 3-methyl-pentane, n-hexane, 1-hexene, n-heptane, n-octane, 1-octene and 2,2,4-trimethylpentane) just to find out that no significant deviations from the 0.978-1.080 range are obtained. As a result, the 3-methyl-pentane absolute response factor of 1.347 x 10^{-6} mg/ml.unit-area was used as reference value together with unitary relative response factors for all other species.

The identification of all the species present at every reaction product for all the experimental runs was accomplished by means of matching their corresponding mass spectrum to the most similar spectrum found in the Wiley 138K mass spectral database.[24] Table 4 reports 24 alkanes experimentally observed at the GC/MS out of 38 possible ones.

Table 4. Identified Alkanes Distribution. A propane trace (0.3 mol %) is introduced together with isobutane feed as internal standard. n-pentane is obtained from hydride transfers involving linear pentenes. Reaction network does not predict the formation of 3-ethyl-pentane. In total, 8 alkanes predicted by the reaction network were not observed at the experiments. Non-observed species might have been present below the detection limit for the electron ionization detector. Numbers in parenthesis indicate a lack of correspondence between experiments and reaction network prediction.

Alkane	Component Group	Sequencing	# of Possible Isomers	# Predicted by Reaction Network	Experimentally Observed #
propane	P3	-	1	0	0
n-butane	NP4	1	1	1	1
i-butane	MP4	2	1	1	1
n-pentane	NP5	3	1	(1)	0
2-methyl-butane	MP5	4	1	1	1
2,2-dimethyl-propane	DP5	-	1	0	0
n-hexane	NP6	-	1	0	0
2-methyl-pentane	MP6	5	1	1	1
3-methyl-pentane	MP6	6	1	1	1
2,2-dimethyl-butane	DP6	7	1	(1)	0
2,3-dimethyl-butane	DP6	8	1	1	1
n-heptane	NP7	-	1	0	0
3-methyl-hexane	MP7	9	1	1	1
2-methyl-hexane	MP7	10	1	1	1
3-ethyl-pentane	MP7	-	1	0	(1)
2,2-dimethyl-pentane	DP7	11	1	(1)	0
2,3-dimethyl-pentane	DP7	12	1	1	1
2,4-dimethyl-pentane	DP7	13	1	1	1
3,3-dimethyl-pentane	DP7	14	1	(1)	0
2,3,3-trimethyl-butane	TP7	15	1	1	1
n-octane	NP8	-	1	0	0
3-methyl-heptane	MP8	16	1	1	1
2-methyl-heptane	MP8	17	1	1	1
4-methyl-heptane	MP8	18	1	1	1
3-ethyl-hexane	MP8	19	1	(1)	0
3,4-dimethyl-hexane	DP8	20	1	1	1
2,4-dimethyl-hexane	DP8	21	1	1	1
2,3-dimethyl-hexane	DP8	22	1	1	1
3,3-dimethyl-hexane	DP8	23	1	(1)	0
3-ethyl-4-methyl-pentane	DP8	24	1	1	1
2,2-dimethyl-hexane	DP8	25	1	(1)	0
2,5-dimethyl-hexane	DP8	26	1	1	1
3-ethyl-3-methyl-pentane	DP8	27	1	(1)	0
2,2,3-trimethyl-pentane	TP8	28	1	1	1
2,2,4-trimethyl-pentane	TP8	29	1	1	1
3,3,4-trimethyl-pentane	TP8	30	1	1	1
2,3,4-trimethyl-pentane	TP8	31	1	1	1
2,2,4,4-tetramethyl-butane	QP8	-	1	0	0
Total	18	31	38	31	24

Among all the 31 molecules predicted by the reaction network, only 8 of them were not detected

in the product. On the other hand, there is only one molecule, 3-ethyl-pentane, that was actually detected at the reaction product but not predicted by the model. In addition, the characterization of the reaction product shows that no linear alkanes were neither predicted by the model nor detected in the experimental products.

In the particular case of alkenes, Table 5 presents their distribution according to their molecular structure described in terms degree of branching and carbon number. Here, from a total of 103 species predicted by the model, only 29 were experimentally detected at the reaction product. The distribution also shows that almost every single type of structure is present in the reaction product but not in such a large variety of isomers as it is expected from the results of the reaction network generation. Most likely, this is the result of two important conditions: equilibrium among species with the same degree of branching for a given carbon number and species acting as fast disappearing intermediates within the reaction network. Besides, only 4 types of alkenes were not experimentally observed even though they were predicted: propene, isobutylene, linear pentenes and 2,3,3-trimethyl-1-butene.

Table 5. Identified Alkenes Distribution. According to the reaction network, 1-propene & linear pentenes are formed through methylheptene/ethylhexene β-scissions. 1-propene and 2-methyl-propene are not experimentally observed. However, the reaction network predicts their formation so they might be fast disappearing intermediates. 2,3,3-trimethyl-1-butene can only be obtained from 2,4-dimethyl-2-pentene PCP-Branching. Numbers in parenthesis indicate a lack of correspondence between experiments and reaction network prediction.

Alkene Structure	Component Group	Sequencing	# Possible Isomers	# Predicted by Reaction Network	Experimentally Observed #
Propene	O3	32	1	(1)	0
Linear Butenes	O4	33	2	2	2
Isobutylene	MO4	34	1	(1)	0
Linear Pentenes	O5	35	2	(2)	0
Methylbutenes	MO5	36	3	3	2
Linear Hexenes	O6	-	3	0	0
Methylpentenes	MO6	37	7	7	1
Dimethylbutenes	DO6	38	3	3	1
Linear Heptenes	O7	-	3	0	0
Methylhexenes, Ethylpentenes	MO7	39	13	11	3
Dimethylpentenes	DO7	40	10	10	2
Trimethylbutene	TO7	41	1	(1)	0
Linear Octenes	O8	-	4	0	0
Methylheptenes, Ethylhexenes	MO8	42	24	22	6
Dimethylhexenes, Ethylmethylpentenes	DO8	43	32	30	9
Trimethylpentenes,Ethyldimethylbutenes	TO8	44	10	10	3
Total	16	13 lumps	119	103	29 (9 lumps)

The absence of propylene and isobutylene in the reaction product is an unexpected result, given the role that these two species play in the formation of many other species within the reaction network. The most likely explanation for their absence is to assume that these species are

actually working as fast disappearing intermediates. In order to confirm this result, samples of propylene in isobutane were tested for proper resolution at the GC/MS. Resolution tests confirmed that propylene, if present, could have been detected.

In summary 53 different molecules were identified in the reaction product through the GC/MS analysis. Based on their structure type, degree of branching and carbon number; all these species were grouped into 44 different component groups that will serve as basis set for the kinetics model formulation.

Experimental Results and Discussion

A series of nine experimental runs with a 8:1 molar mixture of isobutane with 1-butene in liquid phase was carried out in a tubular fixed bed reactor on a proton-exchanged Y-zeolite at 35 bar were carried out for the reaction temperatures: 353, 373 and 393 K as well as for the butene space-time values: 1.1, 2.1 and 4.4 h^{-1}. Based on a complete factorial experimental design as shown in Table 6, both reaction temperature and butene space-time were chosen to ensure a significant initial butene conversion towards isooctanes.

Table 6. Experimental Program. Experiments carried out in liquid phase at 35 bar with an isobutane/1-butene ratio of 8 mol/mol. Program includes up to 15 reaction product samples taken along 8-hour runs. Catalyst particle size: 290 – 510 µm 1:1 diluted with 3 mm glass beads. Average superficial velocity (void reactor): 2.1 cm/s. Reactor diameter to particle diameter ratio > 17.4. Catalyst bed length to reactor diameter ratio: 9.8 – 21.2.

Run #	1	2	3	4	5	6	7	8	9
Reaction Temperature, K	373	373	393	393	353	353	353	373	393
Butene Space-Time, $W/F^{\circ}_{O4}.M_{O4}$, h	1.1	2.1	1.7	1.2	1.1	1.8	4.3	4.6	4.4
Total Processed Butenes, g/gCat.	5.8	3.5	4.0	6.0	6.2	3.7	1.7	1.6	1.4
Run Time, h	6.8	7.0	7.1	7.0	6.5	6.5	7.3	7.3	6.5
Isobutane/1-butene molar ratio	8.4	9.3	8.4	8.9	7.9	8.2	7.7	8.3	8.8
Isobutane Flowrate, ml/min Std.	135	139	142	143	142	139	139	141	140
1-Butene Flowrate, ml/min Std.	16	15	17	16	18	17	18	17	16
Catalyst Load, g	4.13	2.58	2.58	4.13	4.13	2.58	10.34	10.34	10.34

Particle size, catalyst bed length and superficial velocity are chosen so that external and internal mass transfer resistances, axial dispersion and reactor wall effects would result negligible. As stated on the experimental procedure, once a run starts only two type of measurements along the run-time are necessary to calculate each component group product yield in the reaction product: the purge gas flow rate and composition. For the product yields calculation, material balances for each component are formulated in terms of available measurements. The product

yield is defined as the mass of a particular component group produced per 100-unit mass fed. This definition results in the following expression:

$$Y_i = \frac{X_i'' \, MW_i \, V_T^{out} \, \left(1 - X_{MP4} - X_{P3}\right)}{V_{MP4}^{in} \, MW_{MP4} \, X_{P3} + \left(X_{NP4}^{'in} \, MW_{NP4} + X_{O4}^{'in} \, MW_{O4}\right)\left(V_{O4}^{in} + X_{P3} \, V_{MP4}^{in}\right)} \tag{1}$$

where the i^{th}-component product yield (Y_i) is expressed as a function of the isobutane and propane free i^{th}-component molar fraction in the product (X_i"), the purge gas volumetric flowrate (V_T^{out}), the isobutane and propane total molar fractions in the product (X_{MP4} and X_{P3}), the inlet isobutane and 1-butene streams volumetric flowrates (V^{in}_{MP4} and V^{in}_{O4}), the isobutane-free inlet composition (X^{in}_{NP4} and X^{in}_{O4}) and the propane content of the isobutane stream (χ_{P3}). The reaction mixture, comprising both the inlet isobutane and 1-butene streams is analyzed at the GC/MS in an isobutane free-basis (isobutane works as a solvent) in order to determine not only the isobutane/1-butene molar ratio but also the amount of propane in isobutane and n-butane in 1-butane traces that comes with the feeding cylinders. Among these two impurities, propane plays a very important role as a non-reactive tracer in the material balance calculation. Thus, the propane content of the isobutane stream resulted in 0.30 ± 0.05 mol % ($\chi_{P3} \pm \Delta\chi_{P3}$) calculated from the direct analysis of the isobutane cylinder plus the results of 9 analyses for the reaction mixture at the beginning of each run (0.25 – 0.32 mol %),.

Along each material balance calculation, three conservation constraints are checked for consistency in order to accept or reject the outcome: conservation of the total mass within a 100±2 wt% recovery range, the conservation of the total number of moles of alkanes (±0.1 mmol/h) and the conservation of propane (±0.01 mmol/h). From a total of 135 observations taken along 9 runs, 37 were not processed because of operational problems, 19 were rejected because they failed to comply with conservation criteria and 79 were accepted as experiments.

Furthermore, absolute errors for all responses (mass product yields) on each experiment were estimated based on the error propagation of error statistics drawn from measurements of the purge gas flow rate and composition according to:

$$\begin{aligned} \Delta Y_i = &\left|\frac{\partial Y_i}{\partial X_i''}\right| \Delta X_i'' + \left|\frac{\partial Y_i}{\partial V_T^{out}}\right| \Delta V_T^{out} + \left|\frac{\partial Y_i}{\partial V_{MP4}^{in}}\right| \Delta V_{MP4}^{in} + \left|\frac{\partial Y_i}{\partial V_{O4}^{in}}\right| \Delta V_{O4}^{in} + \left|\frac{\partial Y_i}{\partial X_{NP4}^{'in}}\right| \Delta X_{NP4}^{'in} \\ &+ \left|\frac{\partial Y_i}{\partial X_{O4}^{'in}}\right| \Delta X_{O4}^{'in} + \left|\frac{\partial Y_i}{\partial X_{P3}}\right| \Delta X_{P3} \end{aligned} \tag{2}$$

where the absolute error on volumetric flow rates was taken as the integer-rounded standard deviation statistic drawn from 27 measurements of a 100 ml/min of nitrogen at the beginning of each run so that $\Delta V_T^{out} = \Delta V^{in}_{MP4} = \Delta V^{in}_{O4} = 1$ ml/min Std.

The absolute error on the inlet 1-butene stream composition was taken as the maximum deviation observed of during the GC/MS calibration with the AllTech® 1000 ppm C_2-C_6 Unsaturated Gas and 1000 ppm C_1-C_6 Saturated Gas Standards. The very same method of analysis (temperature program, sample volume, Etc.) applied to the product samples is used but with splitless injection in order to compensate for the use of a 100-fold more diluted sample. The equivalence is obtained by estimating that a splitless injection of a 0.5 mol% sample should provide with approximately the same dilution level than a 20:1 split injection of a 10 mol % sample. Thus, the maximum deviation observed of 0.05 mol% was chosen not only for $\Delta X'_{NP4}$ and $\Delta X'_{O4}$ but also for $\Delta X''_i$.

Tables 7 and 8 present product yields (17 responses per experiment) as a function of the amount of processed butene (11 experiments per run) for a selected set of operational conditions (2 runs). A full disclosure of the product yields for all the 79 experiments sampled along the nine runs completed within the experimental program can be found in the Appendix.

Table 7. Product Yields from Run 5. Temperature: 353 K, Butene Space-Time ($W/F°_{O4}.M_{O4}$): 1.1 h, Isobutane/1-Butene Molar Ratio: 8.5 mol/mol. Only non-zero responses are reported.

Processed O4, g/gCat	0.45	0.68	0.90	1.13	1.80	2.48	3.15	3.83	4.51	5.18	5.86	5.86
Product Yields (Y_i), g/100g Feed												ΔY_i
NP4	0.1	0.1	0.1	0.1	0.1	0.1	0.1	0.1	0.1	0.1	0.1	0.10
MP4	79.2	89.1	89.6	89.7	89.7	89.7	89.7	89.8	89.8	89.8	89.8	0.12
MP5	0.4	0.0	0.0	0.0	0.0	0.0	0.0	0.0	0.0	0.0	0.0	0.14
MP6	0.1	0.0	0.0	0.0	0.0	0.0	0.0	0.0	0.0	0.0	0.0	0.14
DP6	0.1	0.0	0.0	0.0	0.0	0.0	0.0	0.0	0.0	0.0	0.0	0.17
MP7	0.1	0.0	0.0	0.0	0.0	0.0	0.0	0.0	0.0	0.0	0.0	0.17
DP7	0.3	0.0	0.0	0.0	0.0	0.0	0.0	0.0	0.0	0.0	0.0	0.17
MP8	1.0	0.0	0.0	0.0	0.0	0.0	0.0	0.0	0.0	0.0	0.0	0.19
DP8	4.9	0.9	0.3	0.2	0.1	0.1	0.1	0.1	0.0	0.1	0.1	0.19
TP8	13.4	0.3	0.0	0.0	0.0	0.0	0.0	0.0	0.0	0.0	0.0	0.27
O4	0.4	4.9	6.4	6.7	7.3	7.7	7.7	7.6	8.6	7.8	8.3	0.12
MO6	0.0	0.0	0.0	0.0	0.0	0.0	0.0	0.0	0.0	0.0	0.0	0.14
MO7	0.0	0.0	0.0	0.0	0.0	0.0	0.0	0.0	0.0	0.0	0.0	0.16
DO7	0.0	0.0	0.0	0.0	0.0	0.0	0.0	0.0	0.0	0.0	0.0	0.19
MO8	0.0	0.2	0.2	0.2	0.1	0.1	0.1	0.1	0.1	0.1	0.1	0.22
DO8	0.0	4.3	3.3	3.2	2.6	2.3	2.2	2.4	1.5	2.2	1.7	0.19
TO8	0.0	0.0	0.0	0.0	0.0	0.0	0.0	0.0	0.0	0.0	0.0	0.23

For instance, by plotting data on Table 8 for Run 9, Figures 8 and 9 reveal the evolution of the

product yields with the amount of butene processed at two different levels of precision. Results for major product yields validate the occurrence of selectivity shifts with deactivation as well as the existence of a non-zero steady conversion of butenes after a few hours of operation.

Table 8. Product Yields from Run 9. Temperature: 393 K, Butene Space-Time ($W/F^{\circ}_{O4}.M_{O4}$): 4.4 h, Isobutane/1-Butene Molar Ratio: 8.6 mol/mol. Only non-zero responses are reported.

Processed O4, g/gCat	0.15	0.17	0.23	0.28	0.45	0.62	0.79	1.13	1.30	1.47	1.64	1.64
Product Yields (Y_i), g/100g Feed												ΔY_i
NP4	0.2	0.2	0.1	0.1	0.1	0.1	0.1	0.1	0.1	0.1	0.1	0.09
MP4	77.8	77.8	78.4	85.8	89.0	89.3	89.4	89.5	89.5	89.6	89.6	0.11
MP5	1.4	1.4	0.8	0.1	0.0	0.0	0.0	0.0	0.0	0.0	0.0	0.13
MP6	0.5	0.6	0.4	0.1	0.1	0.1	0.1	0.0	0.0	0.0	0.0	0.13
DP6	0.6	0.6	0.4	0.1	0.0	0.0	0.0	0.0	0.0	0.0	0.0	0.15
MP7	0.3	0.4	0.3	0.1	0.0	0.0	0.0	0.0	0.0	0.0	0.0	0.15
DP7	0.8	0.9	0.6	0.1	0.0	0.0	0.0	0.0	0.0	0.0	0.0	0.15
MP8	1.4	1.1	0.8	0.0	0.0	0.0	0.0	0.0	0.0	0.0	0.0	0.18
DP8	5.4	5.0	2.9	5.8	1.2	0.8	0.6	0.4	0.5	0.4	0.4	0.17
TP8	11.5	12.0	15.2	1.2	0.0	0.0	0.0	0.0	0.0	0.0	0.0	0.22
O4	0.0	0.0	0.1	2.4	5.0	5.6	6.1	7.0	6.0	6.6	6.5	0.11
MO6	0.0	0.0	0.0	0.0	0.1	0.1	0.1	0.1	0.1	0.1	0.1	0.13
MO7	0.0	0.0	0.0	0.0	0.0	0.1	0.1	0.0	0.0	0.0	0.0	0.15
DO7	0.0	0.0	0.0	0.0	0.1	0.1	0.1	0.1	0.1	0.1	0.1	0.17
MO8	0.0	0.0	0.0	0.0	0.0	0.1	0.0	0.0	0.0	0.0	0.0	0.24
DO8	0.0	0.0	0.0	3.9	4.1	3.7	3.2	2.5	3.5	3.1	3.2	0.17
TO8	0.0	0.0	0.0	0.3	0.2	0.1	0.1	0.1	0.1	0.1	0.1	0.21

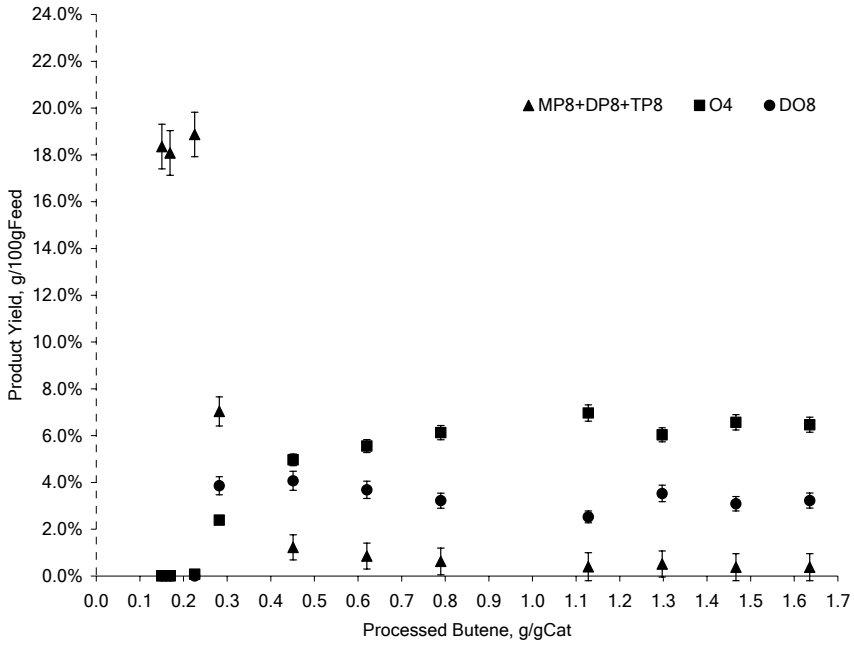

Figure 8. Major Product Yields vs. Processed Butene for Run 9. Temperature: 393 K, Butene Space-Time ($W/F^{\circ}_{O4}.M_{O4}$): 4.4 h, Isobutane/1-Butene Molar Ratio: 8.6 mol/mol.

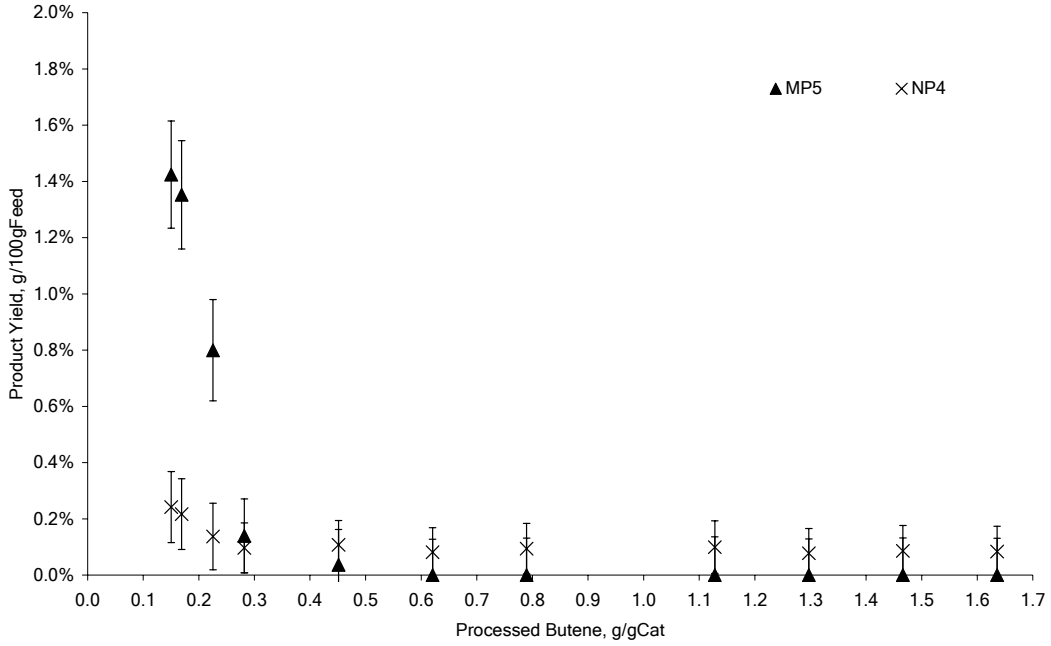

Figure 9. Minor Product Yields vs. Processed Butene for Run 9. Temperature: 393 K, Butene Space-Time ($W/F°_{O4}.M_{O4}$): 4.4 h, Isobutane/1-Butene Molar Ratio: 8.6 mol/mol.

At a lower level of relative precision, Figure 9 shows how the production of methylbutanes disappears completely with deactivation together with the n-butane yield, which reaches its feeding level. This trend is a strong indication that the hydride transfer steps are being deactivated along with the selectivity shift. In fact, when inspecting all possible n-butane formation routes at the proposed reaction network, it turns out that hydride transfer steps on sec-butyl ions are the only elementary steps involved in n-butane production. Thus, the evolution of n-butane with run-time can be directly used as an indicator for hydride transfer activity.

Additionally, the observed trend on methylbutanes is also an indication of a strong deactivation effect on β-scission. This is deduced from the observation that the disappearance of MP5 species from the product is not followed by the production of MO5 species, which should be the case if hydride transfer were the only elementary step deactivating.

In order to illustrate the evolution of the reacting flow with processed butene, Figures 10 to 18 present the most relevant product yields as a function of the processed butene for all the conditions within the experimental program.

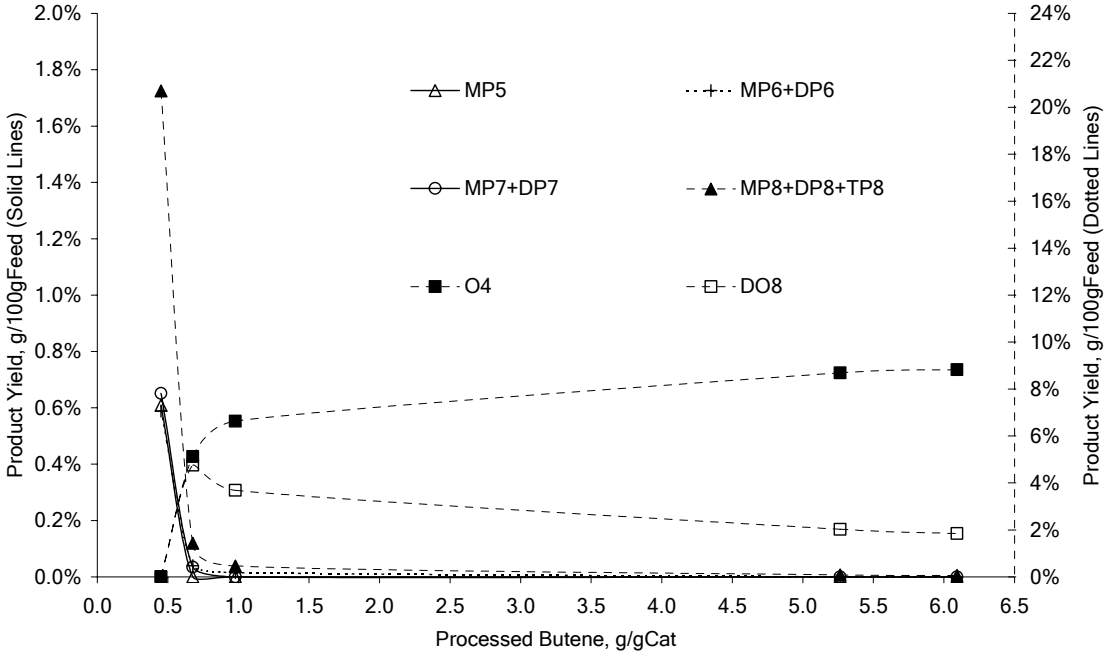

Figure 10. Product Yields vs. Processed Butene for Run 1. Temperature: 373 K, Butene Space-Time ($W/F°_{O4}.M_{O4}$): 1.1 h, Isobutane/1-Butene Molar Ratio: 8.4 mol/mol.

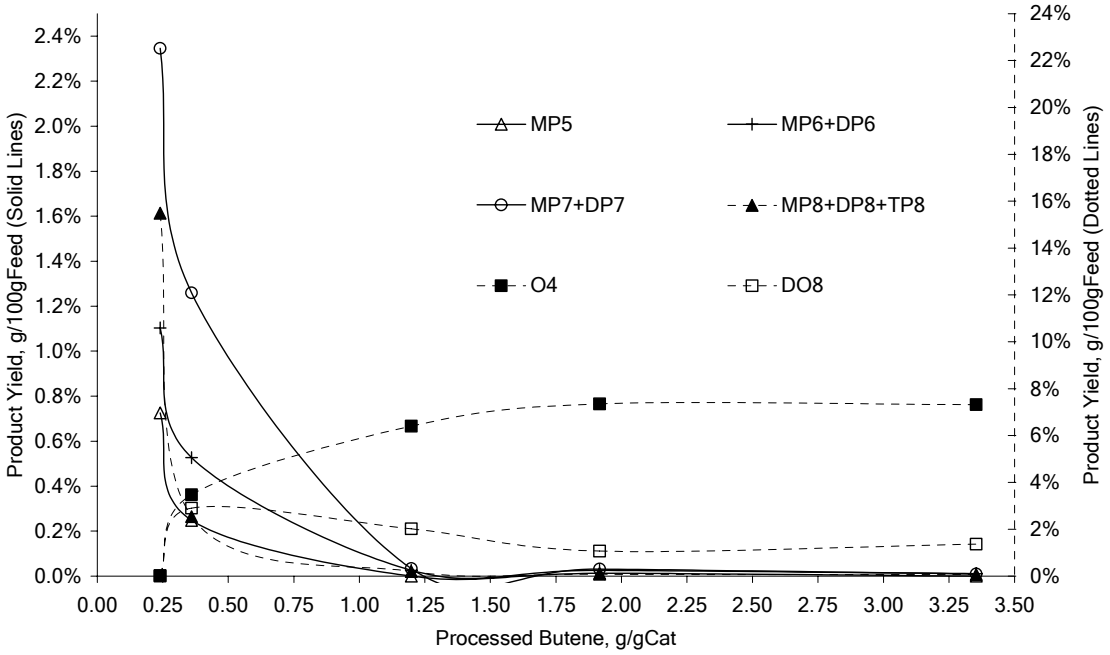

Figure 11. Product Yields vs. Processed Butene for Run 2. Temperature: 373 K, Butene Space-Time ($W/F°_{O4}.M_{O4}$): 2.1 h, Isobutane/1-Butene Molar Ratio: 9.3 mol/mol.

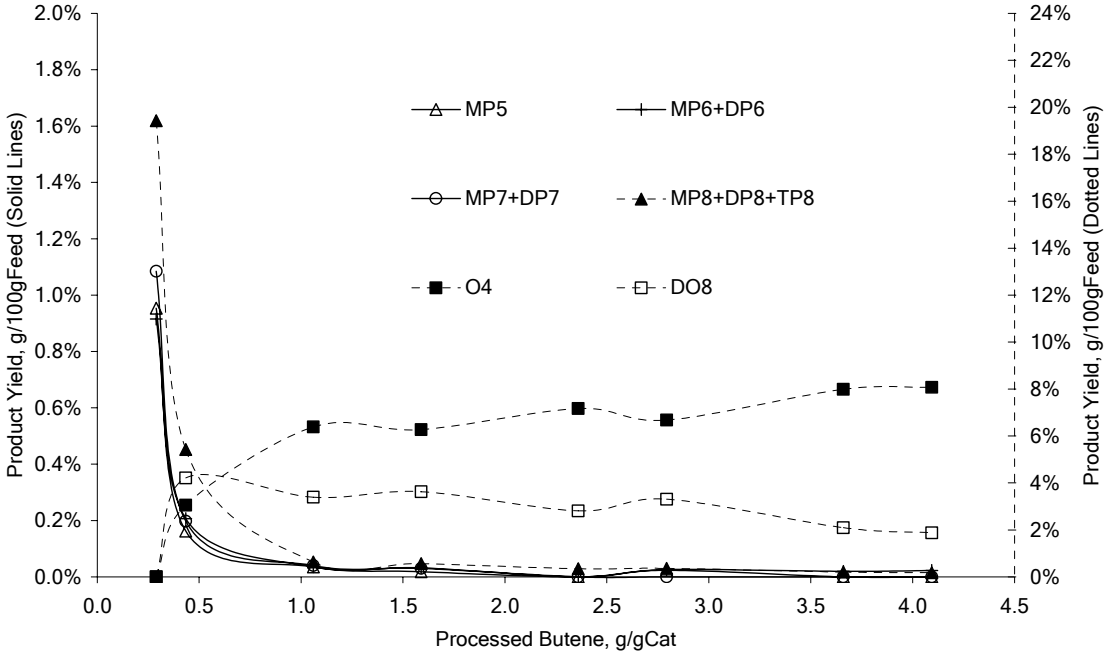

Figure 12. Product Yields vs. Processed Butene for Run 3. Temperature: 393 K, Butene Space-Time ($W/F°_{O4}.M_{O4}$): 1.7 h, Isobutane/1-Butene Molar Ratio: 8.4 mol/mol.

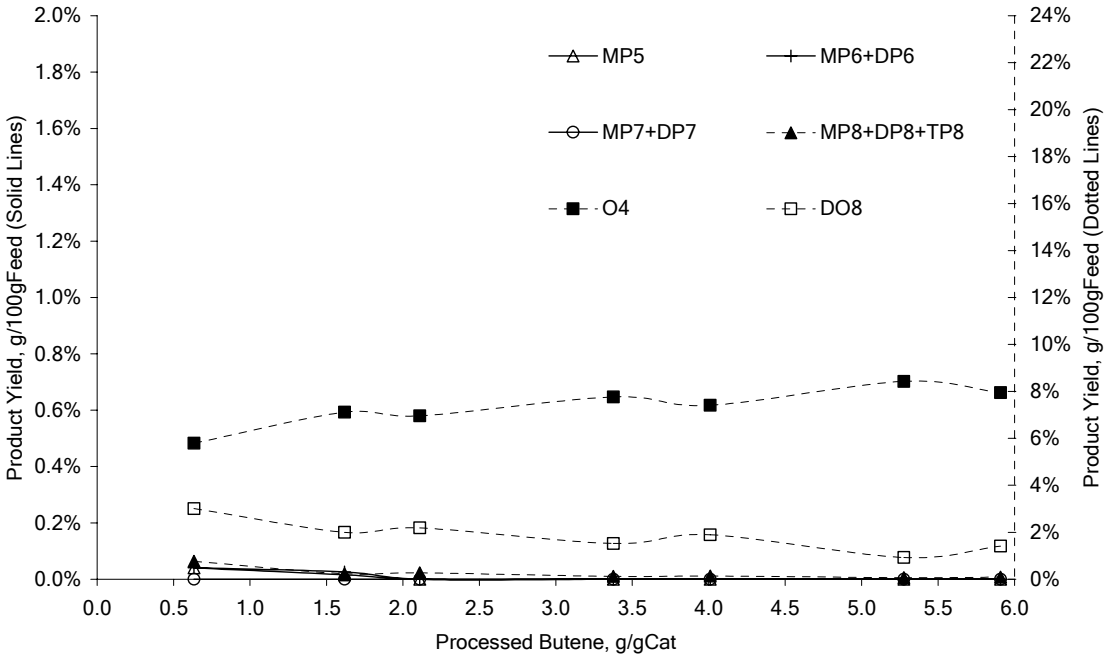

Figure 13. Product Yields vs. Processed Butene for Run 4. Temperature: 393 K, Butene Space-Time ($W/F°_{O4}.M_{O4}$): 1.2 h, Isobutane/1-Butene Molar Ratio: 8.9 mol/mol.

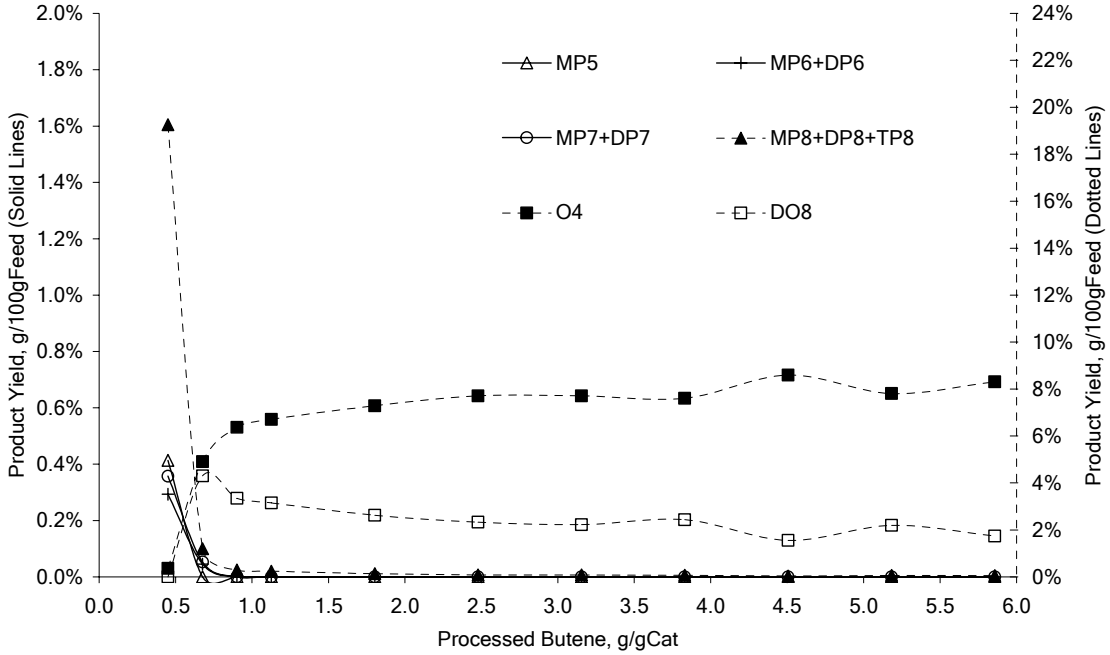

Figure 14. Product Yields vs. Processed Butene for Run 5. Temperature: 353 K, Butene Space-Time ($W/F°_{O4}.M_{O4}$): 1.1 h, Isobutane/1-Butene Molar Ratio: 7.9 mol/mol.

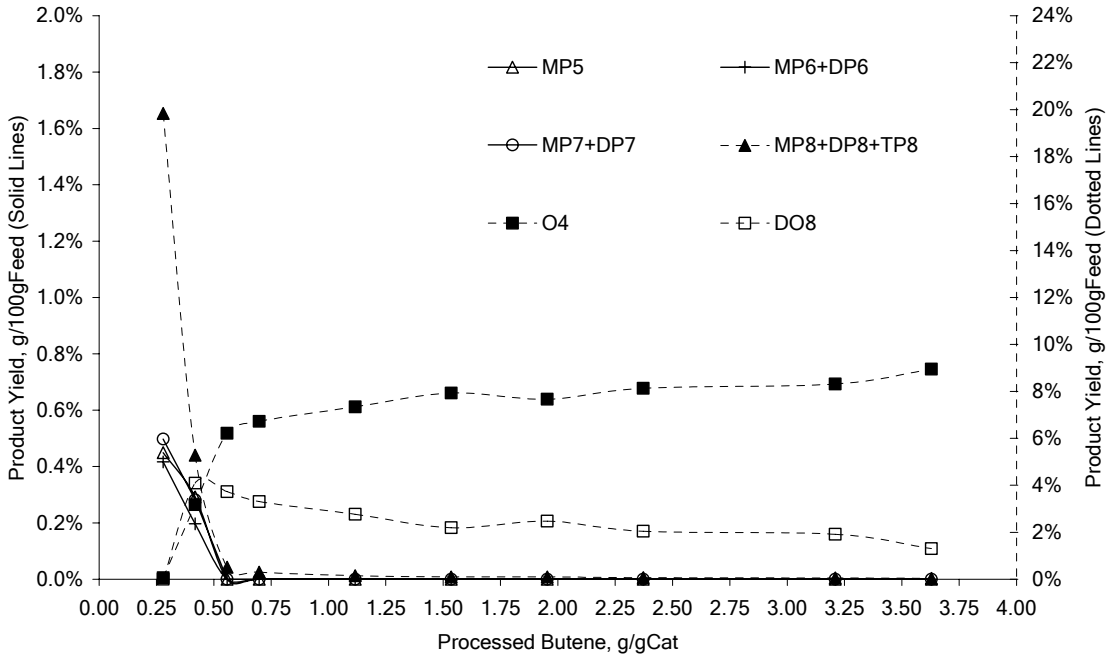

Figure 15. Product Yields vs. Processed Butene for Run 6. Temperature: 353 K, Butene Space-Time ($W/F°_{O4}.M_{O4}$): 1.8 h, Isobutane/1-Butene Molar Ratio: 8.2 mol/mol.

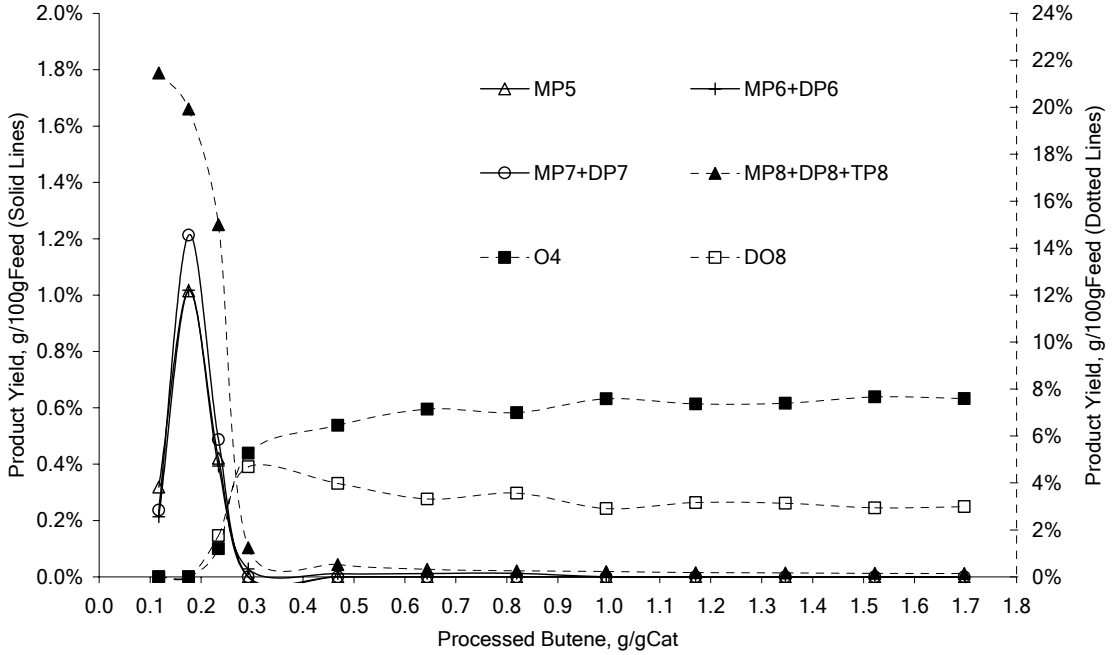

Figure 16. Product Yields vs. Processed Butene for Run 7. Temperature: 353 K, Butene Space-Time ($W/F°_{O4}.M_{O4}$): 4.3 h, Isobutane/1-Butene Molar Ratio: 7.7 mol/mol.

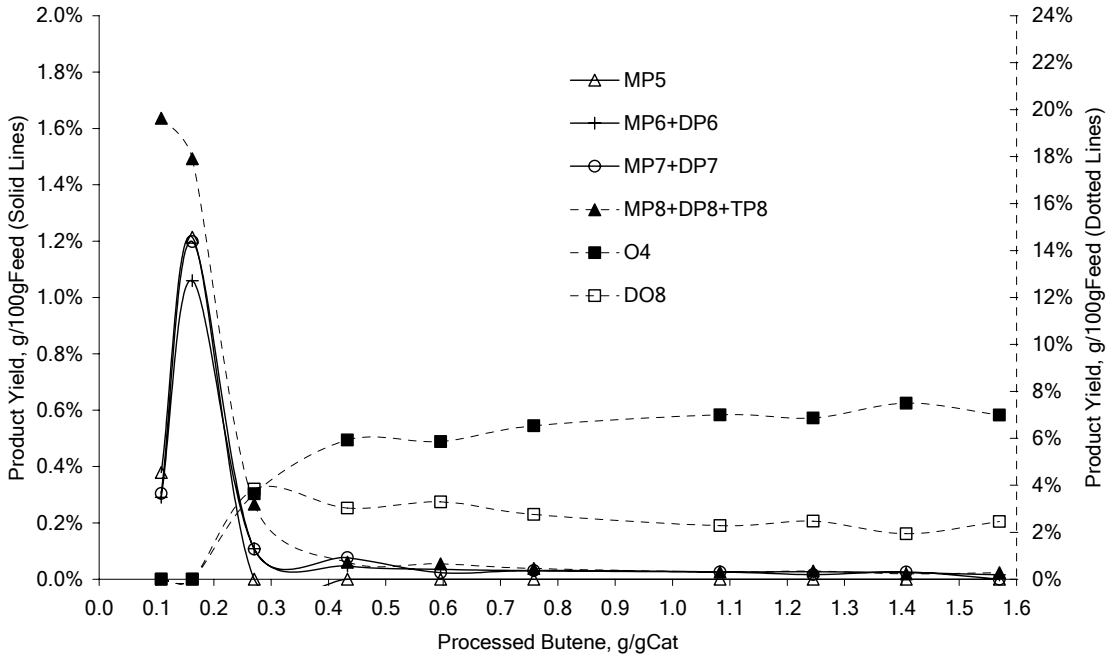

Figure 17. Product Yields vs. Processed Butene for Run 8. Temperature: 373 K, Butene Space-Time ($W/F°_{O4}.M_{O4}$): 4.6 h, Isobutane/1-Butene Molar Ratio: 8.3 mol/mol.

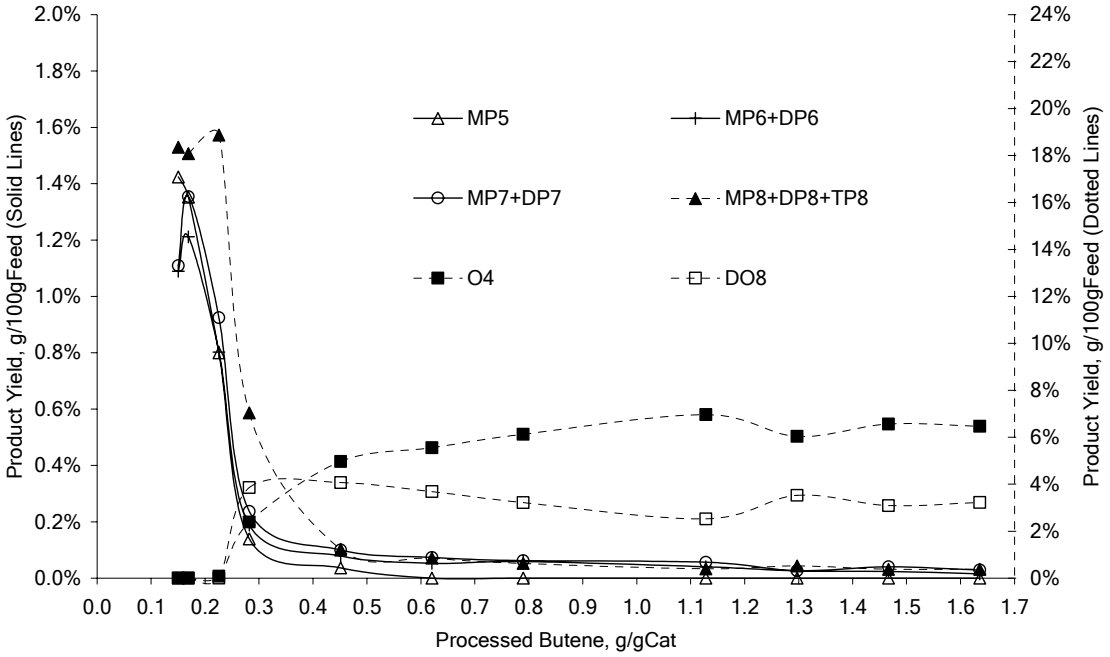

Figure 18. Product Yields vs. Processed Butene for Run 9. Temperature: 393 K, Butene Space-Time ($W/F°_{O4}.M_{O4}$): 4.4 h, Isobutane/1-Butene Molar Ratio: 8.6 mol/mol.

In general, all 9 runs show selectivity shifts not only from saturated octanes to unsaturated ones but also from tribranched species towards dibranched ones. This is a strong indication that PCP-branching and hydride transfer would be following similar deactivation pathways.

All conditions evaluated achieve steady conversion of butene towards dibranched octanes with deactivation. Thus, depending on the butene space-time, every run reaches steady conversion at some point within the processed butene interval of 0.25 to 0.75 g/gCat. The production of TP8 and DP8 isoalkanes decreases rapidly giving up to the formation of DO8 isoalkenes at a much smaller level of butene conversion which changes from levels of about 100 mol% (0 wt% O4 yield) to steady values around 20-35 mol% (6-8 wt% O4 yields). In addition, for all butene conversion levels along 9 runs, no O3 or MO4 formation is observed.

The absence of propene or isobutylene in the reaction product is a remarkable result. According to the reaction network, the formation of any species within the C_5, C_6 or C_7 carbon fractions involves either propene, isobutylene or both. A plausible explanation for this observation is that these species operate as reaction intermediates.

In the particular case of runs with large butene space-time values such as Run 7, 8 and 9, an additional interesting phenomenon is observed along with the amount of processed butene: the development of a moving deactivation front. As shown in Figures 16-18, part of what it seems to be a characteristic breakthrough curve for a moving deactivation front occurs within a range of 0.1 - 0.2 g/gCat in processed butene. Peak values for MP5-TP8 alkanes strongly suggest that by the time the first experiments were sampled; only a fraction of the deactivation zone had reached the exit of the fixed bed reactor.

When looking at all the deactivation profiles obtained with processed butene, the effect of temperature and butene space-time on the product yields is not easily revealed. They all share similar patterns even though they represent the outcomes for significantly different conditions. Consequently, Figure 19 offers a concise view of the reaction temperature and butene space-time effect over the product yields for the two most abundant component groups in the reaction product.

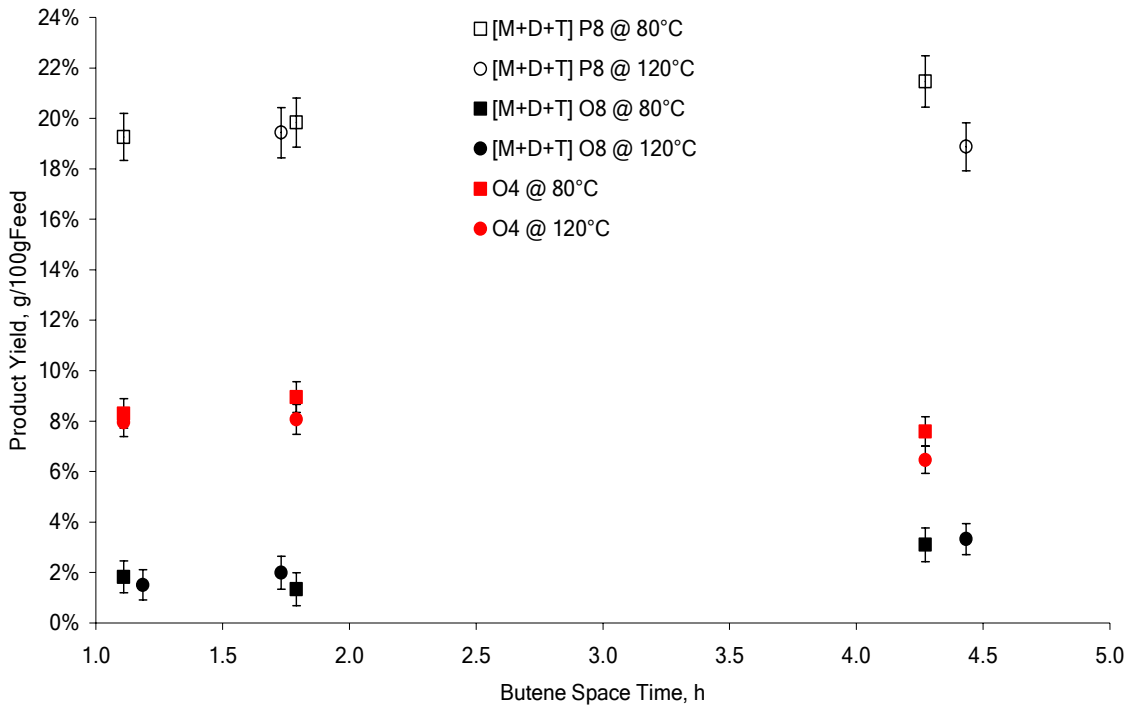

Figure 19. Initial C_8-Alkanes and Final C_4/C_8-Alkenes Product Yields. Dependency on Temperature and Butene Space-Time. All runs but Run 4 included. [M+D+T]P8 yields correspond to peak values within the 0.1-0.2 g/gCat processed butene range. O4 and [M+D+T]O8 yields correspond to steady values after 1.5 g/gCat of processed butene.

In general, the effect of reaction temperature over the main product yields turns out to be weak and in some cases, even smaller than the estimated experimental error so that no effect can be devised. Besides, no further significant expansion of the reaction temperature range of 80-120 °C would be tested without either approaching the lower bound set by the minimum temperature required to achieve measurable butene conversion at the acidity level available in a proton-exchanged Y-zeolite or reaching the upper bound imposed by the isobutane critical temperature of 134.5 °C. Only at high conversion levels and larger butene space-time (>4.4 h) a significant decrease in the amount of [M+D+T]P8 produced with increasing temperature can be observed. This suggests oligomerization and β-scission steps approaching equilibrium conditions (large butene space-time) where thermodynamic effects prevail so that endothermic steps are favored over their reverse ones with increasing temperature.

On the other hand, as butene space-time increases, an increasing trend for all the product yields is also observed. Thus, an even more interesting effect shows up: achievement of total butene conversion as long as there is a sufficient amount of fresh catalyst available. This observation supports the hypothesis that the phenomena this research pursues to explain (deactivation and selectivity shifts) mostly occurs within the boundaries of the deactivation front and that relevant values of the kinetic constants can be properly estimated from the observed changes along this region regardless of the composition profile evolution with butene space-time out of the front region.

Based on these experimental observations, a fundamental kinetic model at the elementary step level will be formulated.

FUNDAMENTAL MODELING OF SOLID ACID ALKYLATION KINETICS

Modeling Deactivation through Site Coverage

The ability of a given solid acid to catalyze a desired hydrocarbon transformation largely depends on the strength and density of its acid sites as well as on the temperature level at which the reaction is carried out. In the particular case of solid acid alkylation of isobutane with butenes over proton-exchanged zeolites, transformations at the elementary step level involve either one or two Brönsted acid sites, which are assumed to be distributed with uniform acid strength. As it was described in previous sections, a set of eight types of elementary steps are identified as the most likely transformations occurring within the reaction network at the acidity and temperature range of interest. Among all the elementary steps considered, alkene (de)protonation turns out being the only interaction occurring between a molecule in the fluid phase and a catalyst acid site on the surface. In consequence, it becomes a *de facto* initiation or termination step since all the other elementary steps involve transformations among surface-bonded carbenium ions. Accordingly, alkene protonation operates as an adsorption process in the zeolite chemistry.

Experimental findings indicate that for the temperature range relevant to the process under study, surface-bonded ions with nine or more carbon numbers are barely desorbed from the catalyst surface. GC/MS analyses indicate that for most product samples, the C_9+ area accounted for less than 1% of the total area in isobutane free basis. Consequently, C_9+ surface-bonded species can be conveniently defined as irreversibly adsorbed ions within the model formulation. As a direct result of this definition, active site coverage by irreversible adsorbed ions becomes an effective deactivation mechanism for the proposed model. A proper description of this mechanism starts with the conservation of the total concentration of acid sites (C^t_{H+}), which is the sum of the concentrations of free acid sites (C_{H+}) and of those that are respectively reversibly (C_{Rn+}) and irreversibly covered (C_{Rm+}).

$$C^t_{H+} = C_{H+} + \sum_{n=1}^{N} C_{R_n^+} + \sum_{m=1}^{M} C_{R_m^+} \qquad (3)$$

According to the information available from the reaction network, equation (3) accounts for the total conservation of acid sites under the presence of 78 reversibly adsorbed ions (N) and 541

irreversibly adsorbed ones (M).

The cation exchange capacity (CEC) of a Zeolyst CBV600 protonated Y-zeolite with estimated formula: $H^{+}_{58}(AlO_2^{-})_{58}(SiO_2)_{150}$ $240 \cdot H_2O$, provides with an estimate value of 3.46 mol/gCat for (C^{t}_{H+}). The catalyst-dependent value of (C^{t}_{H+}) is maintained constant in the model.

From a fundamental point of view, the approximation of considering all C_9+ ions as irreversibly adsorbed species does not imply that their ability to react via other elementary steps such as hydride shift, methyl shift, PCP-branching or even β-scission is impaired. On the contrary, the experimental observation of a non-zero steady butene conversion strongly suggests that non-negligible amounts of irreversibly adsorbed material would be reacting via β-scission towards equilibrium with oligomerization. Therefore, a detailed account for the fate of each species present on the catalyst surface is required in order to account for this experimental observation.

Upon rearrangement of equation (3), a local deactivation function (φ) arises as a natural function of the irreversible fractional site coverage (θ_{irr}). This function accounts for the local fraction of acid sites available on the catalyst surface. In addition, an expression for the local concentration of free acid sites (C_{H+}) can also be derived from the conservation of the total number of acid sites, as a function of the reversible fractional site coverage (θ_{rev}) and the deactivation function [equation (5)].

$$\varphi = 1 - \theta_{irr} = 1 - \sum_{m=1}^{M} \frac{C_{R_m^+}}{C^{t}_{H+}} \tag{4}$$

$$\frac{C_{H+}}{C^{t}_{H+}} = \varphi \left(1 + \sum_{n=1}^{N} \frac{C_{R_n^+}}{C_{H+}} \right)^{-1} = \frac{\varphi}{1 + \theta_{rev}} \tag{5}$$

According to equation (4), the deactivation function shows a linear dependency with respect to the irreversible fractional site coverage. However, depending on the number of acid sites required for a particular type of elementary step to proceed, higher orders on the dependency with fractional site coverage may result for the deactivation function as described by Froment *et al.*[25]

Rate Controlling Steps and Liquid Sorption in Zeolites

Following the identification of (de)protonation steps as the only interaction occurring between molecules in liquid phase and acid sites, together with the definition of C_9+ species as irreversibly adsorbed ions whose serve as deactivation agents, comes the assumption that surface reactions are rate-controlling steps. Even though this assumption is fundamentally different from assuming initiation and termination steps in pseudo-steady state, both approaches end up setting (de)protonation elementary steps in a quasi-equilibrium condition. Thus, upon application of this condition to the present model, sorption partition coefficients relating surface concentrations of reaction intermediates to liquid-phase concentrations corresponding to alkenes inside of zeolite cages can be calculated as state functions.

$$C_{R_n^+} = K_p(R_i^=;R_n^+)\frac{C_i^s\ C_{H+}}{C^o} = K_p(R_i^=;R_n^+)\left(\frac{V_L}{V_p}\right)C_i^s\ C_{H+}^t\left(\frac{1-\theta_{irr}}{1+\theta_{rev}}\right) \tag{6}$$

In equation (6), the local surface concentration of the n^{th}-ion (C_{Rn+}) is expressed in terms of the corresponding liquid-phase concentration for the zeolite-sorbed i^{th}-alkene (C^s_i) and the surface concentration of the free acid sites. The temperature-dependent protonation equilibrium constant (K_p) can be directly related to the change of the Gibbs free energy upon reaction as follows.

$$\left[\frac{C_{R_n^+}\ C^\circ}{C_i^s\ C_{H+}}\right] = K_p(R_i^=;R_n^+) = \exp\left(-\frac{\Delta G_p}{R\,T}\right) \tag{7}$$

In equation (7), concentration of the pure liquid (C^o) shows up because the standard state of the liquid reactant turns out being different from unity. In order to calculate the value of C^o, the inverse value of the standard molar volume for the pure liquid (V_L) together with the catalyst pore volume (V_p) are used to express the resulting concentration in engineering units concerning matter per unit of catalyst weight (mol/gCat). Calculation pathways from pure components in the perfect gas state at standard conditions to the liquid mixture assume ideal solution and negligible pressure effects since the total pressure (35 bar) is much greater than the vapor pressures at the reaction temperature for all the species present in liquid phase.

The liquid-phase concentration of the i^{th}-alkene sorbed inside the zeolite cannot be measured directly. This concentration is the product of a diffusion process that transports species from the

liquid bulk to the confined liquid inside zeolite cages. Thus, it is convenient to express the unknown concentration of the confined liquid in terms of a measurable quantity such as the liquid bulk concentration (C_{Ri+}). Consequently, a unique sorption partition coefficient for all alkene species is proposed based on the assumption that zeolite cages are completely filled with liquid and a that all the mixture components are highly diluted in isobutane. The proposed model follows the premises found by Denayer *et al.*[26] where a similar model is reported to properly fit experimental data for the liquid-phase hydroconversion of a heptane/nonane mixture over Pt-USY zeolite. Based on this description, equation (8) relates the concentration of the zeolite-sorbed i^{th}-alkene to its corresponding molar fraction in the liquid bulk.

$$C^{s}_{R_i^{=}} = K_s\, C_{R_i^{=}} = \overline{C}_{sat} \left(\frac{V_L}{V_p}\right) C_i = \overline{C}_{sat}\, x_{R_i^{=}} \tag{8}$$

Assuming saturation inside the zeolite cages, the sorption partition coefficient becomes the average saturation concentration for all species considered.

$$C_{R_n^{+}} = K_p(R_i^{=};R_n^{+}) \left(\frac{V_L}{V_p}\right) \overline{C}_{sat}\, x_{R_i^{=}}\, C^{t}_{H+} \left(\frac{\varphi}{1+\theta_{rev}}\right) \tag{9}$$

As a result, equation (9) entitles to relate the surface concentration of the reaction intermediates to quantities that can be estimated from thermodynamics as well as to measurable quantities such as molar fractions for species in the liquid bulk ($x_{Ri=}$). In addition, equation (9) can also be used to express the reversible fractional site coverage as a function of the molar fractions in the liquid bulk as indicated by equation (10).

$$\theta_{rev} = \sum_{n=1}^{N} \frac{C_{R_n^{+}}}{C^{t}_{H+}} = \sum_{n=1}^{N} K_p(R_i^{=};R_n^{+}) \left(\frac{V_L}{V_p}\right) \overline{C}_{sat}\, x_{R_i^{=}} \tag{10}$$

Up to this point, a set of key assumptions comprising uniform distribution of Brönsted acid sites, C_9+ species as irreversibly adsorbed deactivation agents, surface reactions as rate-controlling steps and saturation conditions for the confined liquid inside zeolite cages. These assumptions, together with conservation laws for the total number of acid sites serve to achieve not only a fundamental description of the deactivation process but also to establish a feasible solution pathway for the entire kinetic model at the elementary step level by allowing to express most of

the unknowns associated to the solid phase as a function of measurable quantities. Finally, a complete kinetic model formulation requires expressions for the reaction rates. Consequently, in what follows, expressions for the reaction rates at the elementary step level are formulated as the most basic description for the reaction kinetics of the proposed model.

Rate Expressions at the Elementary Step Level

Only two reactant molecules and eight different types of elementary steps are necessary for the computer-generated reaction network to produce 753 species and 3130 elementary steps within the framework of the carbenium ion chemistry. This set of transformations constitutes a fundamental description of the reaction kinetics of the solid acid alkylation process at the elementary step level. However, equilibrium relationships formulated in previous sections for interactions between species in liquid and solid phases open the possibility to significantly reduce the number of rate expressions required to represent the reaction network. To accomplish this reduction, rates for 294 (de)protonation elementary steps are replaced with their corresponding equilibrium relationships by means of equation (9). As a result, a model is formulated by setting equilibria to all possible adsorption/desorption interactions among the 134 molecules present in liquid phase and the 78 reversibly adsorbed ions serving as intermediates on surface elementary steps.

Surface elementary steps comprise 2836 transformations among surface-bonded carbenium ions. In what follows, rate expressions for every surface elementary step are formulated according to the principles of the Transition State Theory (TST). TST establishes that for an elementary step, reactants are in equilibrium with the transition state. Moreover, TST also states that the reaction rate of an elementary step depends on an intensive measure of the amount of each reactant raised to the absolute value of its stochiometric coefficient. This dependency is a direct consequence of the application of the principle of microscopic reversibility. This principle establishes that the transition state for a given reaction and its reverse must be the same. Upon the application of the TST to the definition of the reaction rate of an elementary step, three different types of rate expressions can be written for the six types of elementary steps considered.

First in the formulation, common expressions result for all monomolecular steps (β-scission, pcp-branching, methyl-shift and hydride shift) as indicated on equations (11) and (12). These

expressions state that the reaction rate of the j^{th}-elementary step (r_j) depends on the product of the elementary step rate coefficient (k'_j, s^{-1}) times the surface concentration of the reacting carbenium ion (C_{Rn+} or C_{Rm+}).

$$r_j = k'_j\, C_{R_n^+} = k'_j\, K_p(R_i^=;R_n^+)\left(\frac{V_L}{V_p}\right)\overline{C}_{sat}\;\; C_{H+}^t\left(\frac{\varphi}{1+\theta_{rev}}\right)x_{R_i^=} \tag{11}$$

$$r_j = k'_j\, C_{R_m^+} \tag{12}$$

In the particular case of the transformations involving reversibly adsorbed ions, equation (9) allows rewriting the reaction rate as a function of the liquid bulk composition. In contrast, elementary steps involving irreversibly adsorbed species require track of their local surface concentrations.

Furthermore, reaction rates for bimolecular elementary steps (oligomerization and hydride transfer) occurring over single acid sites are formulated based on TST principles. In the resulting expressions, a second order rate coefficient (k'_j) multiplies the liquid-phase concentration of the zeolite-sorbed reactant (C^s_o or C^s_p) by the surface concentration of the reacting carbenium ion (C_{Rn+}):

$$r_j = k'_j\, C_{R_n^+}\; C_o^s = k'_j\, K_p(R_i^=;R_n^+)\left(\frac{V_L}{V_p}\right)\overline{C}_{sat}^{\,2}\;\; C_{H+}^t\left(\frac{\varphi}{1+\theta_{rev}}\right)x_{R_i^=}\; x_{R^=} \tag{13}$$

$$r_j = k'_j\, C_{R_n^+}\; C_p^s = k'_j\, K_p(R_i^=;R_n^+)\left(\frac{V_L}{V_p}\right)\overline{C}_{sat}^{\,2}\;\; C_{H+}^t\left(\frac{\varphi^2}{1+\theta_{rev}}\right)x_{R_i^=}\; x_{R} \tag{14}$$

Notice that on both expressions (13) and (14), only reversible adsorbed carbenium ions are present as reactants since for any irreversibly adsorbed ion, bimolecular elementary steps would result in model-forbidden outcomes such as the desorption of a C_9+ irreversibly adsorbed ion (hydride transfer) or the formation of a C_{13}+ irreversibly adsorbed ion.

Additionally, in the particular case of hydride transfer, a faster deactivation function (φ^2) is proposed as indicated on rate expression (14) to account for the effect of a weak but necessary interaction between the reacting alkane and a neighboring acid site. Basically it is proposed that this interaction, first identified through quantum chemical calculations by Kazansky, does not

imply adsorption or occupancy of the acid site from the alkane and therefore does not affect the fractional site coverage of acid sites whereas this last one does significantly affect the hydride transfer activity by reducing in great extent the availability of neighboring acid sites. An stochastic description of single- and dual-site reaction mechanisms for deactivating reaction sets can be found in Froment *et al.*[25] Based on his results for the case where main reactions occur on dual-sites and deactivation reactions occur on single-sites, a deactivation function involving a quadratic dependency on the irreversible fractional site coverage is proposed in the present model for the hydride transfer step.

Clearly, the complexity of a kinetic model that comprises about 2836 rate coefficients makes it untractable or even useless for practical purposes. Such a predictive model would require the determination of hundreds of isothermal rate coefficients and consequently an unrealizable amount of experimental data. Current computational capabilities and numerical methods for parameter estimation might be capable of handling problems with several tens or maybe a few hundred model parameters, but even in those cases, their validity would be severely limited because of the uncertainty associated with their determination. In contrast, smaller models based on component lumps and average rates of reaction offer simpler descriptions involving perhaps a reduced but somehow accurate set of parameters. However, the kinetic parameters estimated out of this kind of models are scarcely invariant to changes in reaction conditions or feedstocks and in many cases cannot provide relevant information other than their own predictions about the underlying chemistry involved with the process under study. Consequently, in order to make the proposed model at the elementary step level description tractable, the next step in the model formulation is the introduction of the concept of single event, which delivers the means for a significant reduction in the number of model parameters to be determined.

The Single Event Concept

First introduced by Froment *et al.* in a seminal paper in the area of complex reaction kinetics, the single event concept takes shape from the fundamental framework of TST. This concept is the result of factoring structural contributions associated to possible distinguishable events within a single elementary step out of the TST description of the rate coefficient of an elementary step. Thus, the number of distinct configurations that a reactant and its transition state can take is related to changes in their symmetry numbers in order to account for all possible occurrences of identical single events within an elementary step.

As shown in equation (15), TST provides with a general expression for the rate coefficient of an elementary step. Inside this expression, major contributions to the reaction rate can be identified starting with the vibration frequency along the reaction coordinate converted to a translation that leads the passage from the transition state to products ($\Lambda = k_B T/h$) and followed by the reactant-transition-state equilibrium constant ($K^{\ddagger}$) which is further split into the reactant-transition-state entropy change ($\Delta S^{\circ\ddagger}$) and the energy barrier ($\Delta H^{\circ\ddagger}$).

$$k' = \Lambda K^{\ddagger} = \left(\frac{k_B T}{h}\right) \exp\left(\frac{\Delta S^{\circ\ddagger}}{R}\right) \exp\left(-\frac{\Delta H^{\circ\ddagger}}{RT}\right) \tag{15}$$

In the particular case of the reactant-transition-state entropy change, isolation of structural effects associated with symmetry changes between the reactant and the transition state leads to their separation from the structure-independent intrinsic entropy change ($\Delta \hat{S}^{\circ}$) as indicated in equation (16). Thus, a unique value for all possible single events within a given elementary step is obtained for the intrinsic entropy change.

$$\Delta S^{\circ\ddagger} = \Delta \hat{S}^{\circ} + R \ln\left(\frac{\sigma_{gl}}{\sigma_{gl}^{\ddagger}}\right) \tag{16}$$

Furthermore, by combining equations (15) and (16), structural effects associated with distinguishable single events within an elementary step are factored out from the rate coefficient to yield expression (17).

$$k' = \Lambda \exp\left(\frac{\Delta \hat{S}^{\circ}}{R}\right)\left(\frac{\sigma_{gl}}{\sigma_{gl}^{\ddagger}}\right) \exp\left(-\frac{\Delta H^{\circ\ddagger}}{RT}\right) \tag{17}$$

The ratio of the global symmetry number of the reactant molecule (σ_{gl}) to the global symmetry number of the transition state ($\sigma_{gl}^{\ddagger}$) is defined as the number of single events (n_e) [equation (18)].

$$n_e = \frac{\sigma_{gl}}{\sigma_{gl}^{\ddagger}} \tag{18}$$

As a result, the rate coefficient of an elementary step (k'_j) turns out being a multiple of the single event rate coefficient ($\tilde{k}_j$) in such a way that only those structural effects associated with the stability of the carbenium ions remain present. Hence, equation (19) sets the single event rate coefficient as a function of the surface-bonded carbenium ion types present (t_{Rr+}, t_{Rp+}).

$$k'_j = n_e \, \tilde{k}_j\left(t_{R_r^+}; t_{R_p^+}\right) \tag{19}$$

The introduction of the single event concept allows a significant reduction in the number of model parameters. In fact, by grouping the vibration frequency along the reaction coordinate and the intrinsic entropy change, a structure independent frequency factor is obtained for each type of elementary step (Ã). Hence, all the remaining structure-dependent contributions associated with a particular elementary step end up contained inside the energy barrier. This energy barrier can be approximated to the energy of activation of the elementary step occurring here in liquid phase (Ea ≈ $\Delta H^{\circ\ddagger}$, J/mol) so that an Arrhenius-like expression is obtained for the single event rate coefficient of an elementary step.

$$\tilde{k}_j\left(t_{R_r^+}; t_{R_p^+}\right) = \left[\Lambda \exp\left(\frac{\Delta \hat{S}^\circ}{R}\right)\right] \exp\left(-\frac{\Delta H_j^{\circ\ddagger}}{RT}\right) = \tilde{A}_{ElemStepType} \exp\left(-\frac{Ea_j}{RT}\right) \tag{20}$$

Application of equation (20) brings a dramatic reduction in the number of model parameters. The introduction of the single event concept in the proposed model allows a reduction in the number of distinct frequency factors from 2836 to six: only one per type of elementary step.

Number of Single Events

The application of the single event concept to the proposed model requires previous knowledge of the number of single events for each elementary step. The calculation of the number of single events for a given elementary step goes through the definition of the number of single events as the ratio of the global symmetry numbers of reactants over that of the transition state.

The calculation of the global symmetry number starts with the numerical representation of the molecule by a Boolean matrix.[27] Then the external symmetry number, which corresponds to the number of indistinguishable configurations of the molecule as a rigid rotor, is calculated from the

molecular topology based on the methodology found in Muller *et al.*[28] and Walters *et al.*[29]

The method is based on the identification of the centers of symmetry by recursively removing layers of atoms. Then, simple rules applied to each layer yield contributions to the external symmetry number (σ_{ext}) depending on the hybridization state (sp^2 or sp^3) of each carbon atom. Ulterior identification of 2- and 3-fold internal symmetry axes (n', n'') and quiral centers (n''') within the molecular structure is carried out in order to determine additional contributions to the global symmetry number as indicated on equation (21). The applicability of this method is limited to acyclic hydrocarbon structures where information on hindered internal rotations is not relevant.

$$\sigma_{gl} = \sigma_{ext} \frac{2^{n'} 3^{n''}}{2^{n'''}} \tag{21}$$

In general, the pathway from reactants to transition states along the reaction coordinate involves the creation and/or destruction of symmetry axes and chiral centers by changing the bond distances and positions of the carbon atoms in α- and/or β-position with respect to the one that carries the positive charge or is part of a double bond. This process of creating and/or destroying symmetry axes and chiral centers determines the number of single events for a given elementary step. For instance, Table 9 illustrates this process for both monomolecular and bimolecular elementary steps considered in the present model. In all cases, appearance or disappearance of 2- and 3-fold symmetry axes and/or chiral centers are indicated by changes to the global symmetry number in multiples of two or three.

The validity of representing free carbenium ion structures to represent surface-bonded structures would be questionable. However, Park and Froment[30] studied the effect of the surface bonding of carbenium ions and concluded that both the reactant and the transition state undergo similar reductions in their global symmetry numbers with bonding. Therefore, the number of single events remains constant in the presence of surface-bonded ions.

Table 9. Examples of Symmetry Transformations on Elementary Steps. Based on the most likely transition state structure. Dotted lines indicate variable length bonds. Double dagger indicates transition state structures. Asterisk denotes the position of a chiral center.

(De)Protonation

$\sigma_{gl} = 3$ | $\sigma_{gl} = 3$ | $\sigma_{gl} = 3^2$

$(n_e)_{prot} = \mathbf{1}$ | $(n_e)_{deprot} = \mathbf{3}$

Hydride Shift

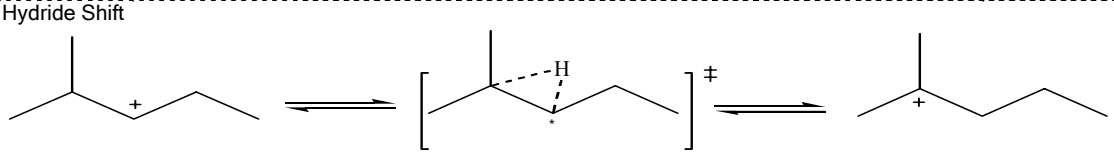

$\sigma_{gl} = 3^3$ | $\sigma_{gl} = 3^3 / 2$ | $\sigma_{gl} = 2 \times 3^3$

$(n_e)_{hs} = \mathbf{2}$ | $(n_e)_{hs} = \mathbf{4}$

Methyl Shift

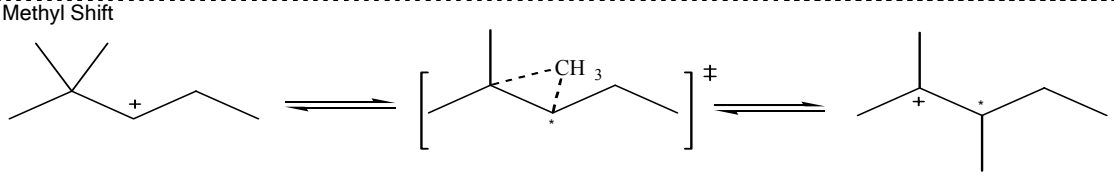

$\sigma_{gl} = 3^5$ | $\sigma_{gl} = 3^4 / 2$ | $\sigma_{gl} = 2 \times 3^4 / 2$

$(n_e)_{ms} = \mathbf{6}$ | $(n_e)_{ms} = \mathbf{2}$

PCP-Branching

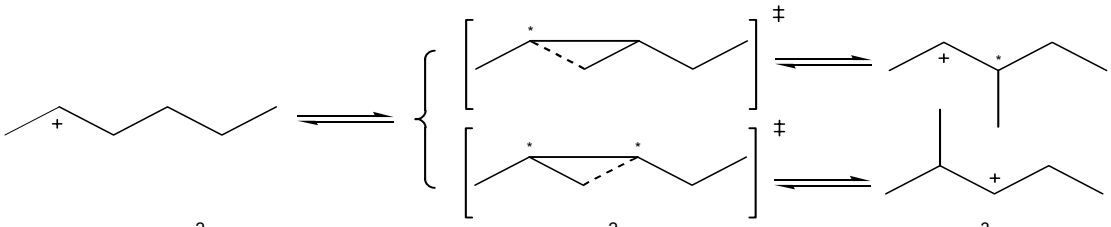

α-cleveage: $\sigma_{gl} = 3^2$ | $\sigma_{gl} = 3^2 / 2$ | $\sigma_{gl} = 3^3 / 2$

$(n_e)_{pcp} = \mathbf{2}$ | $(n_e)_{pcp} = \mathbf{3}$

β-cleveage: $\sigma_{gl} = 3^2$ | $\sigma_{gl} = 3^2 / 2^2$ | $\sigma_{gl} = 3^3$

$(n_e)_{pcp} = \mathbf{4}$ | $(n_e)_{pcp} = \mathbf{12}$

β-Scission & Oligomerization

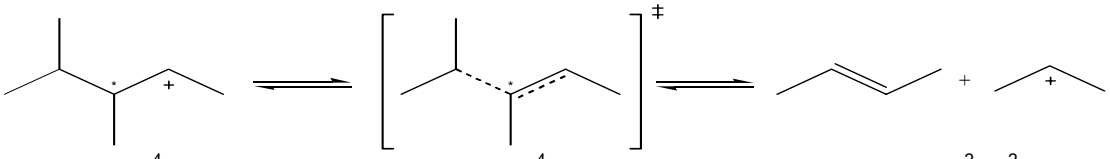

$\sigma_{gl} = 3^4 / 2$ | $\sigma_{gl} = 3^4 / 2$ | $\sigma_{gl} \times \sigma_{gl} = 3^2 \times 3^2$

$(n_e)_{bs} = \mathbf{1}$ | $(n_e)_{oliq} = \mathbf{2}$

Hydride Transfer

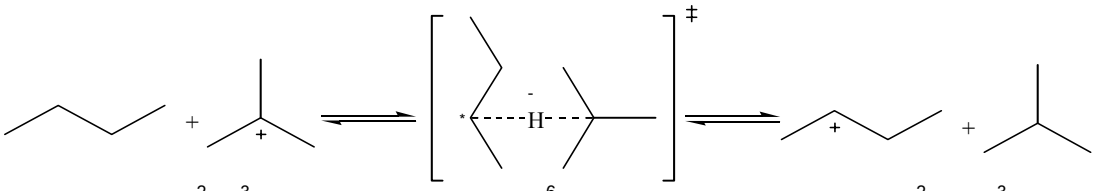

$\sigma_{gl} \times \sigma_{gl} = 2 \times 3^2 \times 3^3$ | $\sigma_{gl} = 3^6 / 2$ | $\sigma_{gl} = 3^2$, $\sigma_{gl} = 3^3$

$(n_e)_{ht} = \mathbf{12}$ | $(n_e)_{ht} = \mathbf{6}$

Furthermore, Park and Froment also validated the independence of the single event frequency factor with the molecular structure for the deprotonation of 2-butylcarbenium ion towards the 1-butene (n_e=3) and 2-butene (n_e=1) products. Accordingly, data on the elementary step transformation of gas-phase carbenium ions from Dumesic *et al.*[31] resulted in very good agreement by turning over an elementary step frequency factor for the deprotonation towards 1-butene three times larger than towards 2-butene. This result strongly suggests a structural independence of the intrinsic entropy change ($\Delta\hat{S}°$) for (de)protonation elementary steps.

One of the practical difficulties in the calculation of the number of single event arises from the fact that the structure of the transition state is frequently unknown. Even though the estimation of the transition state structure is possible by seeking the maximum potential energy structure along the reaction coordinate (minimum energy pathway) in quantum chemistry calculations, this powerful methodology becomes too costly in terms of the computational time when dealing with surface-bonded species and a large number of elementary steps.

In order to overcome the difficulties of estimating a very large number of transition state structures, formulae for the estimation of the number of single events have been developed for elementary steps such as hydride shift, methyl shift, PCP branching, β-scission, oligomerization and hydride transfer. The fundamental assumption in the development of these formulae is that the basic geometry of the transition state is known. The idea is to come up with an educated guess of the basic features of the transition state structure for a given type of elementary step and focus on the creation/destruction of symmetry axes and chiral centers so that a detailed knowledge of the transition state structure would no longer be necessary.

In principle, the basic general structure of the transition state can be obtained from quantum chemistry calculations found in the literature for the elementary steps of interest. Among the key characteristics to identify from transition state structures is the retention of basic structural features from either the reactants (expected on exothermic elementary steps according to the Hammond's postulate) or the products (expected on elementary steps where the intrinsic entropy change equals the entropy change on reaction). In addition, identification of stretching bonds is also a key element to determine possible symmetry changes. Thus, formulae comprising symmetry axes and chiral centers creation and/or destruction yield a straightforward method for estimating the number of single events.

Table 10. Formulae for the Estimation of the Number of Single Events. Letters (r) and (p) denote reactant and product respectively. Double dagger indicates transition state structures. By default: n1=n2=n3=n4=0.

Elementary Step	Formula	Rationale
Alkene Protonation	$(n_e)_{prot}=1$	Transition state preserves the reactant structure: $\sigma^{\ddagger}=\sigma_r$
Alkene Deprotonation	$(n_e)_{deprot}=\sigma_{gl}(r)/\sigma_{gl}(p)$	Alkene protonation reverse reaction
Hydride Shift	$(n_e)_{\beta s}=2^{1+n1+n4}$	A 2-fold internal axis is created when 2 primary carbons are associated with the charge bearing atom: n1=1 A 3-fold internal axis is created when 3 primary carbon atoms are attached to the carbon in β-position: n4=1
Methyl Shift	$(n_e)_{ms}=2\ n_{\beta\text{-Me}\mid\ \alpha\text{-carbon}}$	Transition state yields either 1 or 2 chiral centers depending on the number of methyl groups in β-position with respect to the α-carbon
PCP-Branching α-cleavage: β-cleavage:	$(n_e)_{pcp}= n_{\beta\text{-H}}\ 2^{\ 1+n1+\ n2+\ n3}$ $(n_e)_{pcp}= 2^{\ 1+n1+\ n2+\ n3}$	A 2-fold internal axis is created when 2 primary carbon atoms are associated with the charge bearing atom: n1=1 A chiral center is formed when 3 carbon atoms are attached to the carbon in α-position: n2=1 A chiral center is formed when only 1 carbon atom is attached to the carbon in β-position: n3=1
Oligomerization	$(n_e)_{oliq}=[\ \sigma_{gl}(r_1)\ \sigma_{gl}(r_2)\ ]\ /\ \sigma_{gl}(p)\ (n_e)_{\beta s}$	β-scission reverse reaction
β-Scission	$(n_e)_{\beta s}=(2^{\ n1-\ n2-\ n3})/(3^{\ n4})$	2-fold internal axis is formed when 2 primary carbons are associated with the charged atom: n1=1 A chiral center is formed when 3 carbon atoms are attached to the carbon in α-position: n2=1 A chiral center is formed when only 1 carbon atom is attached to the carbon in β-position: n3=1 3-fold internal axis is removed when 3 primary carbon atoms are attached to the carbon in β-position: n4=1
Hydride Transfer	$(n_e)_{ht}=[\ \sigma_{gl}(r_1)\ \sigma_{gl}(r_2)\ ]\ /\ \sigma_{gl}^{\ddagger}$	Transition state is set such that a 180° bond angle is formed between the two carbon centers: $\sigma^{\ddagger}$

As a result, Table 10 shows a summary of the formulae proposed for the present model accompanied by the rationale applied on their formulation. Notice that by taking advantage of the reversibility relationships, deprotonation and oligomerization formulae are conveniently expressed in terms of the available symmetry numbers of products and reactants. Reactant and product molecular structures are in general readily available making relatively easy their symmetry number estimation. In addition, the number of single events for the corresponding reversible elementary step is necessary to complete the calculation.

The Evans-Polanyi Relationship

Once the number of single events are available, a total of eight frequency factors and 2836 energies of activation remain as required kinetic parameters for a complete description of the

reaction network at the elementary step level, assuming that all protonation equilibrium constants are known. In general, the energy of activation of each elementary step is strongly dependent on the nature and structure of the carbenium ions involved. These species have been identified as the most likely transition states in the transformation of hydrocarbons over solid acids. Therefore, the impact of the carbenium ion stability on the energy of activation is so significant that the exclusion of all steps leading to the formation of primary carbenium ions as transition states in the present model is based on such premises.

On the other hand, surface-bonded carbenium ions, which serve as stable intermediates, have a significant weaker impact on the energy of activation. This is a consequence of the strong stabilization effect that the acid site delivers to the carbenium ion structure by decreasing the energy of the surface-bonded ion to levels much closer to the levels of the species in fluid phase. However, as the carbonyl bond stabilizes the carbenium ion by reducing its net charge, its associated surface-bonded ion retains most of the structural information leading to a free carbenium ion as transition state. Therefore, one of the minima along the reaction coordinate, either the reactant or the product, should resemble the structure of the transition state whereas the other should not, thus establishing a correlation between the reactant-product energy difference and the energy of activation. This is in fact the case for many elementary steps, as stated by the Evans-Polanyi relationship.[32]

The Evans-Polanyi relationship establishes that the magnitude of the energy barrier varies linearly with the energy change on reaction. This functionality is expressed in terms of the energy of activation and the standard heat of reaction by means of equations (22) and (23) for either exothermic or endothermic elementary steps.

$$Ea_j = E^{\circ}_{ElemStepType} - \alpha_{ElemStepType} \left|\Delta H^{\circ}_j\right| = E^{\circ}_{ElemStepType} + \alpha_{ElemStepType}\ \Delta H^{\circ}_j\ ,\ \Delta H^{\circ}_j < 0 \qquad (22)$$

$$Ea_j = E^{\circ}_{ElemStepType} + \left(1-\alpha_{ElemStepType}\right)\left|\Delta H^{\circ}_j\right| = E^{\circ}_{ElemStepType} + \left(1-\alpha_{ElemStepType}\right)\Delta H^{\circ}_j\ ,\ \Delta H^{\circ}_j > 0 \qquad (23)$$

Here, an intrinsic energy barrier (E°) together with a transfer coefficient (α) enter into the energy of activation (Ea_j) as a linearly dependent function of the standard heat of reaction (ΔH°). These expressions are consistent with TST as the subtraction of the energies of activation for reversible elementary steps yields the correct magnitude and sign for the standard heat of reaction.

In order to account for energy differences between surface-bonded carbenium ions and their corresponding alkene isomers, Park and Froment introduced the Evans-Polanyi relationship into the framework of the single event kinetics. Since intrinsic energy barriers and transfer coefficients only depend on the type of elementary step, only twelve different parameters are required to set energy of activation values for all the 2836 elementary steps considered. As a result, only three parameters per type of elementary step are required in order to calculate all the elementary step rate coefficients, assuming that all the standard heats of reaction are available.

Stabilization Energies, Heats of Reaction and Protonation Equilibrium Constants

So far, the proposed model requires only 18 kinetic parameters to calculate 2836 elementary step rate coefficients. The calculation of these reaction rates involves not only the calculation of their corresponding rate coefficients but also the estimation from thermodynamics of values for 78 protonation equilibrium constants and 2282 standard heats of reaction. Consequently, energetic considerations regarding the stabilization effect of a solid acid site on the energy of a surface-bonded carbenium ion must be considered leading to the concept of stabilization energy as a set of additional model parameters required by the proposed model.

Thermodynamics offers the basic framework for the calculation of protonation equilibrium constants and standard heats of reaction. Starting from the definition of the protonation equilibrium constant (K_p) [equation (7)] in the protonation of the i^{th}-alkene to the n^{th}-ion, a more convenient expression is derived in which the Gibbs free energy change with protonation (ΔG_p) is split into different contributions as presented on equation (24).

$$K_p\left(R_i^{=};R_n^{+}\right)=\exp\left(-\frac{\Delta G_p}{RT}\right)=\frac{\sigma_i}{\sigma_n}\exp\left(\frac{\Delta \hat{S}_p^{\circ}}{R}-\frac{\Delta H_p^{\circ}\left(R_i^{=};R_n^{+}\right)}{R\,T}\right) \qquad (24)$$

This expression allows the calculation of the protonation equilibrium constant as a function of the alkene-ion symmetry ratio, the intrinsic entropy change on protonation ($\Delta \hat{S}_p°$) and the heat of protonation at standard conditions ($\Delta H_p°$). The derivation of equation (24) involves the application of the van't Hoff relationship assuming that the heat of protonation at standard conditions for an alkene in liquid phase is a weak function of temperature within the temperature range of interest (< 390 K). As already stated in the formulation of the single event rate coefficient for the intrinsic entropy change of an elementary step, the intrinsic entropy change of

protonation is assumed to be constant and unique all protonation elementary steps. As a result, the intrinsic entropy change of protonation becomes an additional parameter in the proposed model to be determined from experimental data for a given catalyst.

Equation (25) presents the heat of protonation at standard conditions defined as the algebraic sum of the enthalpies of formation for products and reactants.

$$\Delta H_p^\circ\left(R_i^=;R_n^+\right)=\Delta H_{f,s}^\circ\left(R_n^+\right)-\Delta H_{f,l}^\circ\left(R_i^=\right)-\Delta H_{f,s}^\circ\left(H^+\right) \tag{25}$$

In this expression, the enthalpies of formation for the surface-bonded species [$\Delta H°_{f,s}(R_n^+)$ and $\Delta H°_{f,s}(H^+)$] are unknown whereas the enthalpy of formation of the alkene in the liquid phase [$\Delta H°_{f,l}(R_i^=)$] can be calculated from estimates for the alkene standard enthalpy of formation [$\Delta H°_{f,g}(R_i^=)$] and the alkene standard heat of vaporization [$\Delta H°_{vap}(R_i^=)$] by means of equation (26).

$$\Delta H_{vap}^\circ\left(R_i^=\right)=\Delta H_{f,g}^\circ\left(R_i^=\right)-\Delta H_{f,l}^\circ\left(R_i^=\right) \tag{26}$$

In order to calculate the enthalpies of formation for surface-bonded species, the energy change of stabilization (Δq) is introduced as the difference between the energy level of a free carbenium ion and the energy of its corresponding surface-bonded ion after stabilization over a solid acid site. Consequently, equation (27) defines the energy change on stabilization through the difference in the enthalpies of formation for the n^{th}-ion between the gas phase and the surface.

$$\Delta q\left(R_n^+\right)=\Delta H_{f,g}^\circ\left(R_n^+\right)-\Delta H_{f,s}^\circ\left(R_n^+\right) \tag{27}$$

For convenience, the stabilization energy (Δq_+) is defined as the difference between the energy change of stabilization of the proton and the energy change of stabilization of the carbenium ion of interest as indicated on equation (28). The applied definition establishes a convenient reference level for the stabilization energy at the energy level of the stabilized proton on a Brönsted acid site. This reference is specific for a given catalyst and circumvents setting the energy change of stabilization of the proton as a model parameter.

$$\Delta q_+\left(R_n^+\right)=\Delta q\left(H^+\right)-\Delta q\left(R_n^+\right) \tag{28}$$

The stabilization energy definition allows proper calculation of heats of protonation and standard heats of reaction. As shown on equations (29) and (30), calculation of heats of protonation and standard heats of reaction for the six elementary steps considered, only requires previous knowledge of the gas-phase enthalpies of formation and the carbenium-ion-dependent stabilization energies.

$$\Delta H_p^\circ\left(R_i^=;R_n^+\right)=\Delta H_{f,g}^\circ\left(R_n^+\right)-\Delta H_{f,g}^\circ\left(R_i^=\right)-\Delta H_{f,g}^\circ\left(H^+\right)+\Delta H_{vap}^\circ\left(R_i^=\right)+\Delta q_+\left(R_n^+\right) \tag{29}$$

$$\Delta H_j^\circ=\begin{cases} pcp: \Delta H_{f,s}^\circ\left(R_p^+\right)-\Delta H_{f,s}^\circ\left(R_r^+\right)=\Delta H_{f,g}^\circ\left(R_p^+\right)-\Delta H_{f,g}^\circ\left(R_r^+\right) \\ hs: \Delta H_{f,s}^\circ\left(R_p^+\right)-\Delta H_{f,s}^\circ\left(R_r^+\right)=\Delta H_{f,g}^\circ\left(R_p^+\right)-\Delta H_{f,g}^\circ\left(R_r^+\right) \\ ms: \Delta H_{f,s}^\circ\left(R_p^+\right)-\Delta H_{f,s}^\circ\left(R_r^+\right)=\Delta H_{f,g}^\circ\left(R_p^+\right)-\Delta H_{f,g}^\circ\left(R_r^+\right) \\ \beta s: \Delta H_{f,g}^\circ\left(R_p^+\right)-\Delta H_{f,g}^\circ\left(R_r^+\right)+\Delta q_+\left(R_p^+\right)-\Delta q_+\left(R_r^+\right)+\Delta H_{f,g}^\circ\left(R_p^=\right) \\ olig: \Delta H_{f,g}^\circ\left(R_p^+\right)-\Delta H_{f,g}^\circ\left(R_r^+\right)+\Delta q_+\left(R_p^+\right)-\Delta q_+\left(R_r^+\right)-\Delta H_{f,g}^\circ\left(R_r^=\right) \\ ht: \Delta H_{f,g}^\circ\left(R_p^+\right)-\Delta H_{f,g}^\circ\left(R_r^+\right)+\Delta q_+\left(R_p^+\right)-\Delta q_+\left(R_r^+\right)-\Delta H_{f,g}^\circ\left(R_r\right)+\Delta H_{f,g}^\circ\left(R_p\right) \end{cases} \tag{30}$$

The stabilization energy depends on both, the nature of the acid site on the catalyst and the structure of the surface-bonded ion. Based on the assumption of a uniform distribution of acid strength over the active sites, only one stabilization energy value per carbenium ion turns out to be necessary to describe ion-surface interactions, yielding 619 distinct stabilization energies for the proposed model.

In the single-event kinetics modeling of the Methanol-To-Olefins process on ZSM-5 as well as on SAPO-34, Froment *et al.*[30,33] considered a common value for the stabilization energies of ions within the same carbon fraction. This approach allowed them to achieve a significant reduction in the number of independent stabilization energy values.

Application of a similar approach to the present model resulted in 10 stabilization energies, from $\Delta q_+(R^+_{C3})$ to $\Delta q_+(R^+_{C12})$, to be estimated as model parameters. However, the large uncertainty observed in several attempts to estimate these parameters indicated that the available experimental data did not contain enough information. This is in fact the case as inspection of the available experimental results indicates a weak dependency on temperature in the range of 353-393 K. Consequently, the proposed model requires either a further model reduction or additional experimental results within a broader temperature range. Yet, significant broadening of the

reaction temperature range is unfeasible due to a constraint of about 330 K in the minimum temperature required to achieve a measurable butene conversion at the acidity level provided by the proton-exchanged Y-zeolite. Similarly, the maximum temperature is also constrained by the liquid phase condition, which is bounded by the isobutane critical temperature of 408 K.

Because an interaction with an acid site brings down the potential energy of a carbenium ion through the formation of a covalent carbonyl bond between a positively charged carbon atom and a negatively charged oxygen atom, the energy drop associated with the alkene protonation must be strongly dependent not only on the acid strength of the active site but also on the molecular structure of the surface-bonded carbenium ion. Nevertheless, the present model assumes contributions to this drop in energy level for each acid site to be equal because of the unique acid strength among acid sites. In contrast, the dependency of the drop in energy level of surface-bonded ions does vary with structure in gas phase. Hence, it is proposed that values for the energy of stabilization be expressed as a function of the variables that determine the energy level of a carbenium ion in gas phase i.e. nature of the ion and carbon number.

In order to come up with a model for the catalyst-dependent stabilization energy as a function of the nature of the ion and the carbon number, two important contributions to stability are considered. First, there is a large contribution defined as the difference between the energy change on stabilization for a surface-bonded proton and a surface-bonded carbenium ion of a given ion-type (ΔE_+^{sec} or ΔE_+^{tert}). Second, there is a much smaller contribution (γ_c), which accounts for the stabilization effect that an increasing carbon number adds by distributing the positive charge along the carbon chain.

$$\Delta q_+\left(R_n^+\right) = \Delta E_+^{sec} + \gamma_c\, n_c\left(R_n^+\right) \tag{31}$$

$$\Delta q_+\left(R_n^+\right) = \Delta E_+^{tert} + \gamma_c\, n_c\left(R_n^+\right) \tag{32}$$

Application of the proposed equations (31) and (32) is limited to a narrow range of carbon numbers. Assuming uniform neighboring stability effects, a linear decrease in stabilization energy with carbon number is expected for carbon-atom additions occurring relatively close to the charge bearing carbon atom. In contrast, for carbon chain growth occurring far from the charge bearing carbon atom, stability effects become negligible due to diminishing Coulomb interactions. Thus, a more robust model for the stabilization energy would result from a formulation based on a group contribution method so that short-range interactions would be

accounted for. However, such a model would require almost as many stabilization-related parameters as the one involving individual stabilization energy values per carbon number.

The proposed treatment allows reducing the number of model parameters associated to the concept of stabilization energy from 619 to only three. Thus, by adding three parameters from the stabilization energy description to one intrinsic entropy change on protonation plus 18 parameters associated with the reaction kinetics of six different elementary steps, a total of 22 model parameters end up being necessary for a complete description of the proposed model.

Gas-Phase Enthalpies of Formation

In what precedes, reference to gas-phase enthalpies of formation in the calculation of heats of protonation and standard heats of reaction is made under the premises that these properties are available for all the species of interest. Although in the particular case of molecular species such as alkanes and alkenes there are abundant data available in the literature, these data is still insufficient to cover all the molecular species comprised into the reaction network. Consequently, the calculation of the standard enthalpy of formation for alkanes and alkenes in gas phase is carried out by means of the group contribution method formulated by Benson.[34] In principle, the Benson Group Contribution (BGC) method accounts for most of the atom-neighboring interactions within the molecule assuming that these interactions are very short-ranged and that no strain energies exist along the molecule.

Once the basic structure of an aliphatic hydrocarbon molecule is available, the application of BGC method is straightforward by means of equation (33). The gas-phase enthalpy of formation at standard conditions (ΔH_f°) is obtained by adding up all the corresponding atomic contributions as listed on Table 11.

$$\Delta H_f^\circ = \sum_{i=1}^{n_c} ng_i \, gc_i \qquad (33)$$

Table 11. Alkane Standard Enthalpy of Formation. ΔH_f° Values from BGC method with gc1[C-CH3]=-42.19, gc2[C-C2H2]=-20.64, gc3[C-C3H]=-7.95, gc4[C-C4]=2.09 in kJ/mol. [A] From Linstrom *et al*.[35]

		ng				ΔH_f°,kJ/mol	ΔH_f°,kJ/mol
Molecule	Group	1	2	3	4	(Exp)[A]	(Calc)
Propane	P3	2	1	0	0	-105.0	-105.0
n-butane	NP4	2	2	0	0	-125.7	-125.7
2-methyl-propane	MP4	3	0	1	0	-134.5	-134.5
n-pentane	NP5	2	3	0	0	-146.3	-146.3
2-methyl-butane	MP5	3	1	1	0	-155.2	-155.2
2,2-dimethyl-propane	DP5	4	0	0	1	-166.7	-166.7
n-hexane	NP6	2	4	0	0	-166.9	-166.9
2-methyl-pentane	MP6	3	2	1	0	-175.8	-175.8
3-methyl-pentane	MP6	3	2	1	0	-175.8	-175.8
2,3-dimethyl-butane	DP6	4	0	2	0	-184.7	-184.7
2,2-dimethyl-butane	DP6	4	1	0	1	-187.3	-187.3
n-heptane	NP7	2	5	0	0	-187.6	-187.6
2-methyl-hexane	MP7	3	3	1	0	-196.4	-196.4
3-methyl-hexane	MP7	3	3	1	0	-196.4	-196.4
3-ethyl-pentane	MP7	3	3	1	0	-196.4	-196.4
3-methyl-hexane	MP7	3	3	1	0	-196.4	-196.4
2,4-dimethyl-pentane	DP7	4	1	2	0	-205.3	-205.3
2,2-dimethyl-pentane	DP7	4	2	0	1	-208.0	-208.0
3,3-dimethyl-pentane	DP7	4	2	0	1	-208.0	-208.0
2,3-dimethyl-pentane	DP7	4	1	2	0	-205.3	-205.3
2,2,3-trimethyl-butane	TP7	5	0	1	1	-216.8	-216.8
n-octane	NP8	2	6	0	0	-208.2	-208.2
2-methyl-heptane	MP8	3	4	1	0	-217.1	-217.1
3-methyl-heptane	MP8	3	4	1	0	-217.1	-217.1
3-ethyl-hexane	MP8	3	4	1	0	-217.1	-217.1
4-methyl-heptane	MP8	3	4	1	0	-217.1	-217.1
3-ethyl-3-methyl-pentane	DP8	4	3	0	1	-228.6	-228.6
2,3-dimethyl-hexane	DP8	4	2	2	0	-225.9	-225.9
3,4-dimethyl-hexane	DP8	4	2	2	0	-225.9	-225.9
3-ethyl-2-methyl-pentane	DP8	4	2	2	0	-225.9	-225.9
2,2-dimethyl-hexane	DP8	4	3	0	1	-228.6	-228.6
2,4-dimethyl-hexane	DP8	4	2	2	0	-225.9	-225.9
3,3-dimethyl-hexane	DP8	4	3	0	1	-228.6	-228.6
2,3,4-trimehtyl-pentane	TP8	5	0	3	0	-234.8	-234.8
2,2,4-trimethyl-pentane	TP8	5	1	1	1	-237.5	-237.5
2,3,3-trimethyl-pentane	TP8	5	1	1	1	-237.5	-237.5
2,2,3-trimethyl-pentane	TP8	5	1	1	1	-237.5	-237.5
2,2,3,3-tetramethyl-butane	QP8	6	0	0	2	-249.0	-249.0
n-nonane	NP9	2	7	0	0	-228.9	-228.9
2-methyl-octane	MP9	3	5	1	0	-237.7	-237.7
2,2-dimethyl-heptane	DP9	4	4	0	1	-249.2	-249.2
2,2,5-trimethyl-hexane	TP9	5	2	1	1	-258.1	-258.1
2,2,3,3-tetramethyl-pentane	QP9	6	1	0	2	-269.6	-269.6
2,2,4,4-tetramethyl-pentane	QP9	6	1	0	2	-269.6	-269.6
2,2,3,4-tetramethyl-pentane	QP9	6	0	2	1	-267.0	-266.9
2,3,3,4-tetramethyl-pentane	QP9	6	0	2	1	-267.0	-266.9
n-decane	NP10	2	8	0	0	-249.5	-249.5
2,2,5-trimethyl-heptane	TP10	5	3	1	1	-278.7	-278.7
3,3,5-trimethyl-heptane	TP10	5	3	1	1	-278.7	-278.7
2,2,3,3-tetramethyl-hexane	QP10	6	2	0	2	-290.2	-290.2
2,2,5,5-tetramethyl-hexane	QP10	6	2	0	2	-290.2	-290.2
n-undecane	NP11	2	9	0	0	-270.1	-270.1
n-dodecane	NP12	2	10	0	0	-290.8	-290.8

In order to properly represent all possible configurations (conformational information is not available with the current Boolean matrix representation) for alkane and alkene species, eleven different types of contributions are required (gc_i). Consequently, Table 11 presents not only the values for all the alkane-related contributions but also how BGC method predictions compare with a database comprising experimental values for 53 alkanes obtained from literature.

Furthermore, Figure 20 presents a parity plot of the data on Table 11. Here, BGC method estimates resulted in good agreement with experimental values taken from literature. In the particular case of alkanes, the standard enthalpy of formation turned over an accuracy of ±9.5 kJ/mol, calculated from the sample standard error as an approximate measure of error.

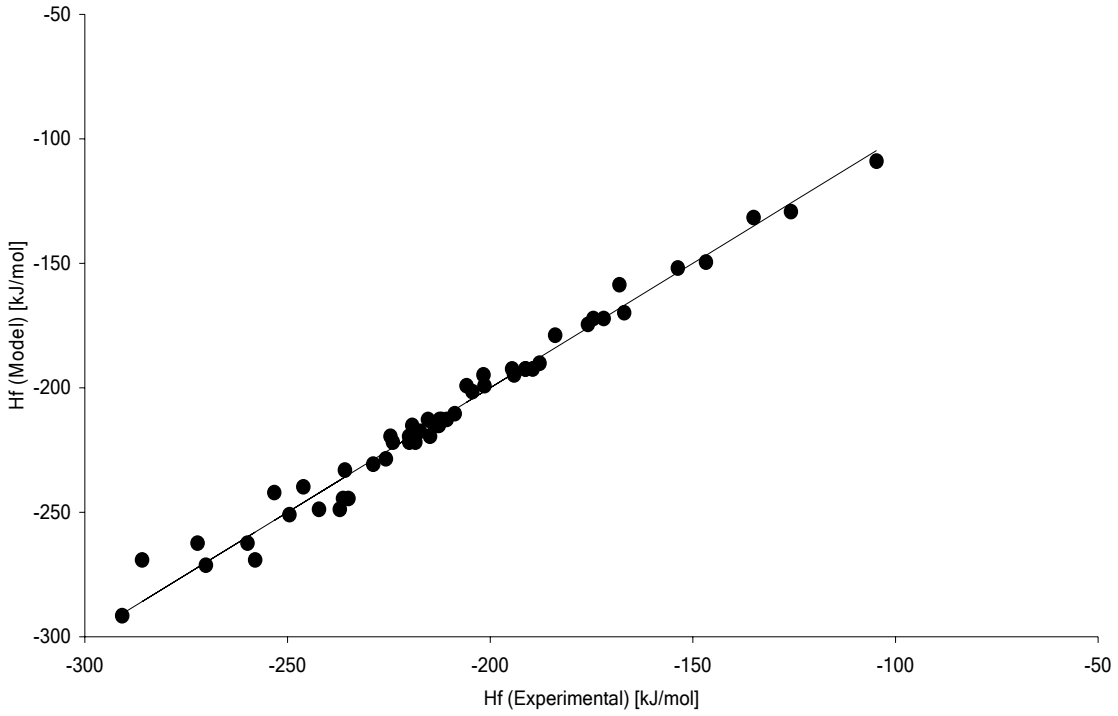

Figure 20. Alkane Standard Enthalpy of Formation Parity Plot.

Similarly, experimental data from the literature for alkenes are applied to evaluate the predictive capabilities of an expanded set of seven additional BGC contributions as presented in Table 12. The data comprises 25 alkenes including several degrees of branching and with carbon numbers ranging from C_3 to C_{12}.

Table 12. Alkene Standard Enthalpy of Formation. ΔHf° Values from BGC method with gc1[C-CH3]=-42.19, gc2[C-C2H2]=-20.64, gc3[C-C3H]=-7.95, gc4[C-C4]=2.09, gc5[Cdb-H2]=26.20, gc6[Cdb-CH]=35.96, gc7[Cdb-C2]=43.28, gc8[C-CdbH3]=-42.19, gc9[C-CdbCH2]=-19.92, gc10[C-CdbC2H]=-6.20, gc11[C-CdbC3]=7.03 in kJ/mol. [A] From Linstrom *et al.*[35]

		ng											ΔHf°,kJ/mol	ΔHf°,kJ/mol
Molecule	Group	1	2	3	4	5	6	7	8	9	10	11	(Exp) [A]	(Calc)
Propene	O3	0	0	0	0	1	1	0	1	0	0	0	20.0	20.0
1-butene	O4	1	0	0	0	1	1	0	0	1	0	0	-0.5	0.1
2-butene(z-/e-)	O4	0	0	0	0	0	2	0	2	0	0	0	-9.2	-12.5
2-methyl-1-propene	MO4	0	0	0	0	1	0	1	2	0	0	0	-17.1	-14.9
1-pentene	O5	1	1	0	0	1	1	0	0	1	0	0	-21.3	-20.6
2-pentene(z-)	O5	1	0	0	0	0	2	0	1	1	0	0	-26.3	-32.4
2-methyl-2-butene	MO5	0	0	0	0	0	1	1	3	0	0	0	-40.8	-47.3
3-methyl-1-butene	MO5	2	0	0	0	1	1	0	0	0	1	0	-27.6	-28.4
1-hexene	O6	1	2	0	0	1	1	0	0	1	0	0	-42.0	-41.2
4-methyl-1-pentene	MO6	2	0	1	0	1	1	0	0	1	0	0	-49.4	-50.1
1-heptene	O7	1	3	0	0	1	1	0	0	1	0	0	-62.8	-61.9
1-octene	O8	1	4	0	0	1	1	0	0	1	0	0	-81.2	-82.5
2-octene(z-/e-)	O8	1	3	0	0	0	2	0	1	1	0	0	-94.2	-94.3
3-octene(z-/e-)	O8	2	2	0	0	0	2	0	0	2	0	0	-92.1	-93.6
4-octene(z-/e-)	O8	2	2	0	0	0	2	0	0	2	0	0	-90.0	-93.6
3-ethyl-3-hexene	MO8	3	0	0	0	0	1	1	0	3	0	0	-104.7	-107.1
2,5-dimethyl-3-hexene(z-/e-)	DO8	4	0	0	0	0	2	0	0	0	2	0	-106.8	-109.2
2,3-dimethyl-2-hexene	DO8	1	1	0	0	0	0	2	3	1	0	0	-108.9	-122.8
3,4-dimethyl-3-hexene(z-/e-)	DO8	2	0	0	0	0	0	2	2	2	0	0	-108.9	-122.0
3-ethyl-4-methyl-3-pentene	DO8	2	0	0	0	0	0	2	2	2	0	0	-108.9	-122.0
2,4,4-trimethyl-1-pentene	TO8	3	0	0	1	1	0	1	1	1	0	0	-110.5	-117.1
2,3,4-trimethyl-2-pentene	TO8	2	0	0	0	0	0	2	3	0	1	0	-117.2	-130.6
1-nonene	O9	1	5	0	0	1	1	0	0	1	0	0	-104.0	-103.2
1-decene	O10	1	6	0	0	1	1	0	0	1	0	0	-124.2	-123.8
1-dodecene	O12	1	8	0	0	1	1	0	0	1	0	0	-165.5	-165.1

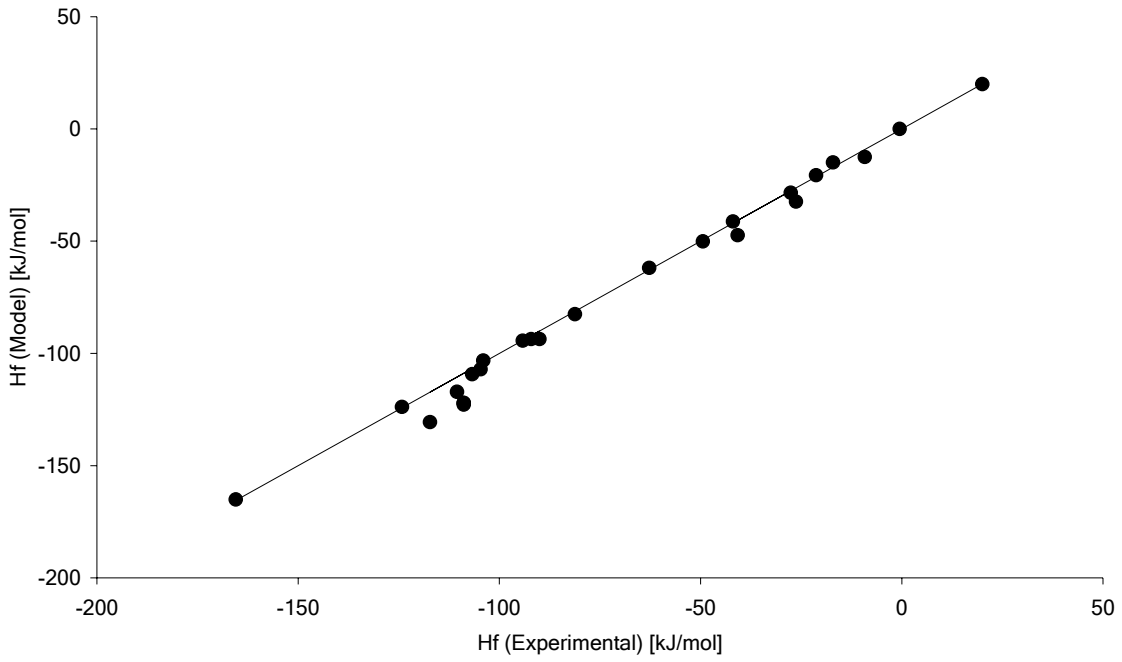

Figure 21. Alkene Standard Enthalpy of Formation Parity Plot.

Moreover, data in Figure 21 also turned out being in very good agreement with the BGC method estimates. Estimates for alkene standard enthalpies of formation resulted in an accuracy of about ±5.1 kJ/mol. Once again, the approximate measure of error is calculated using the sample standard error. As expected, higher values for the standard enthalpy of formation are observed for alkenes than for alkanes within the same carbon fraction, reflecting the lower stability of these species and the higher reactivity in the presence of electrophiles such as acid sites.

Carbenium Ion Energies

The proposed model includes 619 carbenium ions acting either as intermediates (78) or deactivation agents (541). Consequently, previous knowledge of standard enthalpies of formation in gas phase for these species is mandatory in the calculation of thermodynamic properties associated with protonation equilibria and energies of activation. However, available data on carbenium ion energetics is scarce and in most cases inaccurate. Even though precise energy estimations by means of quantum chemical calculations can be accomplished for these species, it turns out being non-practical when a large number of molecules are present because of the tremendous amount of computational power required. Therefore, an approach based on the structure of the BGC method, adapted to account for the short-ranged interactions present within a carbenium ion, is proposed so that it can be effectively applied to the estimation of standard energies of formation on carbenium ions.

The goal of the proposed method is to provide a straightforward mechanism for estimating the standard energy of formation of carbenium ions with decent accuracy. In principle, the BGC structure offers this possibility based on its ability to quantify most atom-neighboring interactions within the molecule by adding up atom-by-atom contributions. Thus, a well-selected set of data involving replications for most of the seven additional ion-focused contributions that would be present in carbenium ion structures is necessary in order to solve for the resulting BGC-like set of linear equations. By definition, the rank of constant coefficient matrix associated to the linear set of equations is always less than the number of BGC-like contributions (unknowns) and therefore the number of species (equations) to use should be greater than the number of BGC-like contributions so that the last ones could be determined by multidimensional linear regression.

Since the BGC-like contributions have to be determined by regression, the composition of the data set turns out being critical for a useful outcome. However, due to the lack of sufficient data on carbenium ion energetics, a combination of literature data and quantum chemical calculations was compiled. In the case of estimated data, ab initio calculations were performed in Gaussian98® at the MP2/6-31G++(d,p) level of theory and brought to standard conditions by means of isodesmic reactions.

The use of isodesmic reactions, which are defined as reactions where the total number of bonds and electrons are conserved, not only permits to avoid error prone calculations such as those required to take the quantum chemical result for the ion energy at 0K plus the zero point energy to the enthalpy of a perfect gas at standard conditions, but also increases the accuracy of the estimation by canceling out electron correlation effects which are often missed at moderate levels of theory. For instance, Table 13 illustrates the use of isodesmic reactions on the estimation of carbenium ion standard enthalpies of formation.

Table 13. Isodesmic Reactions. A Calculated in Gaussian 98®. [A] Level of Theory: PM2/6-31G++(d,p). [B] From Linstrom *et al.* [35]

	Ion Reactant	Reactant Molecule	Product Molecule	Ion Product	Δ
Formula	CH_3CH_2+	CH_4	CH_3CH_3	CH_3+	
Energy,Hartree/particle[A]	-78.525616	-40.316154	-79.464885	-39.311039	0.065846
Energy, kcal/mol[B]	219.0	-17.9	-20.0	**262.5**	41.3
Energy, kcal/mol (Exp.)[B]				261.3	
Formula	CH_3CH_2+	$CH_3CH_2CH_3$	CH_3CH_3	$CH_3CH_2CH_2$+	
Energy,Hartree/particle[A]	-78.525616	-118.618098	-79.464885	-117.696194	-0.017365
Energy, kcal/mol[B]	219.0	-25.0	-20.0	**203.1**	-10.9
Energy, kcal/mol (Exp.)[B]				208.0	
Formula	$(CH_3)_2CH$+	$(CH_3CH_2)_2CH_2$	$CH_3CH_2CH_3$	$(CH_3CH_2)_2CH$+	
Energy,Hartree/particle[A]	-117.705733	-197.625783	-118.618098	-196.714381	-0.000963
Energy, kcal/mol[B]	186.5	-35.1	-25.0	**175.8**	-0.6
Energy, kcal/mol (Exp.)[B]				173.0	

Table 14 presents a data set comprising 19 different gas-phase carbenium ions used on the BGCM contributions estimation. In the set, four primary carbenium ions are included looking forward to bring consistency to the BGC-like structure in the formulation. Indeed, the method turned out remarkably accurate with a sample standard error of about 8.1 kJ/mol.

Table 14. Gas Phase Carbenium Ion Standard Enthalpy of Formation. ΔHf° Values from BGC-like method with gc1[C-CH3]=-42.19, gc2[C-C2H2]=-20.64, gc3[C-C3H]=-7.95, gc4[C-C4]=2.09, gc12[C+-CH2]=942.8, gc13[C+-C2H]=861.2, gc14[C+-C3]=806.3, gc15[C-C+H3]=-42.18, gc16[C-C+CH2]=-29.33, gc17[C-C+C2H]=-29.41, gc18[C-C+C3]=-18.03 in kJ/mol. [A] From Park.[36] [B] From Gaussian 98® with Level of Theory: PM2/6-31G++(d,p).

		ng											ΔHf° kJ/mol	ΔHf° kJ/mol
Carbenium Ion	Group	1	2	3	4	12	13	14	15	16	17	18	(Exp)[A]	(Calc)
ethyl	O2[p]	0	0	0	0	1	0	0	1	0	0	0	917	901
n-propyl	O3[p]	1	0	0	0	1	0	0	0	1	0	0	871	871
n-butyl	O4[p]	1	1	0	0	1	0	0	0	1	0	0	842	851
n-pentyl	O5[p]	1	2	0	0	1	0	0	0	1	0	0	833	830
s-propyl	O3[s]	0	0	0	0	0	1	0	2	0	0	0	781	777
s-butyl	O4[s]	1	0	0	0	0	1	0	1	1	0	0	747	748
s-pentyl(2)	O5[s]	2	0	0	0	0	1	0	0	2	0	0	724[B]	718
s-hexyl(2)	O6[s]	1	2	0	0	0	1	0	1	1	0	0	712	706
s-heptyl(2)	O7[s]	1	3	0	0	0	1	0	1	1	0	0	678	686
2,4-dimethylpentyl(3)	DO7[s]	4	0	0	0	0	1	0	0	0	2	0	649[B]	634
2,2,4,4-tetramethylpentyl(3)	QO9[s]	6	0	0	0	0	1	0	0	0	0	2	596[B]	572
t-butyl	MO4[t]	0	0	0	0	0	0	1	3	0	0	0	687	680
2-methylbutyl(2)	MO5[t]	1	0	0	0	0	0	1	2	1	0	0	654	650
2-methylpentyl(2)	MO6[t]	1	1	0	0	0	0	1	2	1	0	0	631	630
3-methylpentyl(3)	MO6[t]	2	0	0	0	0	0	1	1	2	0	0	629	621
2,3-dimethylbutyl(2)	DO6[t]	2	0	0	0	0	0	1	2	0	1	0	620	608
2-methylhexyl(2)	MO7[t]	1	2	0	0	0	0	1	2	1	0	0	619	609
2,4-dimethylpentyl(2)	DO7[t]	2	0	1	0	0	0	1	2	1	0	0	609	600
2,3,3-trimethylbutyl(3)	TO7[t]	3	0	0	0	0	0	1	2	0	0	1	593	577

Additionally, Figure 22 provides with a parity plot comparing BGC-like estimates with values for the standard energies of formation of carbenium ions from Table 14. As expected, the most influential element on the energy level of a gas-phase carbenium ion is its nature. The data clearly show an important overlapping among the energies of some secondary and tertiary ions due to the impact of the carbon number in their relative stability.

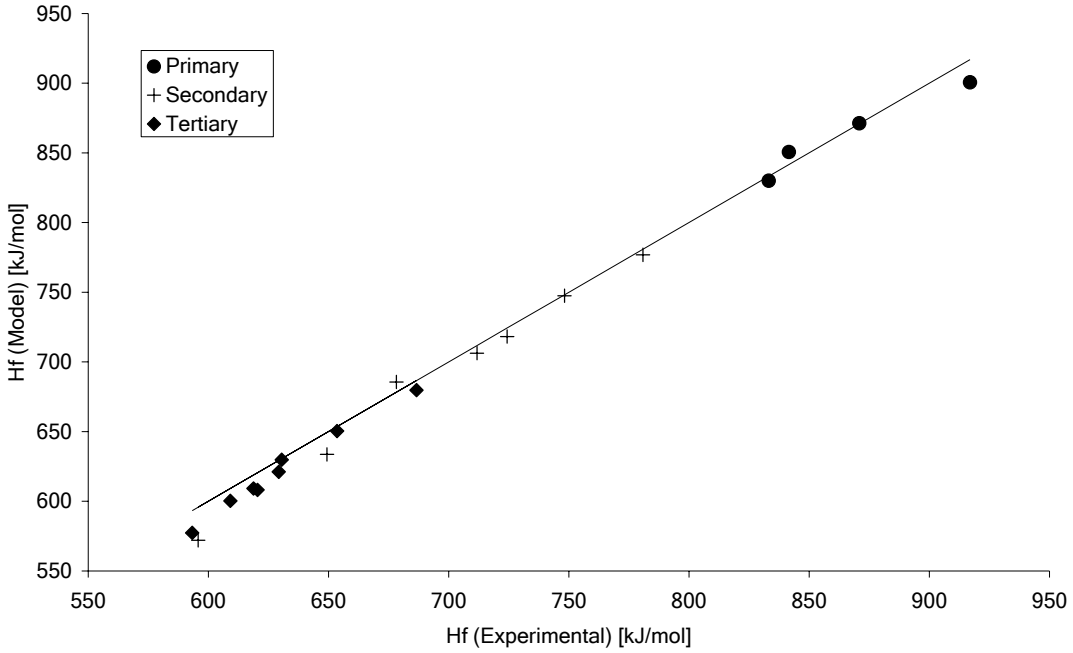

Figure 22. Carbenium Ion Standard Enthalpy of Formation Parity Plot.

In what follows, thermodynamic constraints inferred from experimental facts will be applied to obtain further reductions in the number of model parameters as well as in the number of species required to characterize the reaction mixture without losing detail at the elementary step level description. Further reduction is necessary in order to make the model tractable in terms of the number of species involve in the analysis of the reaction products.

Thermodynamic Constraints and Component Groups

By looking at the reaction product composition, there is some indication that species sharing the same degree of branching within a given carbon fraction might be very close to equilibrium. For instance, partition coefficients for butene isomers, extracted from experimental data at 393 K, turned out in good agreement with calculated values for equilibrium conditions as shown in Table 15. In this table, an estimated 1-butene/2-butene partition coefficient is obtained from Gibbs free energy minimization calculations performed in ASPEN PLUS®. Then, this value is compared to others drawn from a sample comprising three different experiments distributed along with the run-time.

Table 15. Non-Branching Isomerization Equilibrium Test. Alkenes within the O4 Component Group. [A] From Gibbs free energy minimization in ASPEN PLUS®. [B] Experimental values at run-time 1.17 h, 0.5 h and 0.40 h.

Species	Equilibrium Composition[A] @ 393K	Experimental Composition[B] @ 393 K		
Butene Space-Time ($W/F°_{O4}.M_{O4}$), h		0.4 h	0.7 h	1.0 h
1-butene	0.091	0.091	0.105	0.096
2-butene (z-/e-)	0.909	0.909	0.895	0.904
2-butene/1-butene Partition Coefficient	10.0	10.0	8.5	9.5

Based on the assumption that non-branching isomerization reaction rates for aliphatic hydrocarbons increase with carbon number, it is inferred that equilibrium conditions prevail for all species with carbon number larger than four atoms. These premises imply that the reaction rates for non-branching isomerization elementary steps such as hydride shift and methyl shift are fast enough to achieve equilibrium at reaction conditions. Thus, under this scenario, the introduction of these thermodynamic constraints would allow extending the treatment already given to alkene (de)protonation steps to those involving non-branching isomerization. Accordingly, reaction rates corresponding to 65 hydride shifts and 29 methyl shifts can now be dropped from the reaction network and replaced by equilibrium relationships. This removal reduces in six the number of model parameters to yield 16 and sets in 2742 the number of elementary step reaction rates to be calculated.

Additionally, under the non-branching isomerization equilibrium condition, the composition within a component group, comprising alkene species with similar carbon number and degree of branching at a given temperature, becomes fixed. This thermodynamic constraint permits the definition of 13 component groups for alkene species (O3, O4, MO4, MO5, DO5, MO6, DO6, MO7, DO7, TO7, MO8, DO8, TO8) entitled to simplify the number of components in the liquid phase (v-responses) to deal with from 134 (103 alkene species + 31 alkane species) to 44 (13 alkene component groups + 31 alkane species).

Based on the non-branching equilibrium condition, thermodynamic relationships among alkene species comprised within a single component group are formulated in equation (34). This equation relates the molar fraction of any member species [$x(R_r^=)$] within the component group to the overall molar fraction of the component group [$x^{cg}(R_r^=)$], which is defined as the sum over the molar fractions of the species belonging to a given component group, through the use of lumping coefficients [$LC(R_r^=)$].

$$x^{cg}(R_r^{=}) = \sum_{k=1}^{N} x(R_k^{=}) = x(R_r^{=})\,LC(R_r^{=}) = x(R_r^{=})\left[\,1 + \sum_{k\neq r}^{N-1}\left(\frac{\Delta G_{f,l}(R_k^{=}) - \Delta G_{f,l}(R_r^{=})}{R\,T}\right)\right] \tag{34}$$

The lumping coefficient of a given r^{th}-alkene species is defined by equation (34) by means of the sum of the equilibrium constants among alkene species within a given component group with respect to the r^{th}-alkene species expressed as a function of their Gibbs free energies of formation in liquid phase ($\Delta G_{f,l}$). Therefore, the lumping coefficient is indeed a thermodynamic quantity that only depends on temperature and thereof it can be expressed on equation (35) as a function of the enthalpies of formation in liquid phase ($\Delta H_{f,l}$) after canceling out all non-structural contributions related to the entropy.

$$LC(R_r^{=}) = 1 + \sum_{k\neq r}^{N-1}\left(\frac{\sigma_{gl}(R_r^{=})}{\sigma_{gl}(R_k^{=})}\right)\left(-\frac{\Delta Hf_{f,l}(R_k^{=}) - \Delta H_{f,l}(R_r^{=})}{R\,T}\right) \tag{35}$$

In order to estimate the enthalpies of formation in liquid phase, the present model follows the calculation pathway described in equation (36). The pathway starts with the standard enthalpy of formation ($\Delta H°_{f,g}$). After neglecting the enthalpy change with pressure from the perfect gas condition, follows an isothermal enthalpy change through the enthalpy change of vaporization ($\Delta H°_{vap}$) at standard conditions towards the liquid phase state. Finally, the temperature of interest is reached by an isobaric enthalpy change, estimated by means of the liquid heat capacity (C_{liq}).

$$\Delta H_{f,l}(R_k^{=}) = \Delta H°_{f,g}(R_k^{=}) - \Delta H°_{vap}(R_k^{=}) + \int_{T°}^{T} C_{liq}(R_k^{=})\,dT \tag{36}$$

In what precedes, liquid heat capacities and enthalpy changes of vaporization are required to apply calculation pathways leading to obtain temperature-dependent lumping coefficients and heats of protonation for all species. Therefore, reliable estimation methods based on molecular structural information would be desirable for the estimation of these thermodynamic properties. Consequently, the present model adopted two group contribution methods taken from the literature and set them as property estimators for the 134 species in liquid phase.

First, a method reported by Rùzicka *et al.*[37] is applied as a group contribution method developed to the estimation of the liquid heat capacity of aliphatic hydrocarbons as a function of temperature in the range from the melting temperature to the normal boiling temperature. It is based on a set of structural contribution parameters adjusted by means of liquid heat capacity data compiled

from over 1300 organic liquids. Contributions include atom-neighboring interactions within the molecule. As indicated by equation (37), structural contributions (c_i), conveniently reported on Table 16, must be properly added in order to calculate a set of temperature-independent coefficients (C_l) to be used at equation (38), which yields the liquid heat capacity as a polynomial function of temperature.

$$C_l(\bar{R_k}) = \sum_{i=1}^{n_c} ng_i \; c_{i,l} \tag{37}$$

Table 16. Group Contribution Method for Liquid Heat Capacity.

Group	c_1	c_2	c_3	Temp. Range, K
C-CH_3	3.8452	-0.35997	0.19489	80 - 490
C-C_2H_2	2.7972	-0.054967	0.10679	80 - 490
C-C_3H	-0.42867	0.93805	0.0029498	85 - 385
C-C_4	-2.9353	1.4255	-0.085271	145 - 395
C_{db}-H_2	4.1763	-0.47392	0.099928	90 - 355
C_{db}-CH	4.0749	-1.0735	0.21413	90 - 355
C_{db}-C_2	1.9570	-0.31938	0.11911	140 - 315
C-$C_{db}CH_2$	2.0268	0.20137	0.11624	90 - 355
C-$C_{db}C_2H$	-0.87558	0.82109	0.18415	110 - 300
C-$C_{db}C_3$	-4.8006	2.6004	-0.040688	165 - 295

$$C_{liq}\left(\bar{R_k}\right) = R\left[\, C_1 + C_2\left(T/100\right) + C_3\left(T/100\right)^2 \,\right] \tag{38}$$

Then, a group contribution method developed by Constantinou *et al.*[38] is applied to the estimation of the enthalpy change of vaporization at standard conditions. The method is based on tabulated values for the different structural contributions present among aliphatic hydrocarbons. Corresponding values for these contributions are presented on Table 17.

In general, the present method does not consider atom-neighboring interactions. Instead, it sets individual contributions to particular groups of atoms independently of their bonding. Thus, once individual group contributions within the molecule have been identified, equation (39) is used to estimate the value of the enthalpy change of vaporization.

Table 17. Group Contribution Method for Enthalpy Change of Vaporization.

Group	d_i
CH_3	0.49504
CH_2	0.55926
CH	0.33327
C	0.15443
CH_2=CH	0.80750
CH=CH	0.88640
CH_2=C	0.81749
CH=C	0.98358
C=C	1.1236

$$\Delta H^{\circ}_{vap}\left(\bar{R_k}\right) = R\left[0.8213 + \sum_{i=1}^{n_c} ng_i\, d_i\right] \tag{39}$$

Finally, an additional thermodynamic constraint leading to a further reduction in the number of model parameters is identified. This additional constraint results from the reversibility condition relating oligomerization and β-scission elementary steps. Because of this condition, TST establishes that common values for the intrinsic energy barrier (E°) and the transfer coefficient (α) must be applied to both elementary steps since the subtraction of the energies of activation for reversible elementary steps must yield the standard heat of reaction. Thus, the β-scission single event frequency factor ends up being the only model parameter necessary to determine the rates of 554 β-scission elementary steps.

In conclusion, thermodynamic constraints comprising the rigorous lumping of species in equilibrium and the reversibility of oligomerization/β-scission elementary steps entitle the formulation of a feasible kinetic model at the elementary step level for the solid acid alkylation of isobutane with butenes by achieving such a reduction in the number of parameters so that only 14 model parameters can properly describe a reaction kinetics involving 2742 elementary step rates and 753 species.

Rate Expressions at the Single Event Level

Along with this section, a consistent methodology has been applied to the elementary step level description of the kinetics of solid acid alkylation towards the derivation of a more tractable model formulation by means of the single event kinetics. In such a way, the original rates at the

elementary step level can now be expressed in terms of the rates at the single event level where only 14 model parameters, 44 component groups molar fractions for the liquid bulk and 541 surface concentrations for irreversibly adsorbed species are needed for a complete model description.

In summary, equation (40) devises the most relevant features of a 2742-dimensional reaction rate vector (r_j), which comprises the reaction rate expressions at the single event level, derived from equations (11)-(14), (20), (22), (23) and (34).

$$r_j = \begin{cases} n_{e_j}\,\tilde{A}_{pcp}\,\exp\left(-\frac{E^{\circ}_{pcp}+\alpha_{pcp}\,\Delta H^{\circ}_j}{R\,T}\right)K_p(R_i^{=};R_n^{+})\left(\frac{V_L}{V_p}\right)\overline{C}_{sat}\,C^{t}_{H+}\left(\frac{\varphi}{1+\theta_{rev}}\right)\frac{x^{cg}(R_i^{=})}{LC(R_i^{=})} \\ n_{e_j}\,\tilde{A}_{\beta s}\,\exp\left(-\frac{E^{\circ}_{olig}+(1-\alpha_{olig})\,\Delta H^{\circ}_j}{R\,T}\right)K_p(R_i^{=};R_n^{+})\left(\frac{V_L}{V_p}\right)\overline{C}_{sat}\,C^{t}_{H+}\left(\frac{\varphi}{1+\theta_{rev}}\right)\frac{x^{cg}(R_i^{=})}{LC(R_i^{=})} \\ n_{e_j}\,\tilde{A}_{olig}\,\exp\left(-\frac{E^{\circ}_{olig}+\alpha_{olig}\,\Delta H^{\circ}_j}{R\,T}\right)K_p(R_i^{=};R_n^{+})\left(\frac{V_L}{V_p}\right)\overline{C}^{2}_{sat}\,C^{t}_{H+}\left(\frac{\varphi}{1+\theta_{rev}}\right)\frac{x^{cg}(R_i^{=})}{LC(R_i^{=})}\,\frac{x^{cg}(R^{=})}{LC(R^{=})} \\ n_{e_j}\,\tilde{A}_{ht}\,\exp\left(-\frac{E^{\circ}_{ht}+\alpha_{ht}\,\Delta H^{\circ}_j}{R\,T}\right)K_p(R_i^{=};R_n^{+})\left(\frac{V_L}{V_p}\right)\overline{C}^{2}_{sat}\,C^{t}_{H+}\left(\frac{\varphi^2}{1+\theta_{rev}}\right)\frac{x^{cg}(R_i^{=})}{LC(R_i^{=})}\,x(R) \\ n_{e_j}\,\tilde{A}_{\beta s}\,\exp\left(-\frac{E^{\circ}_{olig}+(1-\alpha_{olig})\,\Delta H^{\circ}_j}{R\,T}\right)C_{R_m^{+}} \end{cases} \tag{40}$$

$$\theta_{rev} = \sum_{n=1}^{N} K_p(R_i^{=};R_n^{+})\left(\frac{V_L}{V_p}\right)\overline{C}_{sat}\,\frac{x^{cg}(R_i^{=})}{LC(R_i^{=})} \tag{41}$$

In addition, equation (41) states the final expression for the reversible fractional site coverage (θ_{rev}) as a function of the molar fraction composition of the liquid bulk.

REACTOR MODEL FORMULATION & PARAMETER ESTIMATION

In what follows, a reactor model for the fixed bed solid acid alkylation process is formulated such that, together with the single event kinetic model and the experimental data previously presented, values for the model parameters can be estimated.

The Transient Pseudohomogeneous One-Dimensional Model with Plug Flow

In the present study, the solid acid alkylation of isobutane with butenes at moderate temperatures is carried out in a fixed bed catalytic reactor operating under isothermal conditions. Along this fixed bed reactor, the transformation of reactants into products occurs by heterogeneous reactions occurring on the catalyst surface. These transformations involve a continuous exchange of species between the liquid bulk and the catalyst surface. Diffusion through the stagnant liquid inside the catalyst particles is responsible for this exchange. In addition, chemical reactions develop compositional gradients along and across the catalyst bed causing axial and radial dispersion effects in the convective flow of the liquid bulk.

The selection of experimental conditions such as particle size, superficial velocity and reactor geometry aims to minimize the occurrence of axial and radial dispersion as well as of interfacial and intraparticle gradients. Consequently, instantaneous local equilibria at the interfaces delimiting the liquid bulk, the liquid inside the zeolite cages and the catalyst surface are assumed, leaving the convective flow in axial direction as the only transport mechanism present. Based on this assumption, a pseudohomogeneous one-dimensional model with plug flow is proposed for the experimental reactor.

The application of conservation principles to the one-dimensional plug flow model leads to equation (42). This equation describes the evolution of the vector of product yields ($\hat{Y}$) [equation (43)] with butene space-time ($W/F^{\circ}_{O4}.M_{O4}$) and contains the stochiometric coefficient matrix ($\mathbf{v}^{f}$) for the liquid phase, the diagonal matrix of molecular weights ($\mathbf{M}$) and the vector of reaction rates ($\dot{r}$). The product of the 44 x 2742 stochiometric coefficient matrix, which provides relationships derived from the reaction network, with the 2742-dimensional vector of reaction rates delivers a 44-dimensional vector with the net production rates for each component of the liquid phase.

$$\frac{\partial \hat{Y}}{\partial (W/F^{\circ}_{O4}\, M_{O4})} = \frac{(3600)\,100}{1+F^{\circ}_{MP4}M_{MP4}\,/\,F^{\circ}_{O4}M_{O4}}\,\mathbf{M}\cdot\mathbf{v}^{f}\cdot\bar{r}\,(\hat{Y},\overline{C}_{R_m^+}) \tag{42}$$

$$\hat{Y} = \left\{\hat{Y}_1, \hat{Y}_2, \ldots, \hat{Y}_v\right\}^T \tag{43}$$

As a consequence of the catalyst deactivation, the reactor operates in transient state. The product yield profiles along the reactor change as the irreversible site coverage increases with run-time. These changes are accounted for in equation (42) through the reaction rate dependency on the surface concentrations of the irreversible adsorbed ions (C_{Rm+}). Accumulation of these species on the solid phase is responsible for the catalyst deactivation and dictates the evolution of the profiles with the run-time (t). In contrast, the very small accumulation of matter in the liquid phase makes unnecessary a time derivative in equation (42). Even though there is a significant change in the number of moles of alkene species in the reaction mixture, the accumulation term is neglected because the overall concentration remains almost constant due to its high dilution in isobutane.

As mentioned before, irreversibly adsorbed species are not excluded from acting as reactants for surface elementary steps. Under this scenario, surface elementary steps such as hydride shift, methyl shift and PCP branching can be assumed to be quasi-equilibrated due to the longer residence time associated to irreversibly adsorbed ions. In contrast, surface elementary steps involving the desorption of a C_9+ ion such as hydride transfer and deprotonation are explicitly forbidden. On the other hand, in the case of oligomerization and β-scission, these elementary steps are limited to those required for the formation of the C_9+ ion and their corresponding reverse steps.

In order to account for the irreversibly adsorbed species in the model, conservation principles are applied to the solid surface so that the accumulation of these species can be written in terms of the reaction rates as follows in equation (44). In this expression [equation (45)], the evolution of the vector of surface concentrations for the irreversibly adsorbed ions with run-time, becomes a function of the stochiometric coefficient matrix for the solid phase ($\mathbf{v}^s$) and the vector of reaction rates. Here, the 541 x 2742 stochiometric coefficient matrix comprises all the reaction network relationships involving irreversibly adsorbed ions.

$$\frac{\partial}{\partial t}\overline{C}_{R_m^+} = (3600)\,\mathbf{v}^{s}\cdot\bar{r}\,(\hat{Y},\overline{C}_{R_m^+}) \tag{44}$$

$$\overline{C}_{R_m^+} = \left\{ \overline{C}_{R_1^+}, \overline{C}_{R_2^+}, \ldots, \overline{C}_{R_M^+} \right\}^T \tag{45}$$

Together, equations (42) and (44) form a set of Partial Differential Equations (PDE) describing the evolution of the liquid phase molar flowrates and the surface concentration of irreversible adsorbed ions with butene space-time and run-time. The structure of the PDE suggests an integration strategy based on the discretization of both run-time and butene space-time. Consequently, the discretization process leads to the separation of the PDE problem into a set of non-linear first order Ordinary Differential Equations (ODE) described in equation (42) and a set of linear first order ODE with constant coefficients presented in (46).

$$C_{H+}^t \frac{\partial}{\partial t}\left(\frac{C_{R_m^+}}{C_{H+}^t}\right) = \left(\sum_{j=1} r'_{j,olig}\right)\left(1 - \sum_{k=1}^{M} \frac{C_{R_k^+}}{C_{H+}^t}\right) - \left(\sum_{j=1} r'_{j,\beta s}\right)\left(\frac{C_{R_m^+}}{C_{H+}^t}\right) \tag{46}$$

The adopted integration strategy yields two coupled Initial Value Problems (IVP). In the first IVP, a 44-dimensional ODE set described by equation (42) is integrated along butene space-time by means of the Numerical Differentiation Formula (NDF) scheme for stiff problems implemented by Shampine *et al.*[39,40] Integration of this IVP delivers the product yield profiles with respect to butene space-time for a given run-time. The integrator starts with the reactor inlet yields ($\hat{Y}^\circ$) serving as the initial condition as indicated in (47).

$$\hat{Y}\left(W / F_{O4}^\circ M_{O4} = 0, t\right) = \hat{Y}^\circ \tag{47}$$

The second set, a 541-dimensional eigenvalue problem described in equation (46), has an analytical solution based on the diagonalization of the constant coefficient matrix. The solution of this set for a given butene space-time requires also setting an initial condition. Consequently, expression (48) establishes the adopted initial condition by setting a fresh catalyst load for each experimental run.

$$\overline{C}_{R_m^+}\left(W / F_{O4}^\circ M_{O4}, t = 0\right) = 0 \tag{48}$$

The overall integration of the reactor model proceeds by solving for the profiles along a two-dimensional grid in butene space-time and run-time. Time steps for both dimensions are

sequentially halved until differences between two consecutive solution grids become negligible.

Asymptotic solutions of the reactor model equations provide interesting insights into the fixed bed operation of this process. In the first place, when the butene space-time is large enough (infinite), limiting reactants become extinct and reversible reactions reach equilibrium. In the mathematical model, this is equivalent to neglecting the derivative with respect to butene space-time so that equation (42) turns into expression (49). At equilibrium, the product yields at the reactor exit no longer depend on the butene space-time and therefore a flat profile is achieved for a given level of deactivation (given profile of irreversibly adsorbed ions).

$$\mathbf{v}^{f} \cdot \bar{r}(\hat{Y}^{eq}, \overline{C}_{R_m^+}) = 0 \tag{49}$$

In the second place, when the run-time is large enough (infinite), steady state operation is achieved and therefore both, the product yield and the surface concentrations of the irreversibly adsorbed ions become no longer dependent on the run-time. Equation (50) presents the mathematical expression that reflects this situation.

$$\mathbf{v}^{s} \cdot \bar{r}\left(\hat{Y}, \overline{C}^{\infty}_{R_m^+}\right) = 0 \tag{50}$$

Experimental results showed that for all runs, the operation reaches steady state with respect to the run-time. An even more relevant observation is that the conversion has not dropped to zero when the steady state has been reached. This observation strongly supports the approach taken in the present reactor model concerning the reactivity of the irreversibly adsorbed ions.

A complete solution of the present reactor model for a typical run-time of about 8 hours in a 100 x 100 grid consumes a significant amount of computational time. For instance, the average time of a single run at the Texas A&M University supercomputing facilities (64-processor SGI Origin 3800) can reach up to 2 hours. Therefore, to complete of the parameter estimation process in a realistic amount of time, when the integration code identifies the occurrence of equilibrium or steady state conditions in a given run, it switches to the corresponding asymptotic solution.

The Objective Function

In what precedes, the single event kinetic model of the solid acid alkylation process was embedded into a pseudo-homogeneous one-dimensional plug flow model of a fixed bed reactor in order to reproduce the available experimental observations. In what follows, values for the model parameters are estimated by means of regression methods. The general approach to parameter estimation adopted in the present study is based on the treatment presented in Froment *et al.*[41] and also involves statistical tests.

Let the proposed model be defined as (51). The components of the v-dimensional vector of model responses ($\hat{Y}_h$) correspond to the solution of the model represented by some implicit functionality with components (f_h). This multiresponse function depends on the applied set of experimental conditions for the i^{th}-experiment ($\dot{X}_i$) and the vector of model parameters (β) defined in (52).

$$\hat{Y}_h = f_h(\overline{X}_i, \overline{\beta}) \quad , h=1,\ldots,v \tag{51}$$

$$\overline{\beta} = \left\{\tilde{A}_{pcp}, E^{\circ}_{pcp}, \alpha_{pcp}, \tilde{A}_{olig}, E^{\circ}_{olig}, \alpha_{olig}, \tilde{A}_{ht}, E^{\circ}_{ht}, \alpha_{ht}, \tilde{A}_{\beta s}, \Delta\hat{S}_p, \Delta E^{sec}_{+}, \Delta E^{tert}_{+}, \gamma_c\right\} \tag{52}$$

A multiresponse objective function is defined in (53) based on the least squares minimization criterion assuming that the errors are normally distributed with zero mean and the error variances are not constant but not correlated. This function sums the squares of the errors over all the experiments and depends only on the values of the model parameters.

$$S(\overline{\beta}) = \sum_{h=1}^{v}\sum_{k=1}^{v}\omega_{h,k}\sum_{i=1}^{n}\left[Y_{i,h} - f_h(\overline{X}_i, \overline{\beta})\right]\cdot\left[Y_{i,k} - f_k(\overline{X}_i, \overline{\beta})\right] \tag{53}$$

Proper estimation of the (v x v) elements of the inverse of the error covariance matrix ($\omega_{h,k}$) requires an important number of experiment replications. The diagonal of the error covariance matrix corresponds to the error variances of the responses whereas the off-diagonal elements comprise their covariances. When replicates are not available weighting factors are used instead of $\omega_{h,k}$. In the present study, the adopted weighting factor aims to balance the contribution of each response within the objective function. Equation (54) shows the weighting factor definition according to the nature and value of the responses.

$$\omega_{h,k} = \begin{cases} \dfrac{\sum_{i}^{n} Y_{i,h}^{-1}}{\sum_{i=1}^{n}\sum_{j=1}^{v} Y_{i,j}^{-1}} & , h = k \, , \, Y_{i,h} \neq 0 \\ 1 & , h = k \, , \, Y_{i,h} = 0 \\ 0 & , h \neq k \end{cases} \tag{54}$$

A single evaluation of the objective function (53) for a given set of parameters involves 9 model runs covering 79 experiments (n) with 44 responses (v) per experiment.

Next to the definition of the objective function, there is the process of parameter estimation. In principle, the least squares criterion establishes that the minimization of the objective function as defined must yield the vector of parameter estimates ($\bar{b}$). When the model is adequate and the experimental error is normally distributed with zero mean, this vector is an unbiased estimate of the parameters. Thus, expression (55) presents a general definition of the process of parameter estimation, regardless of the method applied for this.

$$\bar{b} = \min_{\beta} \left\{ S(\bar{\beta}) \right\} \tag{55}$$

In the present formulation, constrained parameter estimation is performed in order to account for the physicochemical constraints inherent to the fundamental nature of the parameters of the proposed model.

Parameter Estimation

Multidimensional nonlinear least squares minimization is applied to parameter estimation. By alternating the use of two algorithms for constrained and unconstrained optimization, the parameters are iteratively improved based along with the minimization of the objective function. For constrained optimization, a Sequential Quadratic Programming (SQP) algorithm is used together with the parameter constraints presented in Table 18. An implementation of the SQP algorithm is used in the present work. In general, the solution of a constrained optimization problem involves the solution of several quadratic programming (QP) sub-problems by means of

an unconstrained optimization algorithm. For problems that are nonlinear in the parameters such as the present one, the formulation of the QP sub-problem involves not only the linearization of the objective function but also the inclusion of linear constraints. Details about the SQP algorithm and its implementation are reported in Grace.[42] Once the constrained optimization procedure is terminated, the solution from this algorithm is fed to an implementation of the Marquardt algorithm in order to ensure that the solution corresponds to a minimum where the gradient of the multiresponse objective function is zero. This zero-gradient condition must be satisfied so that statistics to test the significance of the parameters would be properly applied after regression.

Reparametrization of the vector of parameters shown in (52) results in expression (56). In the first place, single event frequency factors are reparametrized by estimating the normal logarithms instead. This treatment ensures positive values for these parameters and improves convergence by making changes on these large numbers more significant to the method. In the second place, intrinsic energy barriers are reparametrized by introducing their ratios with the transfer coefficients. These ratios aim to reduce the correlation between these two parameters and facilitate the formulation of linear constraints around them.

$$\overline{\beta} = \left\{ \ln \tilde{A}_{pcp}, \frac{E^{\circ}_{pcp}}{R\,\alpha_{pcp}}, \alpha_{pcp}, \ln \tilde{A}_{olig}, \frac{E^{\circ}_{olig}}{R\,\alpha_{olig}}, \alpha_{olig}, \ln \tilde{A}_{ht}, \frac{E^{\circ}_{ht}}{R\,\alpha_{ht}}, \alpha_{ht}, \ln \tilde{A}_{\beta s}, \frac{\Delta \hat{S}_{p}}{R}, \frac{\Delta E^{sec}_{+}}{R}, \frac{\Delta E^{tert}_{+}}{R}, \frac{\gamma_{c}}{R} \right\} \quad (56)$$

In the third place, energy-related parameters are conveniently divided by the universal gas constant (R) in order to scale the problem and to simplify the management of engineering units. The new reparametrized vector shown in (56) is used in both the constrained and the unconstrained optimizations. A detailed description of the advantages of reparametrization as an effective mechanism to improve the accuracy of parameter estimation procedures can be found in Rawlings *et al.*[43]

Table 18. Parameter Constraints Summary. Full application to the proposed model yields 2118 linear constraints.

Parameter(s)	Linear Constraint	Rationale
$\frac{E^{\circ}_{pcp}}{R\,\alpha_{pcp}}, \frac{E^{\circ}_{olig}}{R\,\alpha_{olig}}, \frac{E^{\circ}_{ht}}{R\,\alpha_{ht}}$	$\frac{Ea_j}{R} = \frac{E^{\circ}_{ElemStepType}}{\alpha_{ElemStepType}\,R} + \frac{\Delta H^{\circ}_j}{R}, \Delta H^{\circ}_j < 0$	Energy of activation must be a positive quantity
$\alpha_{pcp}, \alpha_{olig}, \alpha_{ht}$	$0 < \alpha_{ElemStepType} < 1$	Energy of activation must be a fraction of the intrinsic energy barrier
$\frac{\Delta E^{sec}_{+}}{R}, \frac{\Delta E^{tert}_{+}}{R}, \frac{\gamma_c}{R}$	$-200\ {}^{kJ}\!/_{mol} < \frac{\Delta H^{\circ}_p\left(R^{=}_i; R^{+}_n\right)}{R} < 0$	Heat of Protonation must be exothermic with a lower bound of about -200 kJ/mol.
$\frac{\Delta E^{sec}_{+}}{R}, \frac{\Delta E^{tert}_{+}}{R}, \frac{\gamma_c}{R}$	$\frac{\Delta H^{\circ}_p\left(R^{=}_x; R^{+}_{nx}\right)}{R} < \frac{\Delta H^{\circ}_p\left(R^{=}_y; R^{+}_{ny}\right)}{R}, n_C(R^{=}_x) > n_C(R^{=}_y)$	For similar types of carbenium ions, the magnitude of the heat of protonation must increase with the carbon number
$\frac{\Delta \hat{S}_p}{R}$	$\frac{\Delta \hat{S}_p}{R} < 0$	Intrinsic entropy must decrease on protonation
$\frac{\Delta E^{sec}_{+}}{R}$	$\frac{\Delta E^{sec}_{+}}{R} > 0$	Stabilization energy of a secondary carbenium ion must be positive
$\frac{\Delta E^{tert}_{+}}{R}$	$\frac{\Delta E^{tert}_{+}}{R} > 0$	Stabilization energy of a tertiary carbenium ion must be positive
$\frac{\gamma_c}{R}$	$\frac{\gamma_c}{R} < 0$	Stabilization energy should decrease with carbon number

Parameter constraints shown in Table 18 are derived from the fundamentals of the TST and thermodynamics. In most cases their rationale is obvious as well as their implementation. In addition, some constraints involve linear combinations of several parameters in one expression. Therefore, the whole set of parameters can be expressed as a linear set of algebraic inequalities in matrix form making easier its implementation into the QP sub-problem.

In the present work, the task of parameter estimation becomes cumbersome due to the large amount of computing time required to evaluate the objective function. Moreover, the transient nature of the process leading to the occurrence of moving deactivating zone limits the descriptive power of the least squares formulation and makes the convergence of most gradient-based algorithms more difficult to achieve. In order to overcome these limitations, a significant amount of human operator intervention is required. This intervention comprises testing several different

startup values for the parameters on a trial-and-error basis, setting higher weight values to some key responses that define important features observed at the experiments such as peak values and steady state ones and completing the optimization process by using consecutive runs with manual changes in the parameters in between.

In gradient-based methods like Marquardt there is no guarantee that the solution corresponds to a global minimum. Instead, additional tests and different startup values must be tested to validate the solution as a likely global minimum. In addition, powerful statistics derived from the linearization of the model in the vicinity of the solution provide tests which permit to make educated decisions about the accuracy of the estimates. In what follows, those statistics are formulated opening the road to the presentation and discussion of the results for the parameter estimation.

Statistical Tests

In the present work, the formulation of statistical tests for models and parameters associated to nonlinear regression methods follows the treatment found in Froment *et al.*[41] This treatment allows the formulation of statistics from nonlinear regression by means of model linearization as described in Gallant.[44]

Let the model be expressed as a vector of functions (f) depending on a set of experimental conditions (X_i) and on the model parameters (β) as indicated in (57). Assuming that the model is adequate, this vector function should reproduce the vector of experimental responses ($\bar{Y}$) for the i^{th}-experiment with experimental errors (e) normally distributed with zero mean and unknown variance (σ^2). Based on assumptions of variable variance and uncorrelated responses, this description leads to the multiresponse objective function for the weighted least squares method stated already in (53).

$$\overline{Y}_i = \bar{f}\left(\overline{X}_i, \overline{\beta}\right) + \overline{e}_i \quad , \quad e_{i,h} \sim N(0, \sigma^2) \tag{57}$$

The vector of parameter estimates is obtained from the minimization of the multiresponse objective function (53) as indicated in (55). In the vicinity of this vector, the model function is linearized through a truncated Taylor's series expansion according to (58). This approximation

yields the vxp-dimensional Jacobian matrix (**J**), which is defined as the transpose of the matrix of the function gradients. Equation (59) states the derivatives required for the calculation of the Jacobian matrix. After linearization, it is important to set a clear difference between the model function and the objective function by noticing that in parameter estimation, only the gradient of the objective function becomes zero whereas the gradients of the model functions would not. In fact, these gradients within the Jacobian matrix will become key elements in the estimation of the parameter covariance matrix.

$$\bar{f}(\bar{X}_i, \bar{b}) \approx \bar{f}(\bar{X}_i, \bar{\beta}) + \mathbf{J}|_{\bar{X}i, \bar{b}=\bar{\beta}}(\bar{b} - \bar{\beta}) \tag{58}$$

$$J^{(i)}_{h,j} = \frac{\partial f_h(\bar{X}_i, \bar{\beta})}{\partial \beta_j} \tag{59}$$

The testing of models and their parameters greatly depends on the parameter covariance matrix (**V**). For nonlinear models, calculation of this matrix after linearization yields:

$$\mathbf{V}(\bar{b}) = \sum_{i=1}^{n} \left[\mathbf{J}_i^T \boldsymbol{\omega} \mathbf{J}_i \right]^{-1} = \sum_{i=1}^{n} \left(\sum_{h=1}^{v} \sum_{k=1}^{v} J^{(i)}_{j,h} \, \omega_{h,k} \, J^{(i)}_{k,s} \right)^{-1}_{j,s} \tag{60}$$

In the absence of replicated experiments, the elements of the inverse of the experimental covariance matrix are replaced by weights. The pxp-dimensional parameter covariance matrix leads to the formulation of statistics for hypothesis testing of the model and its parameters. Another important statistic required for hypothesis testing is the experimental variance, which is an unknown quantity and therefore has to be estimated from the sample variance. For multiresponse models, the sample variance as an unbiased estimator of the experimental variance can be calculated from (61).

$$s^2 = \frac{S(\bar{b})}{n v - p} \tag{61}$$

To test the model, the significance of the regression is evaluated by means of an F-test (lack-of-fit test). This test is based on a statistic calculated from the ratio between the regression sum of squares and the residual sum of squares:

$$\frac{nv-p}{p}\,\frac{\sum_{h=1}^{v}\sum_{k=1}^{v}\omega_{h,k}\sum_{i=1}^{n}f_h(\overline{X}_i,\overline{b})\,f_k(\overline{X}_i,\overline{b})}{S(\overline{b})} > F(p, nv-p, 1-\alpha) \tag{62}$$

To perform the test, the ratio is compared to the critical value of the F-distribution with nv-p degrees of freedom with a target probability of 1-α (i.e. 95%) as shown in (62). In the test, the model is rejected when the inequality fails because of lack of fit. As a general trend, the larger the calculated ratio is, the better the model fits.

Another important test for parameter estimates is to evaluate the hypothesis (Ho) about whether parameter estimates are significantly different from zero or not at a given confidence level (i.e. 95%). The acceptance or rejection of this hypothesis depends on the statistic presented in (63).

$$Ho: b_j \neq 0 \Leftrightarrow \frac{|b_j|}{\sqrt{s^2\,V_{j,j}(\overline{b})}} > \left| t_{nv-p,\,\alpha/2} \right| \tag{63}$$

This test assumes that the experimental errors are normally distributed and therefore their unbiased estimators (sample errors or residuals) are t-distributed with nv-p degrees of freedom. Rejection of the hypothesis on (63) occurs when the ratio between the absolute value of the parameter and its unbiased estimate for the error is less than the critical value of the t-distribution for nv-p degrees of freedom at a confidence level of 1-α (i.e. 95%).

Finally, a test on each parameter estimate against a single reference value is formulated by means of the approximate confidence intervals (nonlinear model). This intervals comprises all reference values that are not significantly different from the parameter estimate at a given confidence level 1-α (i.e. 95%). Equation (64) presents a formula for the calculation of the symmetric interval based on previously determined statistics.

$$\beta_j = b_j \pm t_{nv-p,\,\alpha/2}\sqrt{\frac{s^2\,V_{j,j}(\overline{b})}{nv-p}} \tag{64}$$

Application of presented statistical tests allows making educated decisions about the predictive capabilities of the model and the quality of the parameter estimates obtained.

Results and Discussion

Figure 23 illustrates the evolution of the values for the objective function with respect to the number of iterations during the application of the SQP and Marquardt algorithms for the last run conducted within the parameter estimation procedure. In this procedure, both constrained (SQP) and unconstrained (Marquardt) optimizers are consecutively applied in order to improve parameter values leading to a minimum of the objective function. At this minimum, statistical tests are applied to the solution leading to changes in the parameter startup values for the next run iteration. Human operator intervention in setting up new startup values between runs is a key step in the overall optimization procedure. This intervention is necessary in order to overcome algorithm limitations in finding out a global minimum. In general, when the algorithm converges to a solution, chances are that this solution corresponds to a local minimum. The value of the objective function and the results of statistical tests permit to discriminate among local minima in order to come up with the most likely set of parameter estimates that would lead to a global minimum. However, there is no other guarantee than the adequacy of the model and the comparison among solutions in a trial-and-error basis that the set of parameter estimates indeed corresponds to a global minimum.

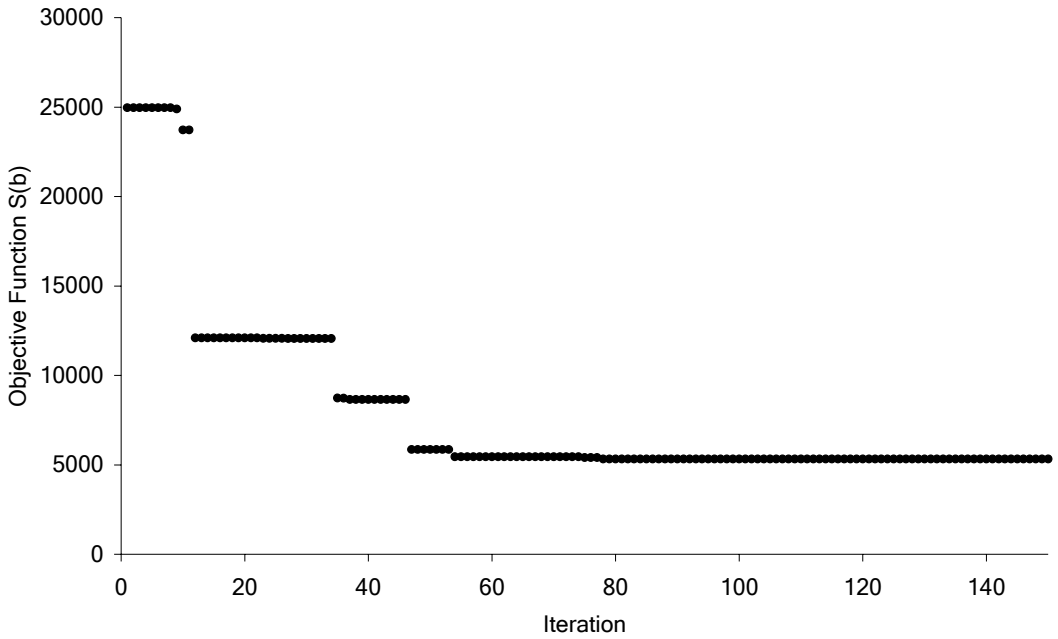

Figure 23. Performance of SQP and Marquardt Algorithms in Parameter Estimation. Evolution of the objective function with respect to the number of iterations for the last run after human operator intervention.

Table 19 presents the results of the parameter estimation for the kinetic model. These results include approximate confidence intervals and t-tests for the reparametrized values of the model parameters. The reported results correspond to the best fit achieved along the optimization procedure described before.

Table 19. Parameter Estimates. [A] After reparametrization. Significance of regression (F-test) yields an F-value of 2589 to reject the lack-of-fit hypothesis with F critical value of 0.70. [B] Estimates significantly different from zero for values greater than the t critical value of 2.24.

Parameters[A]	Estimates	95% Approx. Conf. Interval	| t - value |[B]	Parameters	Values	Units
$\ln\tilde{A}_{pcp}$	2.901×10^{1}	$\pm 4.46 \times 10^{-1}$	4.03	$\tilde{A}_{pcp}$	3.97×10^{12}	s^{-1}
$\frac{E^{\circ}_{pcp}}{R\alpha_{pcp}}$	1.433×10^{4}	$\pm 1.88 \times 10^{2}$	4.77	E°_{pcp}	7.15×10^{1}	kJ/mol
α_{pcp}	6.001×10^{-1}	$\pm 5.30 \times 10^{-3}$	7.02	α_{pcp}	6.00×10^{-1}	dimensionless
$\ln\tilde{A}_{olig}$	1.794×10^{1}	$\pm 5.20 \times 10^{-2}$	21.39	$\tilde{A}_{olig}$	6.18×10^{7}	s^{-1}.gCat/mol
$\frac{E^{\circ}_{olig}}{R\alpha_{olig}}$	1.518×10^{4}	$\pm 1.51 \times 10^{1}$	62.46	E°_{olig}	7.59×10^{1}	kJ/mol
α_{olig}	6.015×10^{-1}	$\pm 2.04 \times 10^{-3}$	18.23	α_{olig}	6.02×10^{-1}	dimensionless
$\ln\tilde{A}_{ht}$	3.523×10^{1}	$\pm 1.13 \times 10^{-1}$	19.39	$\tilde{A}_{ht}$	1.99×10^{15}	s^{-1}.gCat/mol
$\frac{E^{\circ}_{ht}}{R\alpha_{ht}}$	1.262×10^{5}	$\pm 1.33 \times 10^{2}$	58.76	E°_{ht}	9.18×10^{1}	kJ/mol
α_{ht}	8.749×10^{-2}	$\pm 2.01 \times 10^{-4}$	26.93	α_{ht}	8.70×10^{-2}	dimensionless
$\ln\tilde{A}_{\beta s}$	1.382×10^{1}	$\pm 1.30 \times 10^{-2}$	66.09	$\tilde{A}_{\beta s}$	2.04×10^{6}	s^{-1}
$\frac{\Delta\hat{S}_p}{R}$	-2.177×10^{1}	$\pm 2.96 \times 10^{-2}$	45.64	$\Delta\hat{S}_p$	-1.81×10^{2}	J/mol.K
$\frac{\Delta E^{sec}_{+}}{R}$	8.648×10^{4}	$\pm 4.25 \times 10^{1}$	126.04	ΔE^{sec}_{+}	7.19×10^{2}	kJ/mol
$\frac{\Delta E^{tert}_{+}}{R}$	9.141×10^{4}	$\pm 3.33 \times 10^{1}$	170.02	ΔE^{tert}_{+}	7.60×10^{2}	kJ/mol
$\frac{\gamma_c}{R}$	3.019×10^{2}	$\pm 4.82 \times 10^{3}$	0.0039	γ_c	2.51×10^{0}	kJ/mol

Because of the large amount of computing time required to evaluate the objective function, not all the 79 available experiments are used in the parameter estimation. Instead, a careful selection of 53 data sets covering all the experimental conditions considered is conducted to remove from the database those experiments where steady state was long reached.

Parameter confidence intervals shown in Table 19 indicate that for most of the parameters, reasonably accurate and significant estimates are obtained from the regression. Even though a detailed inspection of the relative magnitude of the 95% confidence interval with respect to the parameter value reveals that estimates of those parameters associated with the PCP-branching elementary step have broader confidence intervals and therefore represent less accurate estimates.

In the particular case of the estimate for the carbon number contribution to the stabilization energy, results for the t-test indicate that no statistical difference can be established between this estimate and zero at the 95% confidence level. This result strongly suggests that the stabilization energy dependency on the nature of the carbenium ion has a greater importance than its dependency on the carbon number at least for proton-exchanged Y-zeolites at moderate temperatures. On the other hand, the lack of a trend with the carbon number would also be a consequence of the weak temperature dependence observed in the experimental data.

In general, the values of the estimated parameters are in reasonable agreement with those reported elsewhere[17,33]. However, in the particular case of the Evans-Polanyi transfer coefficient for oligomerization, Froment *et al.*[33,45] obtained estimates significantly smaller than 0.5 from the kinetic modeling of the MTO process over ZSM-5 and SAPO-34. In contrast, the estimate from the present model is greater than 0.5. This result contradicts the general expectancy that values of the transfer coefficient for highly exothermic elementary steps such as oligomerization should be less than 0.5.

In order to illustrate the impact of the parameter estimation results in the predictive capabilities of the model, parity plot for the most relevant product yields are presented in Figures 24, 25 , 26 and 27. In these figures, a good agreement is observed for those component groups that represent a significant fraction of the reaction product at some point during the process such as linear butenes (O4), mono-, di- and tri-branched octanes ([M+D+T]P8) and mono-, di- and tri-branched octenes ([M+D+T]O8). On the other hand, Figure 27 shows that the model has difficulties in reproducing the product yields of those component groups with a short appearance before significant deactivation occurs and that represent a small fraction (< 1.4 wt%) of the reaction product such as pentanes (P5), hexanes (P6) and heptanes (P7). Moreover, parity plots indicate the model underestimates the values for [M+D+T]O8 and P5-P7, whereas it slightly overestimates [M+D+T]P8 values. The occurrence of these deviations suggests that further improvement of the parameter estimates would be worthwhile.

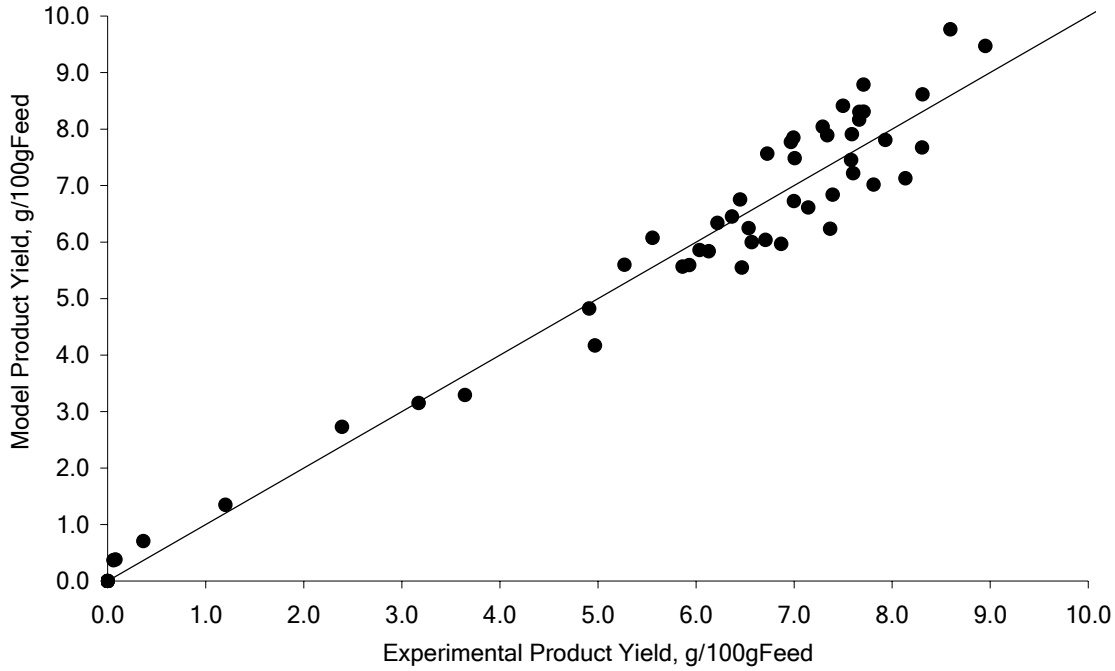

Figure 24. Parity Plot for O4 Product Yield.

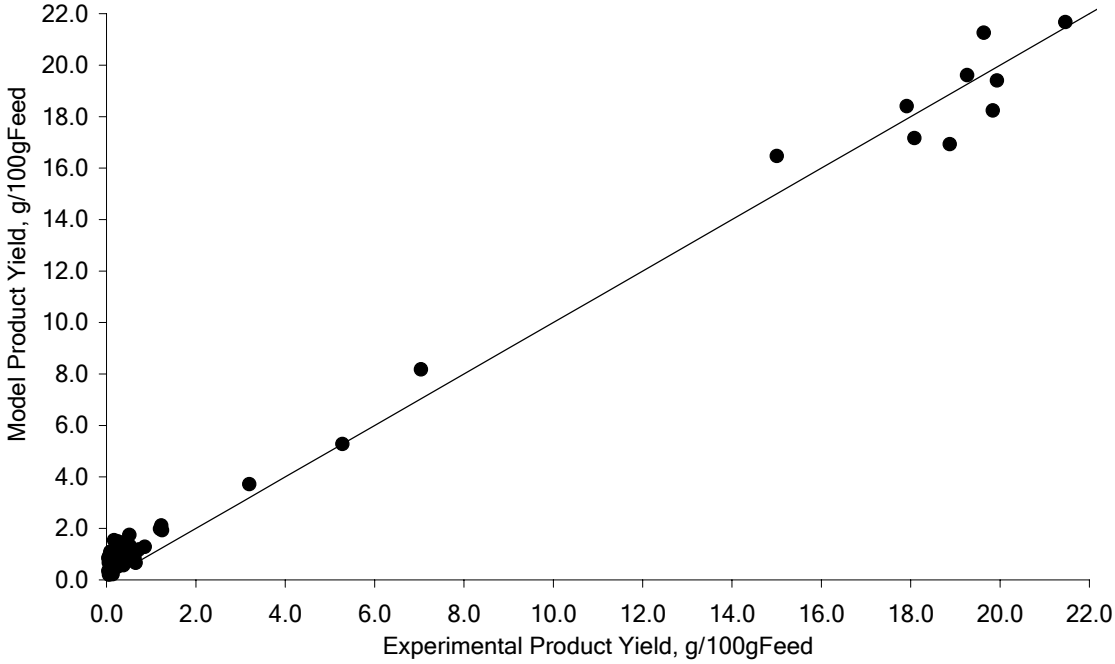

Figure 25. Parity Plot for [M+D+T] P8 Product Yield.

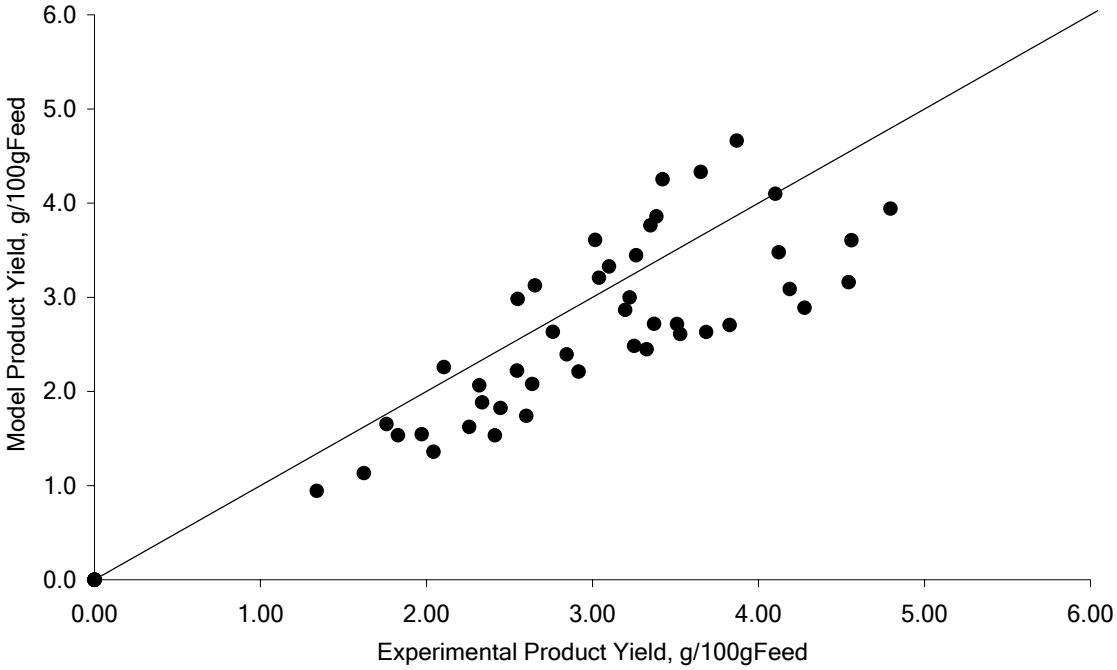

Figure 26. Parity Plot for [M+D+T] O8 Product Yield.

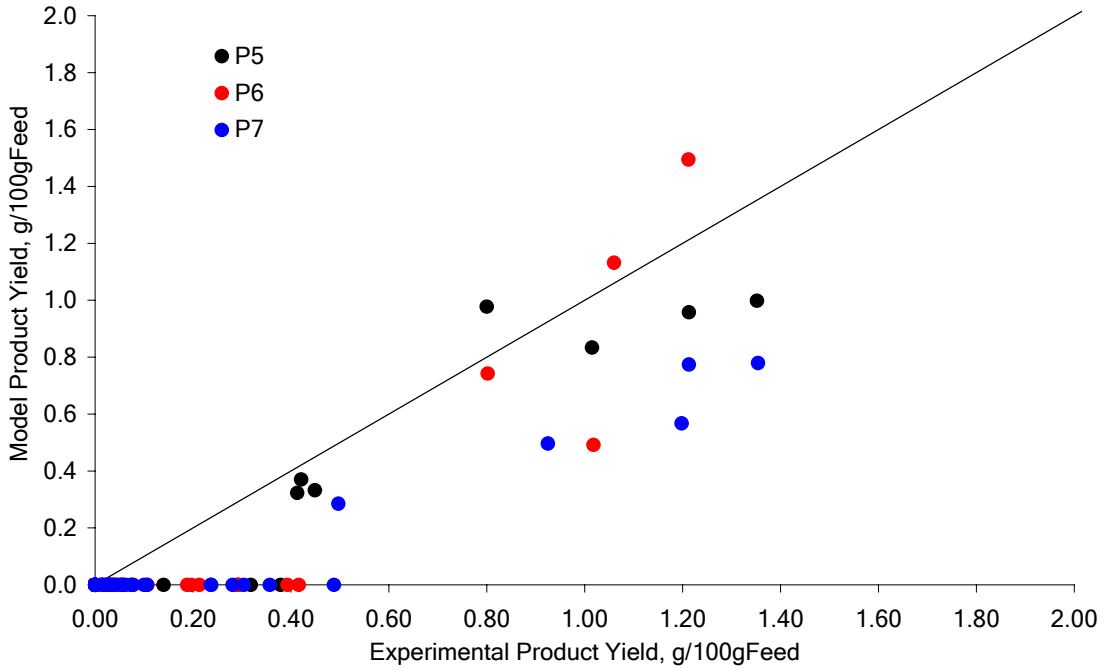

Figure 27. Parity Plot for P5, P6 & P7 Product Yields.

Figure 28 illustrates the predictive capabilities of the model regarding the process of deactivation. In the figure, model-predicted profiles for the most significant component groups resulted in good agreement with the experimental results. Indeed, the calculated trends reproduce the most relevant features of the fixed bed operation such as a strong selectivity shift from saturated to unsaturated products and a non-zero conversion at steady state. In addition, the model offers the possibility to follow the evolution of the deactivation extrema (minimum and maximum deactivation function values for the entire reactor length at a given time as shown in Figure 28) with the run-time, revealing the presence of a well-defined moving deactivation zone.

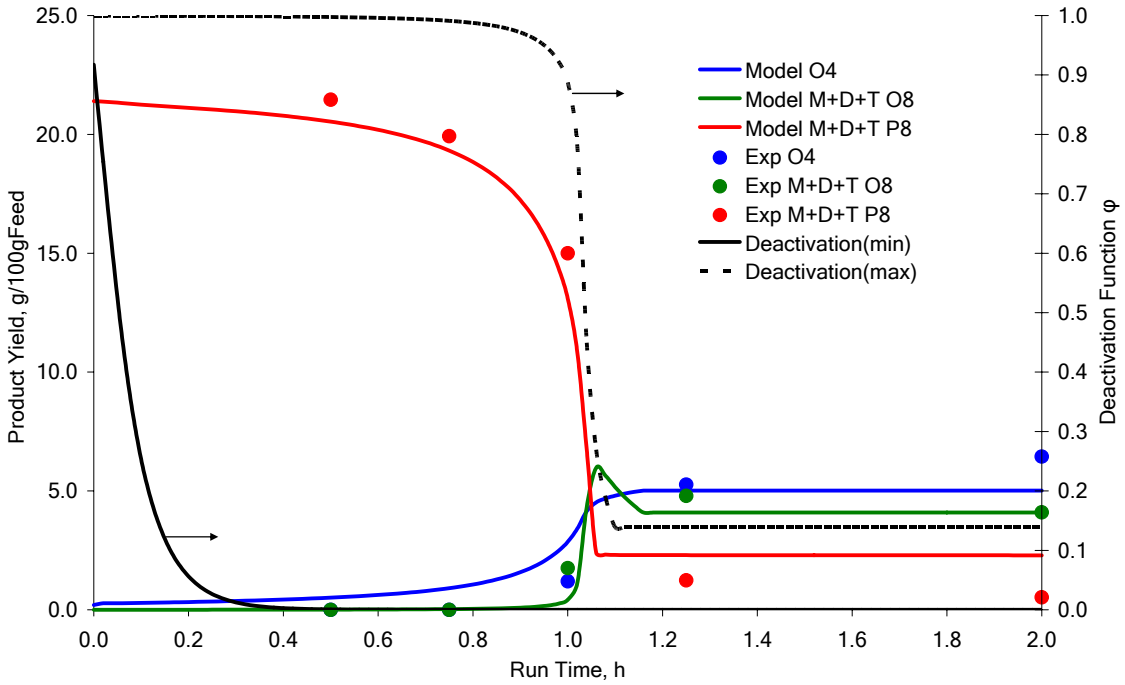

Figure 28. Product Yield Evolution with Run-Time. Temperature: 353 K, Butene Space-Time ($W/F^{\circ}_{O4}.M_{O4}$): 4.3 h, Isobutane/1-Butene Molar Ratio: 7.7 mol/mol.

This result strongly suggests that the proposed deactivation mechanism based on irreversible site coverage by species with a certain remnant reactivity is the predominant mechanism for solid acid alkylation. It also corroborates the hypothesis that in the absence of significant hydride transfer, formation of irreversibly adsorbed species predominates leading to deactivation. Thus, rapid deactivation of hydride transfer yields the characteristic selectivity shift from saturated to unsaturated species as the model correctly predicts. In Figure 28, deactivation of hydride transfer can be observed through a sharp decrease in the formation of saturated species, indicating that

deactivation for this type of elementary step is faster than for any other due to its dependency on the availability of neighboring acid sites.

In addition, Figure 28 shows how the model successfully reaches a non-zero conversion at steady state. This relevant result confirms the hypothesis that irreversibly adsorbed species are indeed reactive for other surface reactions and in particular through β-scission elementary steps equilibrating the formation of deactivation agents and leading to a steady conversion of linear butenes towards the formation of di-branched octenes.

Kinetic models constitute a powerful tool for the analysis and design of industrial reactors as well as for the development of new processes. In the particular case of solid acid alkylation the issue of interest for the present investigation is focused on understanding the underlying phenomena leading to the evolution of the product distribution from saturated to unsaturated species. Consequently, by taking advantage of the model capabilities, calculated profiles along the butene space-time coordinate are generated in order to explore the evolution of the species and deactivation inside of the reactor.

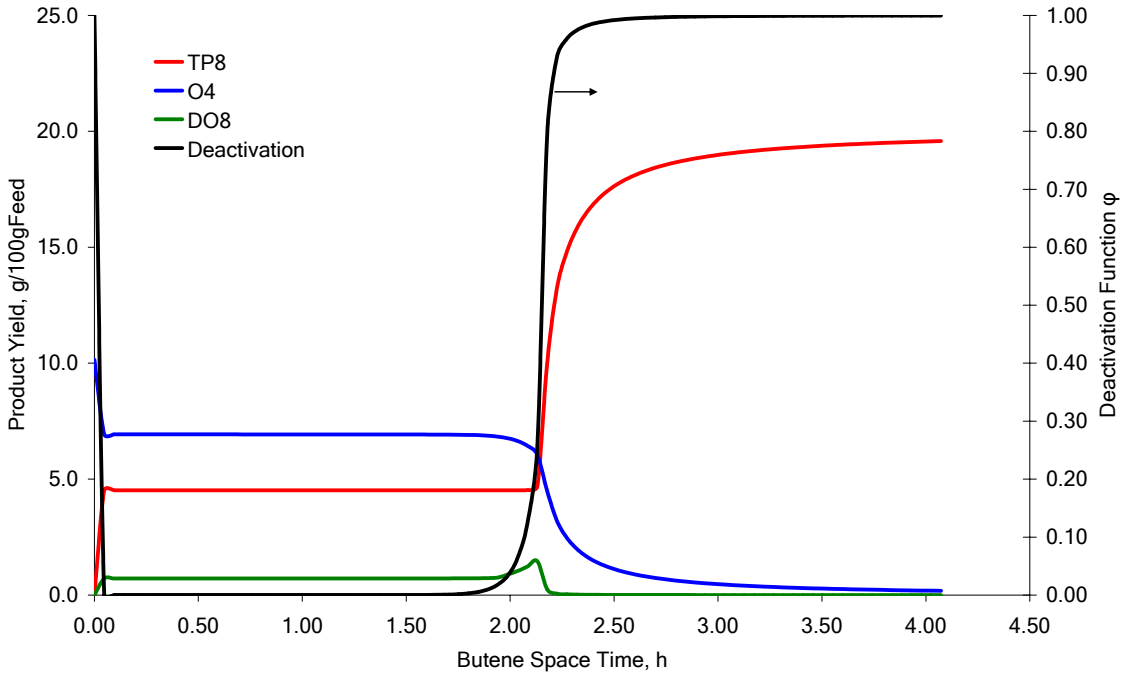

Figure 29. Reach of the Deactivation Zone after 0.5 h of Run-Time: Product Yields. Evolution with Butene Space-Time. Temperature: 373 K, Butene Space-Time ($W/F^{\circ}_{O4}.M_{O4}$): 4.6 h, Isobutane/1-Butene Molar Ratio: 8.3 mol/mol.

Figure 29 provides a clear view of the occurrence of the selectivity shift from tri-branched octanes (TP8) to di-branched octenes (DO8) within the moving deactivation zone. Modeling results indicate that most of the transformations do happen within the moving deactivation zone. Thus, the reactor is in effect separated into two sections. The first one extends from the reactor inlet to the beginning of the deactivation zone where the catalyst presents maximum deactivation under oligomerization/β-scission equilibrium. The second one extends from the moving deactivation zone towards the reactor outlet where fresh catalyst is available and therefore most of the TP8 species are formed.

The model not only generates product yield profiles along the reactor but also net production rates providing additional details about the reaction kinetics of the process. For instance, the net production rates in Figure 30 reveal the role of isobutylene (MO4) as a reaction intermediate leading to a selectivity shift from tri-branched octanes to di-branched octenes because of deactivation. Initially though as a consequence of PCP-branching deactivation, this experimentally observed selectivity shift turned out being a result of the rapid disappearance of isobutylene from the reaction mixture due to the decrease in the formation of t-butyl ions from hydride transfer because of deactivation. Oligomerization of isobutylene and linear butenes with t-butyl ions leads to the formation of tri-branched species.

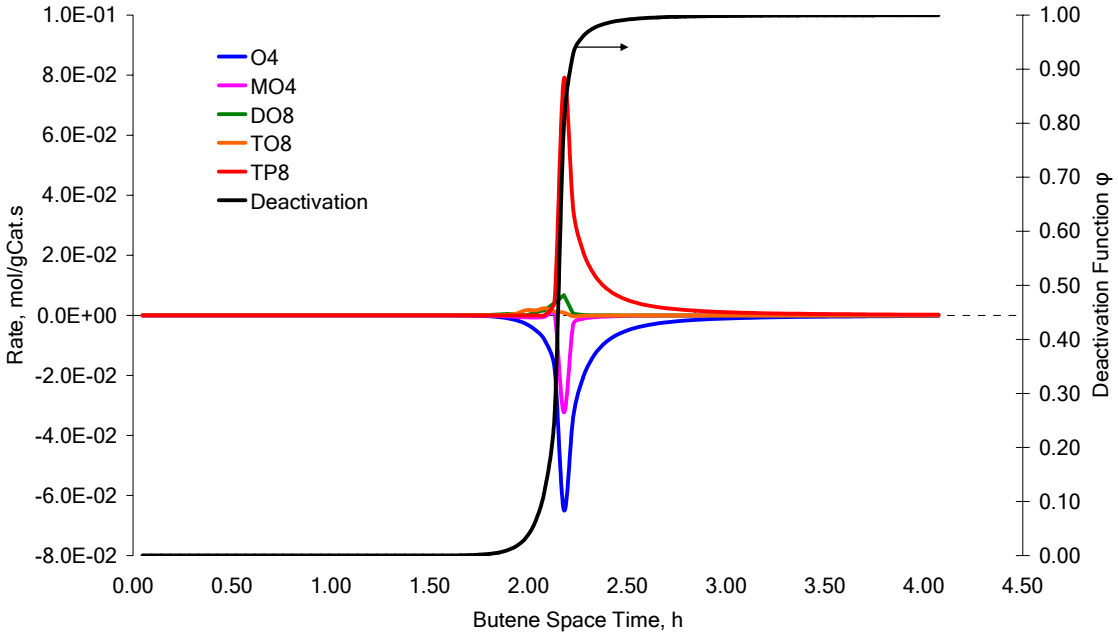

Figure 30. Reach of the Deactivation Zone after 0.5 h of Run-Time: Net Production Rates. Evolution with Butene Space-Time. Temperature: 373 K, Butene Space-Time ($W/F^{\circ}_{O4}.M_{O4}$): 4.6 h, Isobutane/1-Butene Molar Ratio: 8.3 mol/mol.

CONCLUSIONS AND RECOMMENDATIONS

In the present work, a single event kinetic modeling of the solid acid alkylation of isobutane with butenes over proton-exchanged Y-zeolites was formulated in order to achieve a fundamental description of the process at the elementary step level. In the formulation, a significant reduction in the number of model parameters from 3130 to 14 was accomplished by means of expressing the elementary step rate coefficients in terms of the single event concept together with the application of the Evans-Polanyi relationship, the stabilization energy concept and thermodynamic constraints to the rate expressions.

The proposed model provides a rigorous treatment of the deactivation process through site coverage that allows to reproduce most of the features observed in the experimental results. These features included rapid deactivation and non-zero steady conversion accompanied by selectivity shifts in the degree of saturation and branching of the reaction products. In general, the model reveals typical features associated with very rapid reactions some of which leading to very fast deactivation in a narrow zone.

Relevant contributions to the modeling of complex reaction kinetics were made by introducing formulae for the calculation of the number of single events from the identification of transformations leading to the creation/destruction of symmetry axes and chiral centers in the formation of the transition state structure. Additional contributions were made with the introduction of the stabilization energy dependency on the carbenium ion type and carbon number to account for the variations in the stabilization effect of the solid acid site.

An extensive experimental investigation comprising over 135 observations for a set of nine different operating conditions in butene space-time and temperature provided the necessary data for the parameter estimation. The estimation of the 14 model parameters required a substantial effort in terms of computational resources and time. It included constrained (SQP) and unconstrained (Marquardt) optimization along with human operator intervention. Statistical tests on the model and its parameters were performed at the 95% confidence level providing support for an educated decision making concerning the acceptance or rejection of the estimates. Results from one of these tests suggested a negligible contribution of the carbon number to the stabilization energy.

A satisfactory agreement between the model predictions and the experimental results led to the

application of the model to the generation of product yields and net production rates in order to reveal the underlying phenomena controlling the process. For instance, an experimentally observed selectivity shift from saturated products to unsaturated ones was successfully explained by confirming the hypothesis that hydride transfer is responsible for inhibiting deactivation. In contrast, the same results led to the rejection of the hypothesis that PCP-branching deactivation would be responsible for the also experimentally observed selectivity shift from tri-branched products to di-branched ones. Instead, the change in selectivity was attributed to the disappearance of isobutylene and t-butyl ions because of deactivation, implying that these species are intermediates in the formation of tri-branched species along the oligomerization/β-scission reaction pathway.

Another interesting result concerns to the deactivation process where the suggestion from the experimental data of a possible narrow moving deactivation zone was verified by model predictions. Furthermore, the model also permitted to identify the occurrence of oligomerization/β-scission equilibrium at maximum deactivation level in the section preceding the moving deactivation zone. This evolution of this section with butene space-time until the outlet of the reactor is reached leads to the non-zero conversion steady state experimentally observed.

Finally, further research on solid acid alkylation should focus on the design of new materials with mesoporous structures and a high density of strong acid sites. Efforts can be made to decrease the energy of activation of the hydride transfer elementary step so that it could readily proceed with lower acid strength. Materials such as perfluorinated sulfonic acids supported on mesoporous silicas where the distance between neighboring acid sites can be engineered to favor hydride transfer steps are strong candidates for further research.

LITERATURE CITED

[1] *Clean Air Act*, Title II, Part A, Sec. 202, 42, U.S. Code 7521.

[2] Pines, H. The Chemistry of Catalytic Hydrocarbon Conversions. In *Acid-Catalyzed Reactions*; Academic Press: New York, 1981; p 50.

[3] Weitkamp, J.; Traa, Y. Isobutane/Butene Alkylation on Solid Catalysts. Where Do We Stand? *Catalysis Today*. **1999**, *49*, 193.

[4] Diaz-Mendoza, F. A.; Pernett-Bolaño, L.; Cardona-Martínez, N. Effect of Catalyst Deactivation on the Acid Properties of Zeolites Used for Isobutane/Butene Alkylation. *Thermochimica Acta*. **1998**, *312*, 47.

[5] Taylor, R.J.; Sherwood, D.E. Effects of Process Parameters on Isobutane/2-Butene Alkylation Using a Solid Acid Catalyst. *Applied Catalysis A*. **1997**, *155*, 195.

[6] Satoh, K.; Matsuhashi, H.; Arata, K. Alkylation to Form Trimethylpentanes from Isobutane and 1-Butene Catalyzed by Solid Superacids of Sulfate Metal Oxides. *Applied Catalysis A*. **1999**, *189*, 35.

[7] Santana, G.; Akgerman, A. Alkylation of Isobutane with 1-Butene on a Solid Acid Catalyst in Supercritical Reaction Media. *Industrial & Engineering Chemistry Research*. **2001**, *40*, 3879.

[8] de Jong, K.P; Mesters, C.M.A.M.; Peferoen, D.G.R.; van Brugge, P.T.M.; de Groot, C. Paraffin Alkylation Using Zeolite Catalysts in a Slurry Reactor. *Chemical Engineering Science*. **1996**, *51*, 2053.

[9] Querini C.A. Isobutane/Butene Alkylation: Regeneration of Solid Acid Catalyst. *Catalysis Today*. **2000**, *62*, 135.

[10] Feller A.; Zuazo, I.; Guzman, A.; Barth, J.O.; Lercher, J.A. Common Mechanistic Aspects of Liquid and Solid Acid Catalyzed Alkylation of Isobutane with n-Butene. *Journal of Catalysis*. **2003**, *216*, 313.

[11] Gates, B.C.; Katzer, J.R.; Schuit, G.C.A. Chemistry of Catalytic Processes. In *Cracking*; McGraw-Hill: New York, 1979; p 21.

[12] Martens, J.A.; Jacobs, P.A. Theoretical Aspects of Heterogeneous Catalysis. In *Conceptual Background for the Conversion of Hydrocarbons on Heterogeneous Acid Catalysis*; Moffat, J.B. Ed; Van Nostrand Reinhold: New York, 1990; p 52.

[13] Baltanas, M.A.; Van Raemdonck, K.K.; Froment, G.F.; Mohedas, S.R. Fundamental Kinetic Modeling of Hydroisomerization and Hydrocracking on Noble-Metal-Loaded Faujasites. 1. Rate Parameters for Hydroisomerization. *Industrial & Engineering Chemistry Research*. **1989**, *28*, 899.

[14] Boronat, M.; Viruela, P.; Corma, A. Theoretical Study of the Mechanism of Branching Rearrangement of Carbenium Ions. *Applied Catalysis A: General*. **1996**, *146*, 207.

[15] Kazansky, V.B. Adsorbed Carbocations as Transition States in Heterogeneous Acid Catalyzed Transformations of Hydrocarbons. *Catalysis Today*. **1999**, *51*, 419.

[16] Rozanska, X.; van Santen, R.A.; Demuth, T.; Hutschka, F.; Hafner, J. A Periodic DFT Study of Isobutane Chemisorption in Proton-Exchanged Zeolites: Dependence of Reactivity on the Zeolite Framework Structure. *Journal of Physical Chemistry B*. **2003**, *107*, 1309.

[17] Sanchez-Castillo, M.; Agarwall, N.; Miller, C.; Cortright, R.D.; Madon, R.J.; Dumesic, J.A. Reaction Kinetics Study and Analysis of Reaction Schemes for Isobutane Conversion over USY Zeolite. *Journal of Catalysis*. **2002**, *205*, 67.

[18] Kazansky, V.B.;Frash, M.V.; van Santen, R.A. Quantumchemical Study of the Isobutane Cracking on Zeolites. *Applied Catalysis A: General*. **1996**, *146*, 225.

[19] Brouwer, D.M.; Hogeveen, H. Electrophilic Substitutions at Alkanes and in Alkylcarbonium Ions. *Progress in Physical Organic Chemistry*. **1972**, *9*, 179.

[20] Park, T.; Froment, G.F. Analysis of Fundamental Reaction Rates in the Methanol-To-Olefins Process on ZSM-5 as a Basis for Reactor Design and Operation. *Industrial & Engineering Chemistry Research*. **2004**, *43*, 682.

[21] Golender, V.E.;Drboglav, V.V.; Rosenblit, A.B. Graph Potentials Method and Its Application for Chemical Information Processing. *Journal of Chemistry Informatics and Computer Science*. **1981**, *21*, 196.

[22] Clymans, P.J.; Froment, G.F. Computer-Generation of Reaction Paths and Rate Equations in the Thermal Cracking of Normal and Branched Paraffins. *Computers and Chemical Engineering*. **1984**, *8*, 137.

[23] Baltanas, M.A.; Froment, G.F. Computer Generation of Reaction Networks and Calculation of Product Distributions in the Hydroisomerization and Hydrocracking of Paraffins on Pt-Containing Bifunctional Catalysts. *Computers and Chemical Engineering*. **1985**, *9*, 71.

[24] *Wiley 138K Mass Spectral Database*; John Wiley and Sons, Inc: New York, 1990.

[25] Nam, I.; Froment, G.F. Catalyst Deactivation by Site Coverage through Multi-Site Reaction Mechanisms. *Journal of Catalysis*. **1987**, *108*, 271.

[26] Denayer, J.F.M.; De Jonckheere, B.; Loc., M.; Marin G.B; Vanbutsele, G.; Martens, J.A.; Baron, G.V. Molecular Competition of C_7 and C_9 n-alkanes in Vapor- and Liquid-Phase Hydroconversion over Bifunctional Pt-USY Zeolite Catalysts. *Journal of Catalysis*. **2002**, *210*, 445.

[27] Vynckier E.; Froment, G.F. Modeling of the Kinetics of Complex Processes based upon Elementary Steps. In *Kinetic and Thermodynamic Lumping of Multicomponent Mixtures*; Astarita, G., Sandler, S.I., Eds.; Elsevier Science Publishers BV: Amsterdam, The Netherlands, 1984; p 131.

[28] Muller, C.; Scacchi, G.; Come, G.M. A Topological Method for Determining the External Symmetry Number of Molecules. *Computers and Chemistry*. **1991**, *15*, 17.

[29] Walters, W.P.; Yalkowsky, S.H. ESCHER – A Computer Program for the Determination of External Rotational Symmetry Numbers from Molecular Topology. *Journal of Chemical Information and Computer Science*. **1996**, *36*, 1015.

[30] Park, T.; Froment, G.F. Kinetic Modeling of the Methanol to Olefins Process. 1. Model Formulation. *Industrial & Engineering Chemistry Research*. **2001**, *40*, 4172.

[31] Dumesic, J.A.; Rudd, D.F.; Aparicio, L.M.; Rekoske, J.E.; Treviño, A.A. The Microkinetics of Heterogeneous Catalysis. In *Isobutane Cracking Catalyzed by Acid Zeolites*; American Chemical Society: Washington, DC, 1993; p 306.

[32] Evans, M.G.; Polanyi, M. Inertia and Driving Force of Chemical Reactions. *Transactions of the Faraday Society*. **1938**, *31*, 11.

[33] Alwahabi, S.M.; Froment, G.F. Single Event Kinetic Modeling of the Methanol-to-Olefins Process on SAPO-34. *Industrial & Engineering Chemistry Research*. **2004**, *43*, 5098.

[34] Reid, R.C.; Prausnitz, J.M.; Poling, B.E. Properties of Gases and Liquids. In *Thermodynamic Properties of Ideal Gases*; McGraw-Hill, Inc: New York, 1987; p 173.

[35] Linstrom P.J.; Mallard W.G.; Eds. *NIST Chemistry WebBook, NIST Standard Reference Database Number 69*; National Institute of Standards and Technology: Gaithersburg MD, March 2003. (http://webbook.nist.gov).

[36] Park, T. *Kinetic Modeling of MTO Process*. Dissertation. Universiteit Gent: Belgium, 1998; p VI-1.

[37] Rùzicka, V.; Domalski, E.S. Estimation of the Heat Capacities of Organic Liquids as a Function of Temperature Using Group Additivity. I. Hydrocarbon Compounds. *Journal of Physical and Chemical Reference Data*. **1993**, *22*, 597.

[38] Constantinou, L.; Gani, R. New Group Contribution Method for Estimating Properties of Pure

Compounds. *American Institute of Chemical Engineers Journal*. **1994**, *40*, 1697.

[39] Shampine, L. F.; Gladwell I.; Thompson S. Solving ODEs with MATLAB. In *Initial Value Problems*; Cambridge University Press: Cambridge, UK, 2003; p 39.

[40] Shampine, L. F.; Reichelt, M.W. The MATLAB ODE Suite. *SIAM Journal on Scientific Computing*. **1997**, *18*, 1.

[41] Froment, G.F.; Bischoff, K.B. Chemical Reactor Analysis and Design. In *Kinetics of Heterogeneous Catalytic Reactions*; Wiley: New York, 1990; p 98.

[42] Grace, A. *MATLAB Optimization Toolbox User's Guide*; The Math Works, Inc: Natick, MA, 1994.

[43] Rawlings, J.B.; Eckerdt, J.G. Chemical Reactor Analysis and Design Fundamentals. In *Parameter Estimation for Reactor Models*; Nob Hill Publishing, LLC: Madison, WI, 2002; p 519.

[44] Gallant, A.R. Nonlinear Regression. *The American Statistician*. **1975**, *29*, 73.

[45] Park, T.; Froment, G.F. Kinetic Modeling of the Methanol to Olefins Process. 2. Experimental Results, Model Discrimination, and Parameter Estimation. *Industrial & Engineering Chemistry Research*. **2001**, *40*, 4187.

APPENDIX

Nomenclature

Alkene enthalpy of formation in liquid phase, J/mol	$\Delta H°_{f,l}(R_i^=)$
Alkene standard enthalpy of formation, J/mol	$\Delta H°_{f,g}(R_i^=)$
Alkene standard heat of vaporization, J/mol	$\Delta H°_{vap}(R_i^=)$
Benson's group contributions	gc_i
Carbenium ion type contribution to stabilization energy, J/mol	ΔE_+^{sec} or ΔE_+^{tert}
Carbon number	n_c
Carbon number contribution to stabilization energy, J/mol	γ_c
Catalyst pore volume, cm^3/gCat	V_p
Component group molar fraction	x^{cg}
Confidence level	α
Diagonal matrix of molecular weights, g/mol	$\mathbf{M}$
Elementary step energy barrier, J/mol	$\Delta H°^{\ddagger}$
Elementary step energy of activation, J/mol	E_a
Elementary step intrinsic entropy change, J/mol.K	$\Delta \hat{S}°$
Elementary step rate coefficient, s^-1 or s^{-1}.gCat/mol	k'_j
Elementary step reaction rate, mol/gCat.s	r_j
Energy change of stabilization, J/mol	Δq
Enthalpies of formation for the surface-bonded species, J/mol	$\Delta H°_{f,s}(R_n^+)$ or $\Delta H°_{f,s}(H^+)$
Evans-Polanyi intrinsic energy barrier, J/mol	$E°$
Evans-Polanyi transfer coefficient	α
Experiment variance	σ^2
External symmetry number	σ_{ext}
Gibbs free energy change with protonation, J/mol	ΔG_p

Global symmetry number	σ_{gl}
Inlet 1-butene volumetric flowrate, Std. cm^3/h	V^{in}_{O4}
Inlet isobutane volumetric flowrate, Std. cm^3/h	V^{in}_{MP4}
Intrinsic entropy change with protonation, J/mol.K	$\Delta\hat{S}_p^\circ$
Inverse of the error covariance matrix	$\omega_{h,k}$
Irreversible fractional site coverage	θ_{irr}
Isobutane and propane free molar fraction	X_i"
Isobutane free molar fraction	X_i'
Isobutane propane molar content	χ_{P3}
isobutane-free inlet molar fractions	X^{in}_{NP4} and X^{in}_{O4}
Jacobian matrix	**J**
Liquid bulk concentration, mol/cm^3	$C_{Ri}^{=}$
Liquid bulk molar fraction	$x_{Ri}^{=}$
Liquid heat capacity, J/mol.K	C_{liq}
Liquid-phase concentration of a zeolite-sorbed species, mol/gCat	C^s_o or C^s_p
Local concentration of free acid sites, mol/gCat	C_{H+}
Local deactivation function	φ
Local surface concentration of irreversibly adsorbed ions, mol/gCat	C_{Rm+}
Local surface concentration of reversibly adsorbed ions, mol/gCat	C_{Rn}
Lumping coefficient	LC
Molar fraction	X
Molar volume for the pure liquid, cm^3/mol	V_L
Number of 2-fold internal symmetry axes	n'
Number of 3-fold internal symmetry axes	n''
Number of experiments	n
Number of group contributions	ng_i
Number of irreversibly adsorbed ions	M
Number of parameters	p

Number of quiral centers	n'''
Number of responses	v
Number of reversibly adsorbed ions	N
Number of single events	n_e
Parameter covariance matrix	$\mathbf{V}$
Product yield, g/100gFeed	Y_i
Protonation equilibrium constant	K_p
Purge gas volumetric flowrate, Std. cm^3/h	V_T^{out}
Reactant-transition-state entropy change, J.mol.K	$\Delta S^{\circ\ddagger}$
Reactant-transition-state equilibrium constant	$K^{\ddagger}$
Reversible fractional site coverage	θ_{rev}
Run-time	t, h
Single event frequency factor, s^-1 or s^{-1}.gCat/mol	$\tilde{A}$
Single event rate coefficient, s^-1 or s^{-1}.gCat/mol	$\tilde{k}_j$
Stabilization energy, J/mol	Δq_+
Standard heat of protonation, J/mol	ΔH_p°
Standard heat of reaction	ΔH°
Stochiometric coefficient matrix for the liquid phase	$\mathbf{v}^f$
Stochiometric coefficient matrix for the solid phase	$\mathbf{v}^s$
Total concentration of acid sites, mol/gCat	C^t_{H+}
Total concentration of the pure liquid, mol/gCat	C^o
Transition state global symmetry number	$\sigma_{gl}^{\ddagger}$
Universal gas constant, J/mol.K	R
Vector of experimental conditions	$\dot{X}_i$
Vector of experimental errors, g/100gFeed	e
Vector of experimental responses (product yields), g/100gFeed	$\bar{Y}$
Vector of Implicit model functions	f_h
Vector of inlet yields, g/100gFeed	$\hat{Y}^{\circ}$

Vector of model parameters	β
Vector of model responses (product yields), g/100gFeed	$\hat{Y}$, $\hat{Y}_h$
Vector of parameter estimates	$\hat{b}$
Vibration frequency, s^{-1}	Λ

Experimental Run Data

Table. Product Yields from Runs 1-9

Processed O4, g/gCat	0.45	0.68	0.98	5.26	6.09	0.24	0.36	1.20	1.92	3.35	0.29	0.43	1.06	1.59
Temperature, °C	100	100	100	100	100	100	100	100	100	100	120	120	120	120
O4 Space Time, h	1.1	1.1	1.1	1.1	1.1	2.1	2.1	2.1	2.1	2.1	1.7	1.7	1.7	1.7
Inlet Molar MP4/O4 Ratio	7.9	7.9	7.9	7.9	7.9	9.7	9.7	9.7	9.7	9.7	8.2	8.2	8.2	8.2
NP4	0.1	0.1	0.1	0.1	0.1	0.1	0.1	0.1	0.0	0.0	0.2	0.1	0.1	0.1
MP4	77.2	88.3	88.8	89.1	89.1	80.3	88.3	90.8	90.8	90.9	77.4	86.2	89.0	89.1
NP5	0.0	0.0	0.0	0.0	0.0	0.0	0.0	0.0	0.0	0.0	0.0	0.0	0.0	0.0
MP5	0.6	0.0	0.0	0.0	0.0	0.7	0.2	0.0	0.0	0.0	1.0	0.2	0.0	0.0
MP6	0.3	0.0	0.0	0.0	0.0	0.6	0.3	0.0	0.0	0.0	0.5	0.1	0.0	0.0
DP6	0.3	0.0	0.0	0.0	0.0	0.6	0.2	0.0	0.0	0.0	0.5	0.1	0.0	0.0
MP7	0.1	0.0	0.0	0.0	0.0	0.6	0.4	0.0	0.0	0.0	0.3	0.1	0.0	0.0
DP7	0.5	0.0	0.0	0.0	0.0	1.6	0.8	0.0	0.0	0.0	0.8	0.1	0.0	0.0
TP7	0.0	0.0	0.0	0.0	0.0	0.1	0.0	0.0	0.0	0.0	0.0	0.0	0.0	0.0
MP8	0.4	0.0	0.0	0.0	0.0	0.8	0.0	0.0	0.0	0.0	0.6	0.0	0.0	0.0
DP8	6.6	1.2	0.5	0.1	0.1	6.4	1.9	0.2	0.1	0.1	5.6	3.6	0.6	0.6
TP8	13.7	0.3	0.0	0.0	0.0	8.3	0.7	0.0	0.0	0.0	13.2	1.8	0.0	0.0
O3	0.0	0.0	0.0	0.0	0.0	0.0	0.0	0.0	0.0	0.0	0.0	0.0	0.0	0.0
O4	0.0	5.1	6.6	8.7	8.8	0.0	3.5	6.4	7.3	7.3	0.0	3.0	6.4	6.3
MO4	0.0	0.0	0.0	0.0	0.0	0.0	0.0	0.0	0.0	0.0	0.0	0.0	0.0	0.0
O5	0.0	0.0	0.0	0.0	0.0	0.0	0.0	0.0	0.0	0.0	0.0	0.0	0.0	0.0
MO5	0.0	0.0	0.0	0.0	0.0	0.0	0.0	0.0	0.0	0.0	0.0	0.0	0.0	0.0
MO6	0.0	0.0	0.1	0.0	0.0	0.0	0.1	0.1	0.2	0.1	0.0	0.0	0.1	0.1
DO6	0.0	0.0	0.0	0.0	0.0	0.0	0.0	0.0	0.0	0.0	0.0	0.0	0.0	0.0
MO7	0.0	0.0	0.0	0.0	0.0	0.0	0.3	0.2	0.4	0.2	0.0	0.0	0.0	0.0
DO7	0.0	0.0	0.0	0.0	0.0	0.0	0.1	0.0	0.0	0.0	0.0	0.0	0.1	0.1
TO7	0.0	0.0	0.0	0.0	0.0	0.0	0.0	0.0	0.0	0.0	0.0	0.0	0.0	0.0
MO8	0.0	0.0	0.0	0.1	0.0	0.0	0.1	0.1	0.0	0.0	0.0	0.0	0.1	0.1
DO8	0.0	4.8	3.7	2.0	1.8	0.0	2.9	2.0	1.1	1.4	0.0	4.2	3.4	3.6
TO8	0.0	0.1	0.1	0.0	0.0	0.0	0.1	0.1	0.0	0.0	0.0	0.2	0.1	0.1

Table. Continued.

Processed O4, g/gCat	2.36	2.79	3.66	4.09	0.63	1.62	2.11	3.38	4.01	5.28	5.91	0.45	0.68	0.90
Temperature, °C	120	120	120	120	120	120	120	120	120	120	120	80	80	80
O4 Space Time, h	1.7	1.7	1.7	1.7	1.2	1.2	1.2	1.2	1.2	1.2	1.2	1.1	1.1	1.1
Inlet Molar MP4/O4 Ratio	8.2	8.2	8.2	8.2	9.1	9.1	9.1	9.1	9.1	9.1	9.1	8.5	8.5	8.5
NP4	0.1	0.1	0.1	0.1	0.1	0.1	0.1	0.1	0.1	0.1	0.1	0.1	0.1	0.1
MP4	89.2	89.2	89.3	89.3	89.9	90.2	90.2	90.3	90.3	90.3	90.3	79.2	89.1	89.6
NP5	0.0	0.0	0.0	0.0	0.0	0.0	0.0	0.0	0.0	0.0	0.0	0.0	0.0	0.0
MP5	0.0	0.0	0.0	0.0	0.0	0.0	0.0	0.0	0.0	0.0	0.0	0.4	0.0	0.0
MP6	0.0	0.0	0.0	0.0	0.0	0.0	0.0	0.0	0.0	0.0	0.0	0.1	0.0	0.0
DP6	0.0	0.0	0.0	0.0	0.0	0.0	0.0	0.0	0.0	0.0	0.0	0.1	0.0	0.0
MP7	0.0	0.0	0.0	0.0	0.0	0.0	0.0	0.0	0.0	0.0	0.0	0.1	0.0	0.0
DP7	0.0	0.0	0.0	0.0	0.0	0.0	0.0	0.0	0.0	0.0	0.0	0.3	0.0	0.0
TP7	0.0	0.0	0.0	0.0	0.0	0.0	0.0	0.0	0.0	0.0	0.0	0.0	0.0	0.0
MP8	0.0	0.0	0.0	0.0	0.0	0.0	0.0	0.0	0.0	0.0	0.0	1.0	0.0	0.0
DP8	0.4	0.4	0.2	0.2	0.7	0.2	0.3	0.1	0.1	0.1	0.1	4.9	0.9	0.3
TP8	0.0	0.0	0.0	0.0	0.0	0.0	0.0	0.0	0.0	0.0	0.0	13.4	0.3	0.0
O3	0.0	0.0	0.0	0.0	0.0	0.0	0.0	0.0	0.0	0.0	0.0	0.0	0.0	0.0
O4	7.2	6.7	8.0	8.1	5.8	7.1	7.0	7.8	7.4	8.4	7.9	0.4	4.9	6.4
MO4	0.0	0.0	0.0	0.0	0.0	0.0	0.0	0.0	0.0	0.0	0.0	0.0	0.0	0.0
O5	0.0	0.0	0.0	0.0	0.0	0.0	0.0	0.0	0.0	0.0	0.0	0.0	0.0	0.0
MO5	0.0	0.0	0.0	0.0	0.0	0.0	0.0	0.0	0.0	0.0	0.0	0.0	0.0	0.0
MO6	0.1	0.1	0.1	0.1	0.1	0.1	0.1	0.1	0.1	0.1	0.1	0.0	0.0	0.0
DO6	0.0	0.0	0.0	0.0	0.0	0.0	0.0	0.0	0.0	0.0	0.0	0.0	0.0	0.0
MO7	0.0	0.0	0.0	0.0	0.0	0.0	0.0	0.0	0.0	0.1	0.0	0.0	0.0	0.0
DO7	0.1	0.1	0.1	0.3	0.2	0.1	0.1	0.1	0.1	0.1	0.0	0.0	0.0	0.0
TO7	0.0	0.0	0.0	0.0	0.0	0.0	0.0	0.0	0.0	0.0	0.0	0.0	0.0	0.0
MO8	0.1	0.1	0.1	0.1	0.0	0.0	0.0	0.1	0.1	0.0	0.1	0.0	0.2	0.2
DO8	2.8	3.3	2.1	1.9	3.0	2.0	2.2	1.5	1.9	0.9	1.4	0.0	4.3	3.3
TO8	0.1	0.1	0.0	0.0	0.1	0.0	0.1	0.0	0.0	0.0	0.0	0.0	0.0	0.0

Table. Continued.

Processed O4, g/gCat	1.13	1.80	2.48	3.15	3.83	4.51	5.18	5.86	0.28	0.42	0.56	0.70	1.12	1.54
Temperature, °C	80	80	80	80	80	80	80	80	80	80	80	80	80	80
O4 Space Time, h	1.1	1.1	1.1	1.1	1.1	1.1	1.1	1.1	1.8	1.8	1.8	1.8	1.8	1.8
Inlet Molar MP4/O4 Ratio	8.5	8.5	8.5	8.5	8.5	8.5	8.5	8.5	8.4	8.4	8.4	8.4	8.4	8.4
NP4	0.1	0.1	0.1	0.1	0.1	0.1	0.1	0.1	0.1	0.1	0.1	0.1	0.1	0.1
MP4	89.7	89.7	89.7	89.7	89.8	89.8	89.8	89.8	78.6	86.4	89.4	89.5	89.6	89.6
NP5	0.0	0.0	0.0	0.0	0.0	0.0	0.0	0.0	0.0	0.0	0.0	0.0	0.0	0.0
MP5	0.0	0.0	0.0	0.0	0.0	0.0	0.0	0.0	0.4	0.3	0.0	0.0	0.0	0.0
MP6	0.0	0.0	0.0	0.0	0.0	0.0	0.0	0.0	0.2	0.1	0.0	0.0	0.0	0.0
DP6	0.0	0.0	0.0	0.0	0.0	0.0	0.0	0.0	0.2	0.1	0.0	0.0	0.0	0.0
MP7	0.0	0.0	0.0	0.0	0.0	0.0	0.0	0.0	0.1	0.1	0.0	0.0	0.0	0.0
DP7	0.0	0.0	0.0	0.0	0.0	0.0	0.0	0.0	0.4	0.2	0.0	0.0	0.0	0.0
TP7	0.0	0.0	0.0	0.0	0.0	0.0	0.0	0.0	0.0	0.0	0.0	0.0	0.0	0.0
MP8	0.0	0.0	0.0	0.0	0.0	0.0	0.0	0.0	0.6	0.0	0.0	0.0	0.0	0.0
DP8	0.2	0.1	0.1	0.1	0.1	0.0	0.1	0.1	4.4	3.1	0.5	0.3	0.1	0.1
TP8	0.0	0.0	0.0	0.0	0.0	0.0	0.0	0.0	14.9	2.2	0.0	0.0	0.0	0.0
O3	0.0	0.0	0.0	0.0	0.0	0.0	0.0	0.0	0.0	0.0	0.0	0.0	0.0	0.0
O4	6.7	7.3	7.7	7.7	7.6	8.6	7.8	8.3	0.1	3.2	6.2	6.7	7.3	7.9
MO4	0.0	0.0	0.0	0.0	0.0	0.0	0.0	0.0	0.0	0.0	0.0	0.0	0.0	0.0
O5	0.0	0.0	0.0	0.0	0.0	0.0	0.0	0.0	0.0	0.0	0.0	0.0	0.0	0.0
MO5	0.0	0.0	0.0	0.0	0.0	0.0	0.0	0.0	0.0	0.0	0.0	0.0	0.0	0.0
MO6	0.0	0.0	0.0	0.0	0.0	0.0	0.0	0.0	0.0	0.0	0.0	0.0	0.0	0.0
DO6	0.0	0.0	0.0	0.0	0.0	0.0	0.0	0.0	0.0	0.0	0.0	0.0	0.0	0.0
MO7	0.0	0.0	0.0	0.0	0.0	0.0	0.0	0.0	0.0	0.0	0.0	0.0	0.0	0.0
DO7	0.0	0.0	0.0	0.0	0.0	0.0	0.0	0.0	0.0	0.0	0.0	0.0	0.0	0.0
TO7	0.0	0.0	0.0	0.0	0.0	0.0	0.0	0.0	0.0	0.0	0.0	0.0	0.0	0.0
MO8	0.2	0.1	0.1	0.1	0.1	0.1	0.1	0.1	0.0	0.1	0.1	0.1	0.1	0.0
DO8	3.2	2.6	2.3	2.2	2.4	1.5	2.2	1.7	0.0	4.1	3.7	3.3	2.8	2.2
TO8	0.0	0.0	0.0	0.0	0.0	0.0	0.0	0.0	0.0	0.0	0.0	0.0	0.0	0.0

Table. Continued.

Processed O4, g/gCat	1.95	2.37	3.21	3.63	0.12	0.18	0.23	0.29	0.47	0.64	0.82	1.00	1.17	1.35
Temperature, °C	80	80	80	80	80	80	80	80	80	80	80	80	80	80
O4 Space Time, h	1.8	1.8	1.8	1.8	4.3	4.3	4.3	4.3	4.3	4.3	4.3	4.3	4.3	4.3
Inlet Molar MP4/O4 Ratio	8.4	8.4	8.4	8.4	8.0	8.0	8.0	8.0	8.0	8.0	8.0	8.0	8.0	8.0
NP4	0.1	0.1	0.1	0.1	0.1	0.2	0.1	0.1	0.1	0.1	0.1	0.1	0.1	0.1
MP4	89.6	89.6	89.6	89.6	77.7	76.7	80.6	88.5	88.9	89.0	89.0	89.0	89.1	89.1
NP5	0.0	0.0	0.0	0.0	0.0	0.0	0.0	0.0	0.0	0.0	0.0	0.0	0.0	0.0
MP5	0.0	0.0	0.0	0.0	0.3	1.0	0.4	0.0	0.0	0.0	0.0	0.0	0.0	0.0
MP6	0.0	0.0	0.0	0.0	0.1	0.5	0.2	0.0	0.0	0.0	0.0	0.0	0.0	0.0
DP6	0.0	0.0	0.0	0.0	0.1	0.5	0.2	0.0	0.0	0.0	0.0	0.0	0.0	0.0
MP7	0.0	0.0	0.0	0.0	0.1	0.3	0.1	0.0	0.0	0.0	0.0	0.0	0.0	0.0
DP7	0.0	0.0	0.0	0.0	0.2	0.9	0.3	0.0	0.0	0.0	0.0	0.0	0.0	0.0
TP7	0.0	0.0	0.0	0.0	0.0	0.0	0.0	0.0	0.0	0.0	0.0	0.0	0.0	0.0
MP8	0.0	0.0	0.0	0.0	0.8	0.7	0.0	0.0	0.0	0.0	0.0	0.0	0.0	0.0
DP8	0.1	0.1	0.1	0.0	3.8	3.9	10.5	1.2	0.5	0.3	0.3	0.2	0.2	0.2
TP8	0.0	0.0	0.0	0.0	16.8	15.3	4.5	0.0	0.0	0.0	0.0	0.0	0.0	0.0
O3	0.0	0.0	0.0	0.0	0.0	0.0	0.0	0.0	0.0	0.0	0.0	0.0	0.0	0.0
O4	7.7	8.1	8.3	9.0	0.0	0.0	1.2	5.3	6.4	7.1	7.0	7.6	7.4	7.4
MO4	0.0	0.0	0.0	0.0	0.0	0.0	0.0	0.0	0.0	0.0	0.0	0.0	0.0	0.0
O5	0.0	0.0	0.0	0.0	0.0	0.0	0.0	0.0	0.0	0.0	0.0	0.0	0.0	0.0
MO5	0.0	0.0	0.0	0.0	0.0	0.0	0.0	0.0	0.0	0.0	0.0	0.0	0.0	0.0
MO6	0.0	0.1	0.0	0.0	0.0	0.0	0.0	0.0	0.1	0.1	0.0	0.1	0.0	0.0
DO6	0.0	0.0	0.0	0.0	0.0	0.0	0.0	0.0	0.0	0.0	0.0	0.0	0.0	0.0
MO7	0.0	0.0	0.0	0.0	0.0	0.0	0.0	0.0	0.0	0.0	0.0	0.1	0.0	0.0
DO7	0.0	0.0	0.0	0.0	0.0	0.0	0.0	0.0	0.0	0.0	0.0	0.0	0.0	0.0
TO7	0.0	0.0	0.0	0.0	0.0	0.0	0.0	0.0	0.0	0.0	0.0	0.0	0.0	0.0
MO8	0.1	0.0	0.0	0.0	0.0	0.0	0.0	0.1	0.1	0.1	0.1	0.1	0.1	0.1
DO8	2.5	2.0	1.9	1.3	0.0	0.0	1.8	4.7	4.0	3.3	3.6	2.9	3.2	3.1
TO8	0.0	0.0	0.0	0.0	0.0	0.0	0.0	0.0	0.0	0.0	0.0	0.0	0.0	0.0

Table. Continued.

Processed O4, g/gCat	1.52	1.70	0.11	0.16	0.27	0.43	0.60	0.76	1.08	1.25	1.41	1.57	0.15	0.17
Temperature, °C	80	80	100	100	100	100	100	100	100	100	100	100	120	120
O4 Space Time, h	4.3	4.3	4.6	4.6	4.6	4.6	4.6	4.6	4.6	4.6	4.6	4.6	4.4	4.4
Inlet Molar MP4/O4 Ratio	8.0	8.0	8.8	8.8	8.8	8.8	8.8	8.8	8.8	8.8	8.8	8.8	8.6	8.6
NP4	0.1	0.1	0.1	0.2	0.1	0.1	0.1	0.1	0.1	0.1	0.1	0.0	0.2	0.2
MP4	89.1	89.1	79.3	78.4	88.3	89.6	89.7	89.8	89.8	89.8	89.9	90.0	77.8	77.8
NP5	0.0	0.0	0.0	0.0	0.0	0.0	0.0	0.0	0.0	0.0	0.0	0.0	0.0	0.0
MP5	0.0	0.0	0.4	1.2	0.0	0.0	0.0	0.0	0.0	0.0	0.0	0.0	1.4	1.4
MP6	0.0	0.0	0.1	0.5	0.1	0.0	0.0	0.0	0.0	0.0	0.0	0.0	0.5	0.6
DP6	0.0	0.0	0.2	0.5	0.0	0.0	0.0	0.0	0.0	0.0	0.0	0.0	0.6	0.6
MP7	0.0	0.0	0.1	0.3	0.0	0.0	0.0	0.0	0.0	0.0	0.0	0.0	0.3	0.4
DP7	0.0	0.0	0.2	0.9	0.1	0.0	0.0	0.0	0.0	0.0	0.0	0.0	0.8	0.9
TP7	0.0	0.0	0.0	0.0	0.0	0.0	0.0	0.0	0.0	0.0	0.0	0.0	0.0	0.0
MP8	0.0	0.0	0.8	0.9	0.0	0.0	0.0	0.0	0.0	0.0	0.0	0.0	1.4	1.1
DP8	0.1	0.1	3.9	4.3	2.8	0.7	0.7	0.5	0.3	0.3	0.2	0.3	5.4	5.0
TP8	0.0	0.0	14.9	12.7	0.4	0.0	0.0	0.0	0.0	0.0	0.0	0.0	11.5	12.0
O3	0.0	0.0	0.0	0.0	0.0	0.0	0.0	0.0	0.0	0.0	0.0	0.0	0.0	0.0
O4	7.7	7.6	0.0	0.0	3.6	5.9	5.9	6.5	7.0	6.9	7.5	7.0	0.0	0.0
MO4	0.0	0.0	0.0	0.0	0.0	0.0	0.0	0.0	0.0	0.0	0.0	0.0	0.0	0.0
O5	0.0	0.0	0.0	0.0	0.0	0.0	0.0	0.0	0.0	0.0	0.0	0.0	0.0	0.0
MO5	0.0	0.0	0.0	0.0	0.0	0.0	0.0	0.0	0.0	0.0	0.0	0.0	0.0	0.0
MO6	0.1	0.0	0.0	0.0	0.0	0.1	0.1	0.1	0.1	0.1	0.1	0.1	0.0	0.0
DO6	0.0	0.0	0.0	0.0	0.0	0.0	0.0	0.0	0.0	0.0	0.0	0.0	0.0	0.0
MO7	0.0	0.0	0.0	0.0	0.0	0.0	0.0	0.0	0.0	0.0	0.0	0.0	0.0	0.0
DO7	0.0	0.0	0.0	0.0	0.0	0.2	0.1	0.1	0.1	0.1	0.1	0.1	0.0	0.0
TO7	0.0	0.0	0.0	0.0	0.0	0.0	0.0	0.0	0.0	0.0	0.0	0.0	0.0	0.0
MO8	0.1	0.1	0.0	0.0	0.1	0.1	0.1	0.1	0.1	0.1	0.1	0.1	0.0	0.0
DO8	2.9	3.0	0.0	0.0	3.8	3.0	3.3	2.8	2.3	2.5	1.9	2.5	0.0	0.0
TO8	0.0	0.0	0.0	0.0	0.6	0.1	0.1	0.1	0.1	0.1	0.0	0.0	0.0	0.0

VITA

JORGE MAXIMILIANO MARTINIS COLL

Av Raul Leoni Edf Los Pinos #12 • El Cafetal • Caracas, Venezuela, Ph. 58-(212)-986-8449

EDUCATION

2000–2004 Texas A&M University College Station, TX

PhD in Chemical Engineering (3.92/4 GPA)

1989–1994 Universidad Simon Bolivar Caracas, Venezuela

B.S. in Chemical Engineering (4.17/5 GPA), 2nd in 94' Class, 90' Dean's List.

EXPERIENCE

1994–2000 PDVSA Intevep Los Teques, Venezuela

Research Engineer

TRAINING

Fall 1998 AIChE Training Program (#003) Miami, FL

Modeling of Chemical Processes. (Profs. W.D.Seider, J.D.Seader and L.T. Biegler)

Summer 1998 MIT Summer Professional Program (10.35s) Boston, MA

Modeling, Simulation and Optimization of Chemical Processes. (Prof. P. Barton)

PUBLICATIONS

Ovalles, C.; Vallejos, C.; Vásquez, T.; Martinis, J.; Pérez-Pérez, A.; Cotte, E.; Castellanos L.; Rodríguez, H. Extra-Heavy Crude Oil Downhole Upgrading Process using Hydrogen Donors under Steam Injection Conditions. *SPE Journal*. 2001, SPE No. 69692.

Ovalles C.; Martinis, J.; Pérez-Pérez, A.; Cotte, E.; Castellanos, L.; Rodríguez, H. Physical and Numerical Simulation of an Extra-Heavy Crude Oil Downhole Upgrading Process Using Hydrogen Donors Under Cyclic Steam Injection Conditions. *SPE Journal*. 2001, SPE No. 69561.